Deposition, Oxidation, and Adhesion Mechanisms of Conformal Polydopamine Films

Submitted in partial fulfillment of the requirements for

the degree of

Doctor of Philosophy

in

Materials Science and Engineering

Luke J. Klosterman

B.S., Materials Engineering, Iowa State University

Carnegie Mellon University

Pittsburgh, PA

September 2016

Acknowledgements

I would first like to express my gratitude to my advisor, Professor Chris Bettinger for his persistent guidance, patience, and encouragement these past four years. His high standards for scientific communication, along with his wisdom regarding project planning, have greatly helped my development as a professional scientist. I will continue to value the lessons and technical knowledge I have learned during our meetings and discussions. I also thank my committee members, Professor Michael Bockstaller, Professor Elizabeth Holm, and Professor Newell Washburn for the time they have donated providing helpful feedback for my thesis which has helped guide my research. Tremendous thanks goes to Adam Wise for his unending assistance with AFM and Raman measurements and for providing crucial advice that helped me with my first publication. Thanks also to John Riley, Jake Vries, and Professor Paul Sides for their valuable experimental assistance. I also wish to acknowledge financial support from the following organizations: the Defense Advanced Research Projects Agency (D14AP00040), Charles Stark Draper Laboratory University Research & Development Program, the Pennsylvania Infrastructure Technology Alliance (PITA), Pittsburgh Innovation Works, and the Carnegie Mellon University School of Engineering.

I also thank the past and current members of the Bettinger research group for their support and friendship. In particular, I thank Young Jo Kim for his help with figure design and his pioneering work on melanins along with work by Hang Ah Park. Thanks to Hector Becerril, Riddhi Kachole, Haosheng Wu, Ik Soo Kwon, and CongCong Zhu for their technical assistance and fruitful discussions.

Finally, I thank my parents and sisters for their loving support and faith in me which has kept me motivated these past four years.

Abstract

The oxidation of dopamine in aqueous solutions deposits thin conformal films on a wide variety of material surfaces. These films consist of a material known as *polydopamine* (PDA), and they exhibit chemical and structural similarities to melanin pigments and adhesive proteins secreted by mussels. The facile synthesis and versatile adhesion of PDA enable the functional modification of numerous material surfaces for applications in biomedical devices, energy storage, and water purification. This thesis details fundamental investigations into the deposition, oxidation, and adhesive mechanisms of PDA films.

Depositing PDA films on substrates with different controlled chemistries revealed the importance of solution pH and initial deposition rates on the morphology of the films. The deposition of PDA molecules with increasing pH depends on two competing factors: increased generation rate of PDA molecules *versus* increased solubility due to catechol ionization. The areal density and coverage of three-dimensional PDA islands is influenced by the surface charge and hydrophobicity of the substrate in aqueous solutions.

Spectroscopic and electrochemical characterization of PDA films revealed that redox-inactive metal cations can accelerate the oxidation of PDA. The generation of radicals of 5,6-dihydroxyindole were monitored *in situ* via ultraviolet-visible spectroscopy as a function of cation concentration and pH. The extent of oxidation was quantified by cyclic voltammetry. The resulting oxidation modifies the metal sorption properties of PDA by generating more carboxylic acid groups and enhancing the iron chelation of the films.

The adhesive stability of PDA films was characterized by delamination kinetics of films on SiO_2 and indium tin oxide (ITO). PDA film adhesion is a substrate, salt, and oxidation-dependent phenomenon. Long-term adhesive stability of PDA films can be promoted by use of

higher dopamine concentrations during synthesis, incorporation of multivalent cations, and avoiding alkaline conditions and strongly oxidizing electrical bias. Elastic moduli of PDA films were quantified by compressive thin film wrinkling, and the measured value of 2.0 ± 0.9 GPA agrees with simulations of PDA based on an oligomeric aggregate model. This thesis helps develop a framework for understanding the synthesis, composition, microstructure, and stability of PDA films.

Table of Contents

List of Figures

List of Tables

List of Schemes

Chapter 1

Introduction

The catechol and amine-rich composition of adhesive mussel-foot proteins has inspired the rapid development of catecholamine coatings and polymers in the past decade.[1] Oxidative polymerization of dopamine, norepinephrine, and other catecholamines in aqueous solutions deposits conformal nanometer-scale coatings on a wide variety of material surfaces.[2–6] Catechol, quinone, and amine moieties within the films serve as anchoring points for biomolecules,[7] metals,[2,8] minerals,[9] or polymers.[10] The interfacial properties of numerous materials can therefore be extensively modified via catecholamine coatings, and copious applications have been explored in the fields of biomaterials,[11] energy storage,[12] water purification,[13–15] and others.[16]

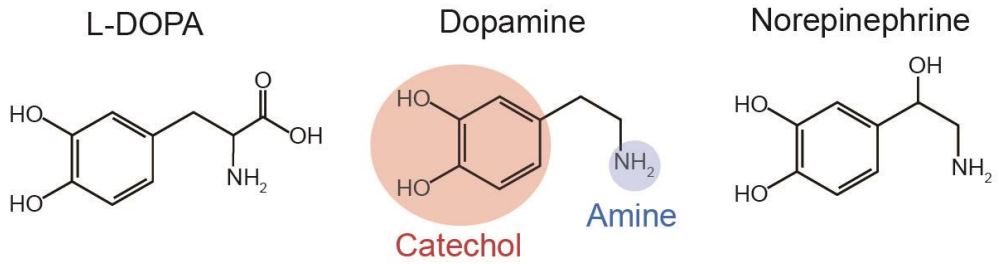

Figure 1.1: Examples of catecholamine molecules used to create versatile functional coatings.

The most prominent example of catecholamine coatings is *polydopamin*e (PDA). This material is typically synthesized by the O_2-induced oxidation of dopamine in alkaline aqueous solutions. Over the course of minutes to hours a brown/black precipitate appears in the form of nanoparticles in the liquid[17] and also as a conformal nanofilm on all surfaces present in the reaction vessel.[2] Two naturally occurring analogs to PDA – mussel-foot proteins and melanin pigments – serve as well-studied perspectives through which the properties of PDA can be

understood. This introductory chapter will discuss the chemical and physical properties of PDA in light of these analogous materials and also the practical applications explored for PDA. Finally, the objectives of this thesis are presented.

1.1 Mussel-Inspired Underwater Adhesion

1.1.1 Adhesion Schemes for Organic Coatings

A fundamental engineering constraint for organic coatings is the interfacial forces that provide their adhesion. These forces can be covalent, electrostatic, polar, or dispersive in nature[18] and define the possible coating-substrate pairings as well as the functional contexts of the coating (Figure 1.2).[19] For example, thiolate[20] and silane[21] coatings can act as robust and precise anchors for desired functional groups but are limited to oriented covalent bonding with metallic and oxide substrates, respectively. Langmuir-Blodgett coatings utilize the competing

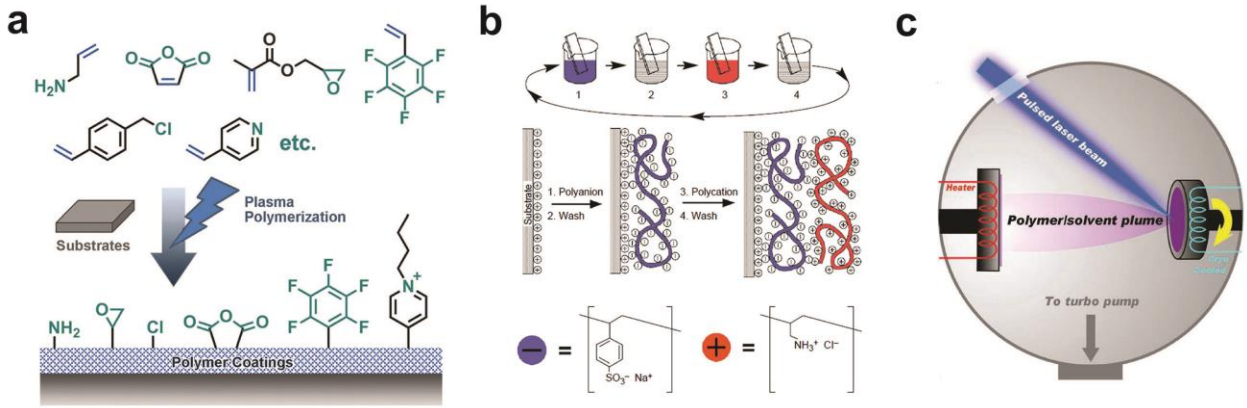

Figure 1.2: Examples of polymer coating approaches that can coat varieties of substrates utilizing different adhesion forces. a) Plasma polymerization with covalent bonding.[19] b) Layer-by-layer coatings utilizing electrostatic forces.[22] c)Laser deposition utilizing dispersive force adhesion.[23] Reproduced from respective sources.

hydrophilic/hydrophobic forces of amphiphiles to create precise homogenous films, but require sensitive preparation and specialized equipment.[24] Electrostatic forces between complementary charged polymers can be employed to form layer-by-layer films with wide applicability,[22] but

require lengthy multistep preparation[25] and can be unstable in strong electrolytes.[19] Several other schemes such as spin coating,[26,27] chemical vapor deposition,[28,29] or laser ablation deposition[23,30] utilize dispersive/nonpolar forces to coat a variety of substrate materials, but require specific equipment and substrate geometries.

A simple, universal organic coating method could greatly diversify the viable substrate materials for various applications via control over their surface properties. This coating method should exploit as many interfacial forces as possible in order to adhere to any given substrate.[31] In addition, this coating method would need to contend with the ubiquitous presence of water[31,32] which typically diminishes adhesion via attenuation of attractive interfacial forces.[1] The robust and promiscuous underwater adhesion of marine mussels has served as a biological inspiration for universal coatings[1] and is discussed in the next section.

1.1.2 Mussel Adhesion and Molecular Mechanisms

Mussels are marine organisms that attach themselves securely to various surfaces in saltwater environments. This versatile surface attachment is accomplished through byssal threads that extend from the mussel and secrete specialized adhesive proteins (Figure 1.3).[1,32] Two of these proteins, termed Mfp-3 and Mfp-5, are located at the interface between the byssal thread and the surface. These proteins are relatively rich in catechol and amine-containing peptides, particularly Mfp-5.[33] Inspired by the high catechol and amine content in these underwater adhesive proteins, several biomimetic materials incorporating these functionalities were created with moderate success in reproducing the versatile moisture-resistant adhesion.[34–37] An extremely simplified approach towards this biomimicry was discovered by Messersmith and coworkers in 2007, wherein the O_2-induced oxidation of dopamine in water produced conformal

adherent coatings on every class of material (Figure 1.3).[2] Other catecholamine molecules can produce similar coatings.[3–5]

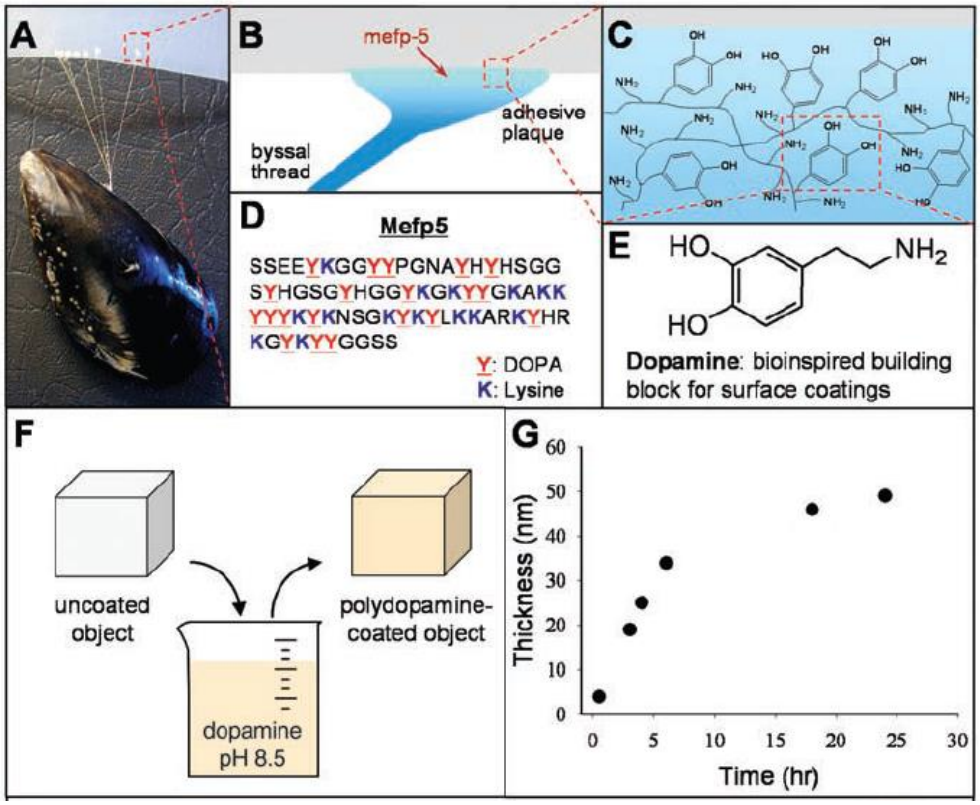

Figure 1.3: Mussel-inspired coating. a) Mussel with adhesive fibers attached to PTFE. b,c) Illustrations of the interfacial location of the adhesive protein and its amino and catechol groups. d) Amino acid sequence of the adhesive protein indicating the abundance of DOPA (catechols) and lysine (amines) e) Dopamine molecule with both primary amine and catechol groups. f) Scheme for polydopamine film synthesis. g) Thickness of the film versus time in solution. Reproduced from [2].

The molecular basis for mussel-inspired adhesion has been explored using atomic force microscopy (AFM), surface force apparatuses (SFA), and spectroscopic techniques. AFM contact force measurements revealed that the adhesive force of a single catechol moiety to wet TiO_2 is ~800 pN (Figure 1.4).[38] In comparison, a typical covalent bond is around 1-2 nN.[39] The adhesive force of oxidized catechol (i.e. quinone) to TiO_2 is ~180 pN, while that of a mono-phenol (tyrosine) is ~100 pN. These and other data[40] highlighted the importance of the un-oxidized, bidentate hydroxyl moiety of catechol for establishing high strength underwater adhesion (at least to TiO_2). The origin of this strong bond is a ligand-to-metal charge transfer

complex between the catecholic oxygens and the Ti^{4+} atoms at the surface,[41–43] exhibiting ~40% covalent and 60% ionic bond character.[44] Similar complexes have been observed between catechols and other metal oxides including Fe_2O_3,[45] Cr_2O_3[45], and Al_2O_3.[46]

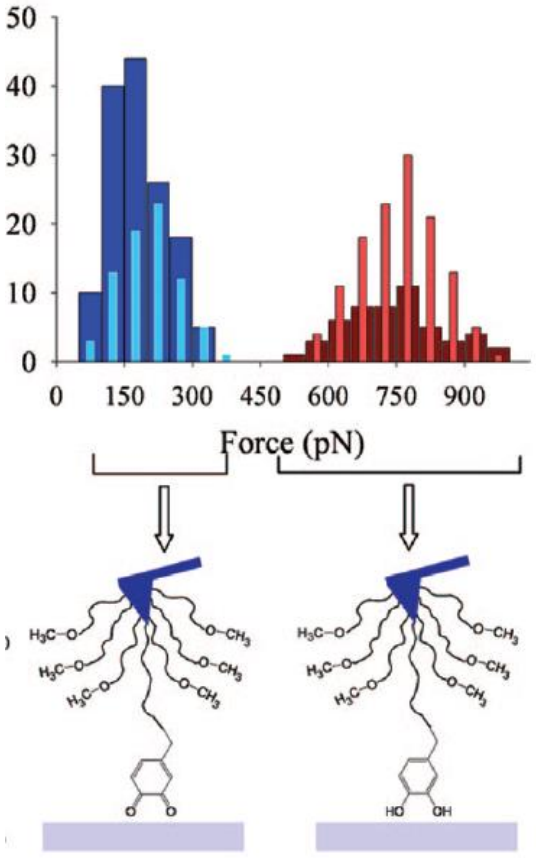

Figure 1.4: Adhesion forces measured between catechol and TiO_2 surface at pH = 8.3 (light bars) and pH = 9.7 (dark bars). The bimodal distribution was attributed to measurements from oxidized (left) vs. reduced catechols, and as the pH is increased more measurements were recorded from the oxidized catechol. Reproduced from [38]

Catechol adhesion to SiO_2 and mica (an aluminosilicate) occurs by a different interaction than with TiO_2. Simulations of dopamine and L-DOPA (i.e. carboxylated dopamine) adsorption to wet SiO_2 surfaces indicated direct, bidentate hydrogen bonding between catechol and SiO_2.[47,48] Increasing the catechol content of mussel-mimetic peptides increased their adhesion force to mica and TiO_2.[49] The magnitude of this force was lower with mica than TiO_2 in all

cases, which the authors attributed to weaker hydrogen bonds with mica than the coordination bonds with TiO_2 (Figure 1.5).

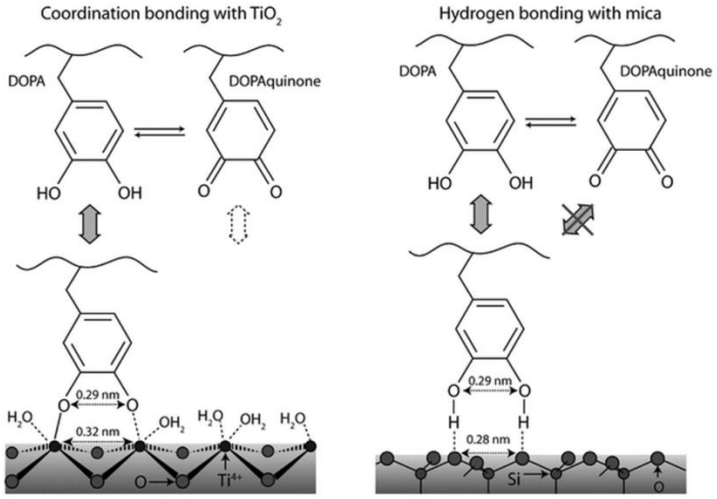

Figure 1.5: Proposed binding mechanism of catechols (e.g. DOPA) to TiO_2 and mica based on the relative strengths of their interactions. Reproduced from [49].

Surface force measurements on catechol and amine-containing molecules between mica surfaces revealed a cooperative adhesive synergy between the catechols and amines.[50] Only molecules with *both* catechols and primary amines exhibited adhesion and close approach between two mica surfaces. Based on the closer interaction distance in the presence of molecules containing primary amines, the amines were proposed to displace adsorbed surface cations and allow the catechols to interact with the mica surfaces (Figure 1.6). Additionally, this cooperative synergy was most effective when both catechol and amine were present on the same molecule,[51] which supports the versatile adhesion observed in polydopamine.

Besides bidentate hydroxyl interactions with oxide surfaces, oxidized catechols (i.e. quinones) can adhere to organic surfaces via covalent bonding with nucleophiles such as primary amines and thiols.[38] Other organic adhesion schemes observed in catecholamine materials include π-π and cation-π attractions involving aromatics and amines,[52] hydrophobic attractions

between nonpolar organics and catechols,[53,54] or the ubiquitous hydrogen bonding present in complex organic systems.[55]

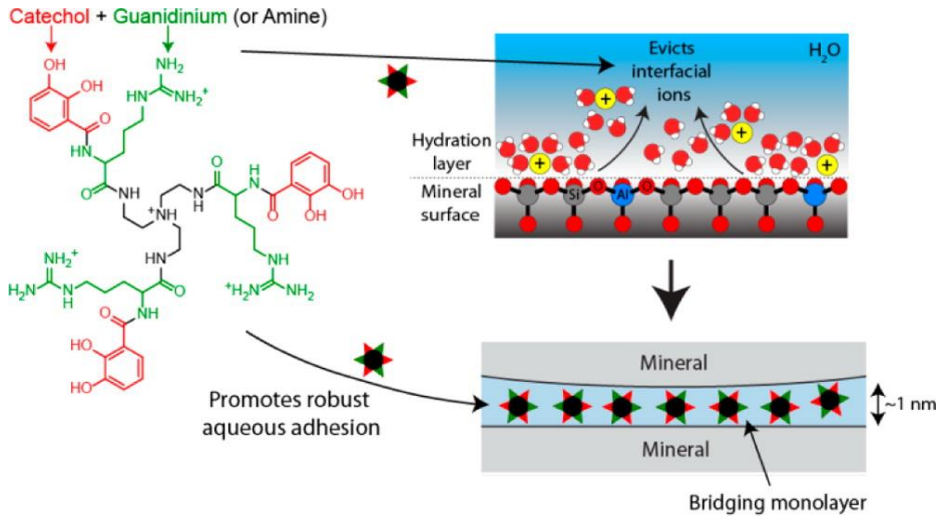

Figure 1.6: Proposed role of positively charged amine groups in displacing hydrated cations from mineral surfaces. The presence of primary amines is necessary for close approach and adhesion of catechol groups to mica. Reproduced from [51].

Taken together, the extensive studies performed on adhesive mussel proteins and derivative materials have revealed a multimodal adhesion scheme that enables versatile and robust adhesion in wet environments.[56] The next section will discuss the internal chemistry and structure of catecholamine coatings in light of their similarity to naturally occurring melanin pigments.

1.2 Chemistry of Melanin Materials

1.2.1 Synthesis of Melanins

Despite the remarkable adhesion and coating properties of polydopamine, dopamine itself does not form coherent, bulk coatings on surfaces.[2] Rather, oxidation of the starting molecule is necessary, and a functioning knowledge of polydopamine coatings requires understanding their oxidative chemistry and resulting structure. The oxidation pathway and products of dopamine have been explained in light of the many decades of work done on the synthesis of melanins.

Melanins are a class of pigments found throughout nature and serve a variety of functions ranging from photoprotection, metal cation homeostasis, and protection from predators. *Eumelanins* are the most well-studied and are derived from the oxidation of 3,4,-dihydroxyphenalalanine (L-DOPA) – a molecule that is equivalent to dopamine with an added carboxylic acid next to the amine. *Neuromelanin* is less well-understood but is derived directly from oxidation of dopamine present in the brain.[57]

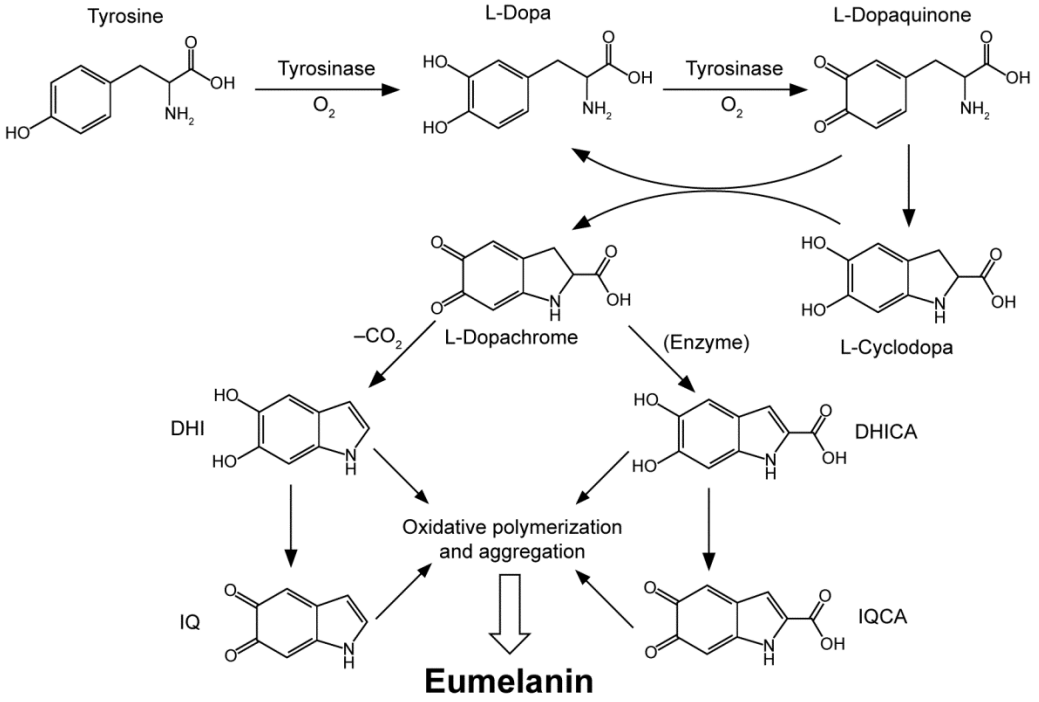

Scheme 1.1: Reaction pathway for natural melanogenesis. Adapted from [58] and [59].

The natural synthesis of eumelanin begins with the enzymatically-controlled creation and oxidation of the catecholamine L-DOPA (Scheme 1.1). Oxidation of the catechol allows the primary amine within L-DOPA to attach to the 6-position on the benzene ring creating a heterocyclic compound called *cyclodopa*. Further oxidation creates a red-colored compound known as *dopachrome*. The structural verification of this red compound was central to the historical understanding of melanogenesis.[60] Dopachrome then tautomerizes and to an extent decarboxylates to produce the immediate precursors to melanin: 5,6-dihydroxyindole-carboxylic

acid (DHICA) and 5,6-dihydroxyindole (DHI). These species then oxidatively bond together into oligomers (possibly through radical-radical coupling[61,62]) producing melanin.[63] Additionally, hydrogen peroxide generated during the catechol oxidation steps[64] can degrade the indolic molecules resulting in pyrrole carboxylic acids, which are also observed in melanins.[65,66] In general however, the pigment can be characterized as indolic oligomers.

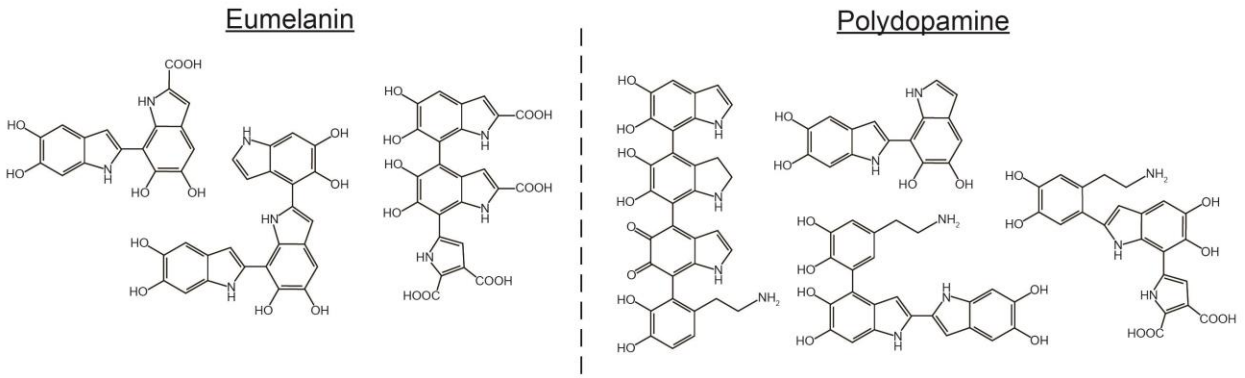

Figure 1.7: Comparison of typical oligomers present in natural eumelanin and polydopamine.

In contrast to eumelanin, the O_2-induced oxidation of polydopamine (PDA) is not enzymatically controlled and therefore produces a more heterogeneous product. A comparison of the oligomers in eumelanin[67] versus PDA[66,68,69] is shown in Figure 1.7, as taken from several studies.[70] The detailed oxidation pathway of PDA is similar to eumelanin and will be discussed in Chapter 3, but suffice to say the oxidation rate of dopamine is directly proportional to the oxygen and dopamine concentration and inversely proportional to hydronium concentration.[71] Chemical oxidants such as Cu^{2+},[72] ammonium persulfate,[73] or sodium periodate[74] can also oxidize dopamine into PDA.

1.2.2 Structure of Melanins

As melanin precursors oxidize in solution, their products precipitate as a brown-black pigment. The oligomers of natural and synthetic melanins aggregate primarily via π-stacking,

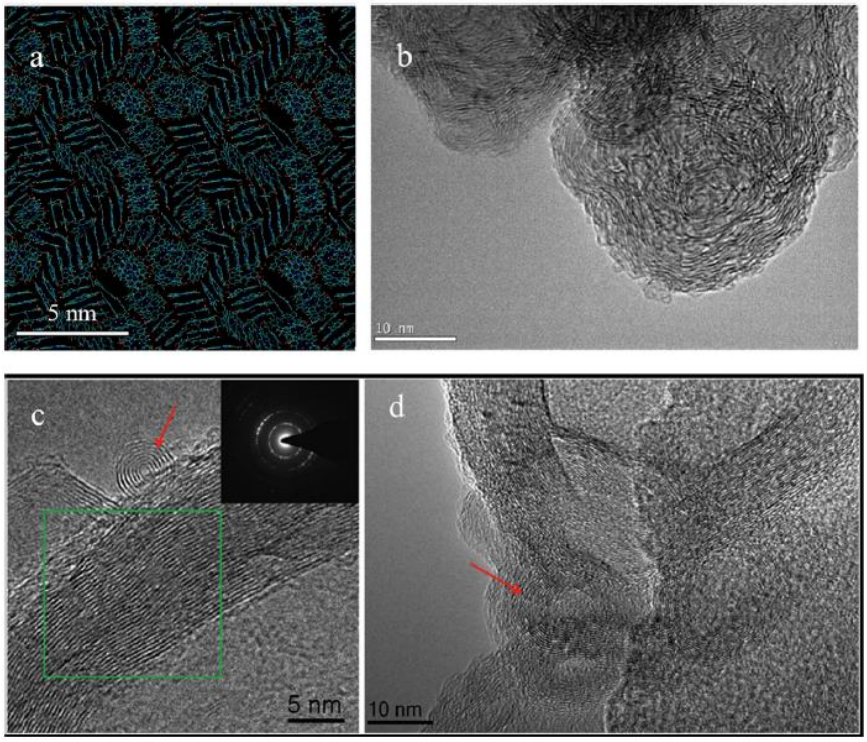

Figure 1.8: Aggregated microstructure of polydopamine. (a) Simulated aggregate of DHI-tetramers (b) typical TEM micrograph of particle (c,d) high-resolution TEM images with red arrows showing graphite-like fringes from stacked oligomers. The inset of C shows a diffraction pattern taken from the green-boxed region. Reproduced from [75]

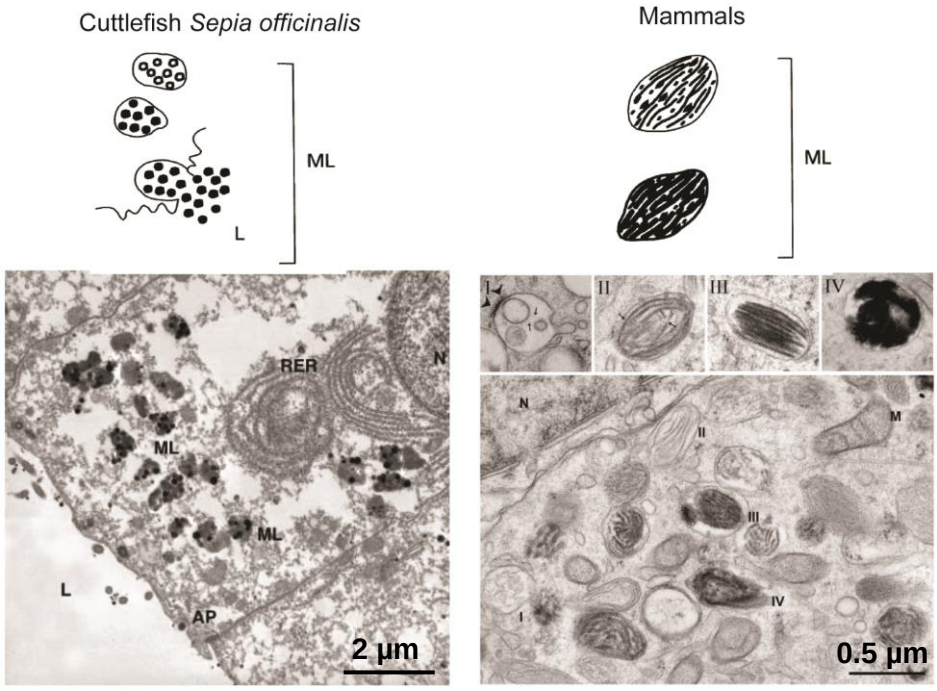

Figure 1.9: Aggregation of melanin oligomers in cuttlefish (left) versus mammals (right). Aggregation occurs heterogeneously in both. ML = melanosome, the organelle in which melanogenesis occurs. Illustrations reproduced from [76], cuttlefish micrograph from [77], and mammal micrograph from [78].

but hydrogen bonding and charge transfer between catechol and quinone groups contributes as well.[69,79] X-ray diffraction[80–83] and TEM measurements[84,75] on natural and synthetic melanins revealed periodic spacings of 3.4–3.8 Å, which is characteristic of π-stacked heteroaromatic molecules (Figure 1.8). TEM micrographs also show a lack of long-range order, as expected from the heterogeneity of the constituent molecules.

Natural melanins preferentially precipitate heterogeneously on protein fibrils[78] or vesicles[77] depending on the organism (Figure 1.9). The precipitation of PDA nanoparticles is sensitive to the reaction conditions and buffer used during synthesis. PDA particles typically range from ~50-300 nm diameter depending on the synthesis condition.[17] Increasing the pH and

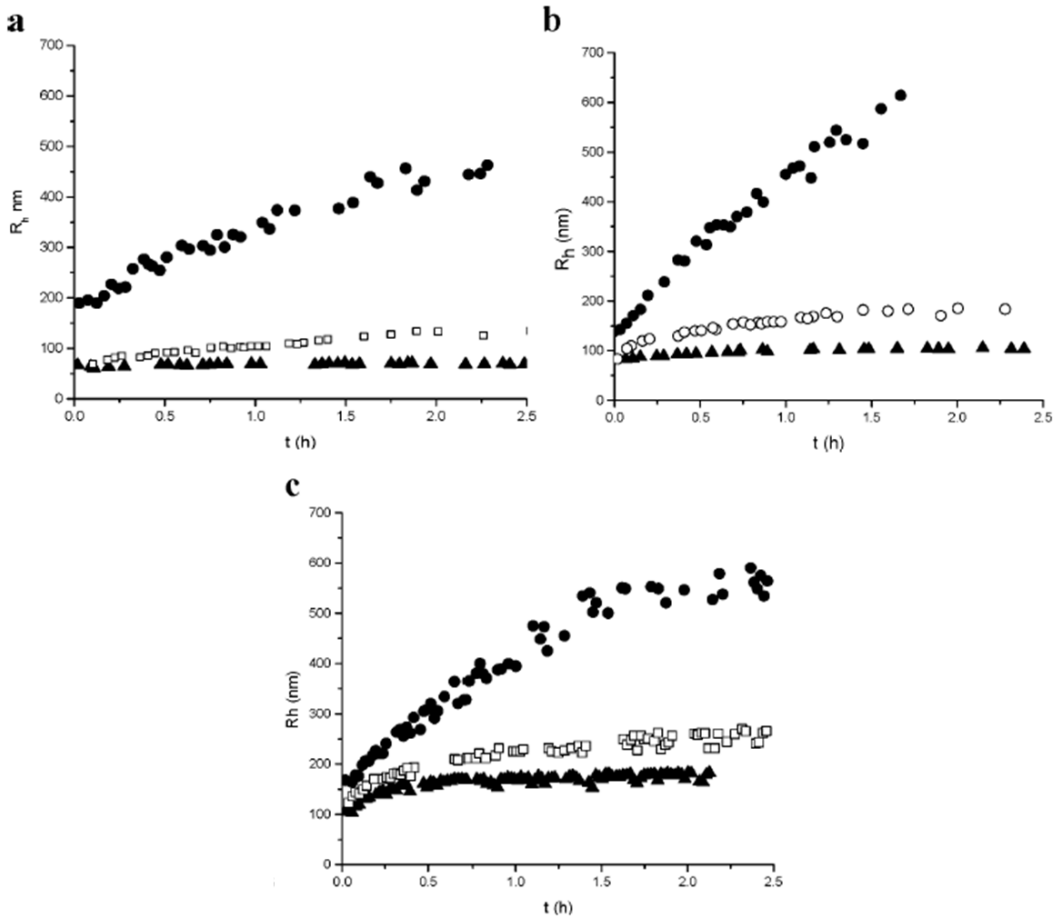

Figure 1.10: Hydrodynamic radii of PDA growing from a) 0.5 mM b) 1.0 mM c) 2.0 mM dopamine in three buffer solutions, K_2PO_4 (circles), $NaHCO_3$ (open squares), and Tris (triangles). Reproduced from [85].

temperature of the dopamine solution creates nanoparticles at the lower end of this range, likely due to increased nucleation rate. Dynamic light scattering revealed that increasing the dopamine precursor concentration increases the size of PDA aggregates, as expected given the greater amount of material available (Figure 1.10).[85] Interestingly, PDA aggregates are larger in phosphate buffer compared to carbonate or Tris buffer, and this is likely due to higher ionic strength in phosphate buffer which would lessen the double-layer repulsion between charged PDA species.[4,85] The large PDA aggregates formed in the reaction liquid are distinct from the PDA formed heterogeneously on surfaces (as will be discussed in Chapter 2) but the aggregates can deposit and adhere to the PDA coatings as shown in Figure 1.11.

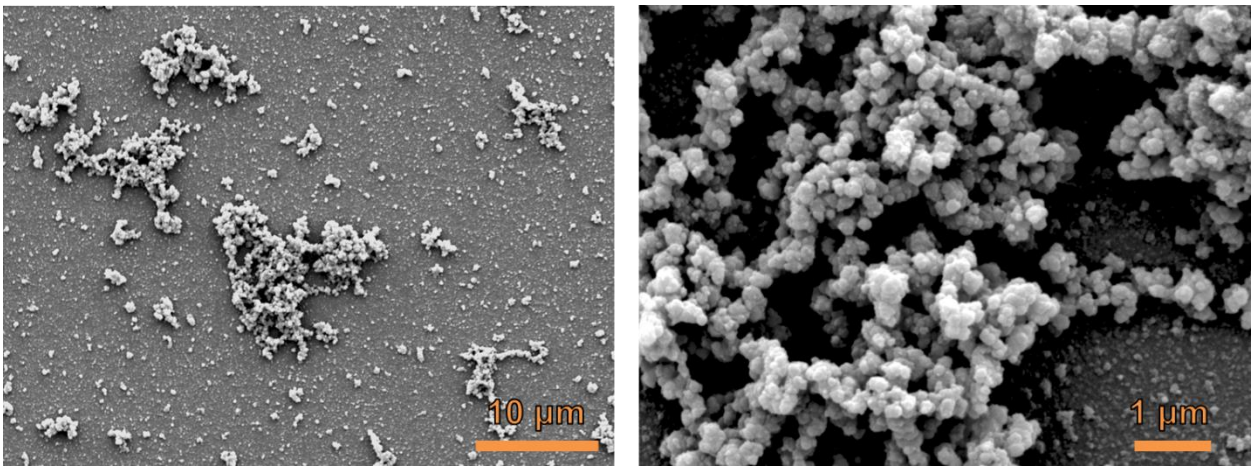

Figure 1.11: Scanning electron microscope images of 59 nm thick PDA films formed in 1 mg/ml dopamine solution. Large aggregates of PDA particles are visible on the surface that are distinct from the underlying film. (Original data.)

1.2.3 Properties of Melanins

Aside from the versatile adhesion of PDA, the other intrinsic properties of melanins primarily derive from their many catechol groups. The redox chemistry of catechols involves two $1e^-$, $1H^+$ steps with a semiquinone intermediate (Figure 1.12). As such, melanins become more susceptible to oxidation at higher pH (Figure 1.13).

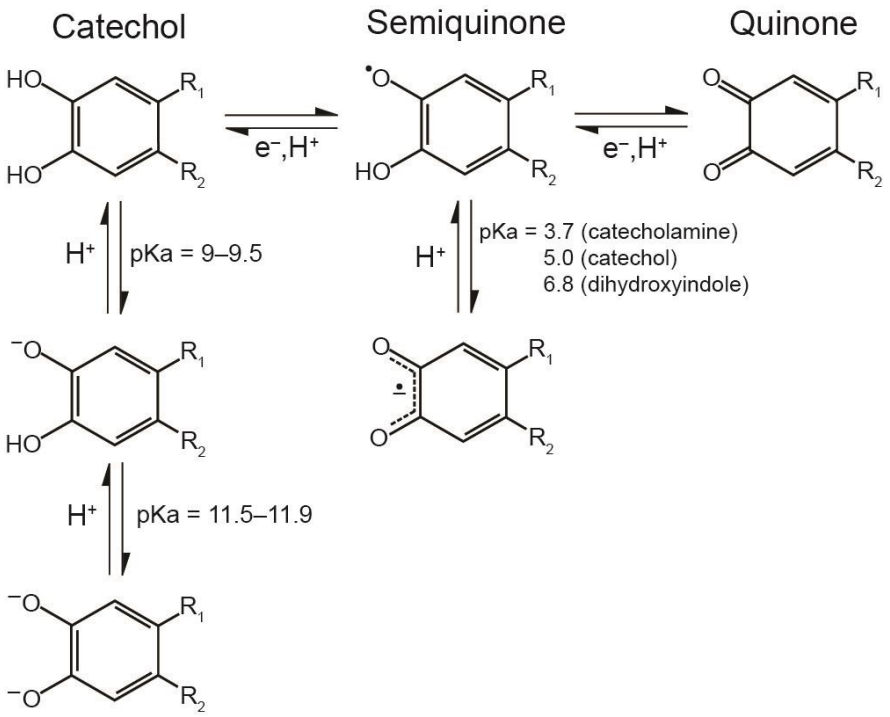

Figure 1.12: Electron and hydrogen equilibria of catechols. pK_as for the catechol column were taken from [86–88]. pK_as for semiquinones were taken from [89] for catecholamine, [90] for catechol, and [91] for dihydroxyindole.

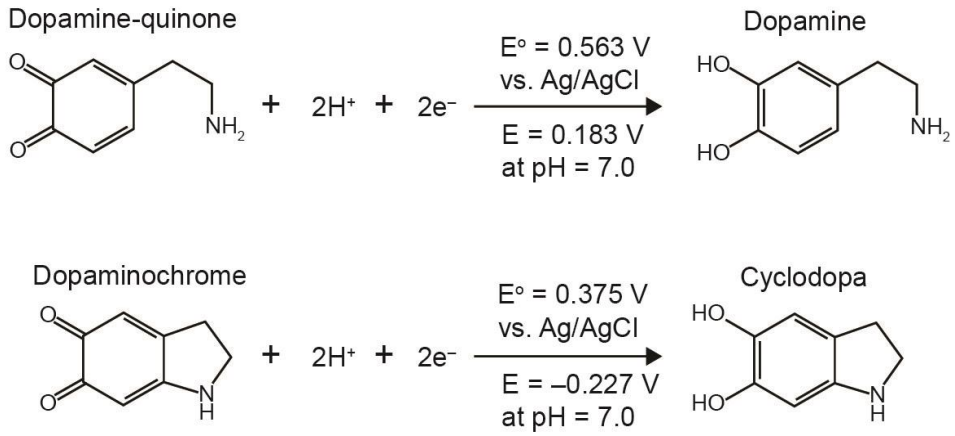

Figure 1.13: Redox potentials for two of the main constituents in PDA.[92]

A comproportionation equilibrium exists between the catechol and quinone species in water producing semiquinone radicals (Figure 1.14). A stable population of semiquinone radicals is a defining feature of melanins (ca. 1 radical per 1700 monomers in PDA[93] or 1 per 1500 in DHI-melanin[86]) and contributes to its mixed electronic-ionic conduction[94] and its metal

ion binding capacity.[95] The semiquinone concentration can be increased by increasing pH[96], hydration level,[94] bound metals[95], and light exposure.[97,98] There is also a population of intrinsic carbon-centered radicals resulting from the polymerization process[99], but they do not appear to contribute to the electrical properties of melanin.

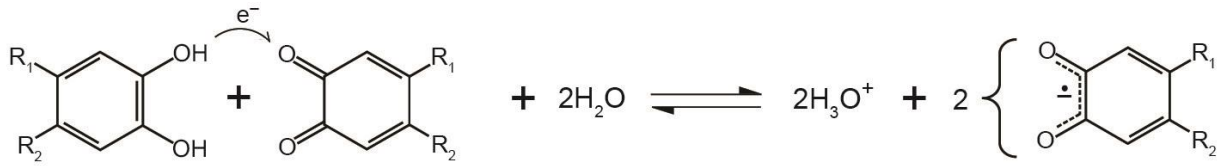

Figure 1.14: Catechols and quinones exist in a comproportionation equilibrium with semiquinones.

The electrical conductivity of melanin is due to a combination of protonic transport and electronic conduction of free radicals. The conductivity of melanin depends strongly on hydration, and is reported to be between 10^{-7} and 10^{-4} S/cm when fully hydrated (Figure 1.15).[100,101] Proposed current conduction mechanisms are based on the evolving redox states of catechols (Figure 1.12–1.13) at electrically biased positive and negative electrodes.[101] Under

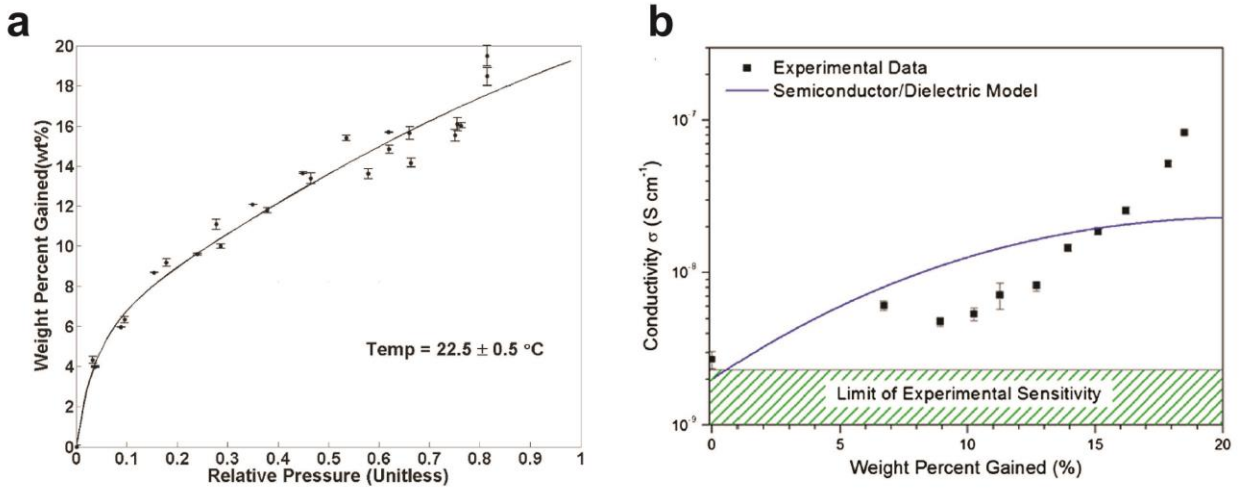

Figure 1.15: a) Water sorption isotherm for a pressed synthetic melanin pellet (~13 mm diameter x 2 mm thickness) with corresponding BET model curve. Reproduced from [102] b) Conductivity of melanin vs. water content (wt%). Fully hydrated melanin is ~18 wt% water. Also shown in the figure is the poor fit of an amorphous semiconductor model of conduction (blue line). Reproduced from [100].

applied electrical bias, positive charge carriers in melanin (hydrogen ions) drift towards the negative electrode via Grotthuss hopping mechanisms[94] within the water and between ionized catechol groups. Negative charge carriers (free radicals) migrate via electronic conduction within oligomers, and also as the complementary effect of proton hopping. This conduction scheme implies that the current flow would eventually stop between electrodes due to complete reduction and oxidation of the melanin oligomers at the electrode interfaces. The high degree of irreversibility observed in cyclic voltammograms of melanins supports this conduction scheme.[101,103,104]

Melanins also exhibit a strong affinity for certain metal cations, and they are believed to play a role in metal homeostasis within certain organisms. Neuromelanin, which exists in certain cells in the human midbrain, contains high concentrations of iron ions, and may act to sequester these and other toxic metals.[105–107] Fungal melanins absorb various transition metal cations from their environment, possibly acting as a protective sequesterant.[108–110] Apart from these

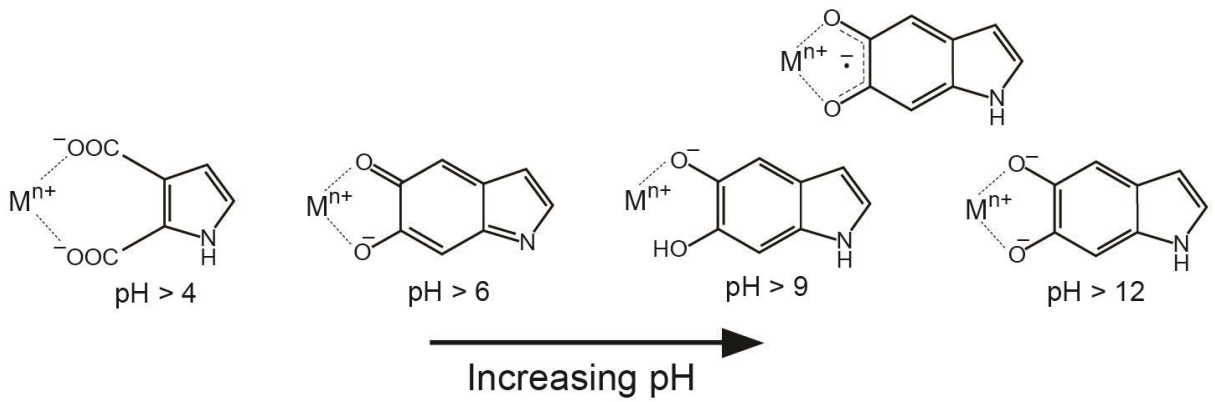

Figure 1.16: The modes of metal binding to melanins as a function of pH.

examples, it has also been observed that melanins in general tend to absorb multivalent cations[111] through semiquinone,[95] quinone-imine,[86] or carboxylic acid[112] groups (Figure 1.16). Multiple catechol groups can also chelate simultaneously with multivalent cations like Fe^{3+} (Figure 1.17),

and catechols in melanin exhibit a greater affinity for Fe^{3+} compared to group II cations such as Mg^{2+} and Ca^{2+}.[88,112]

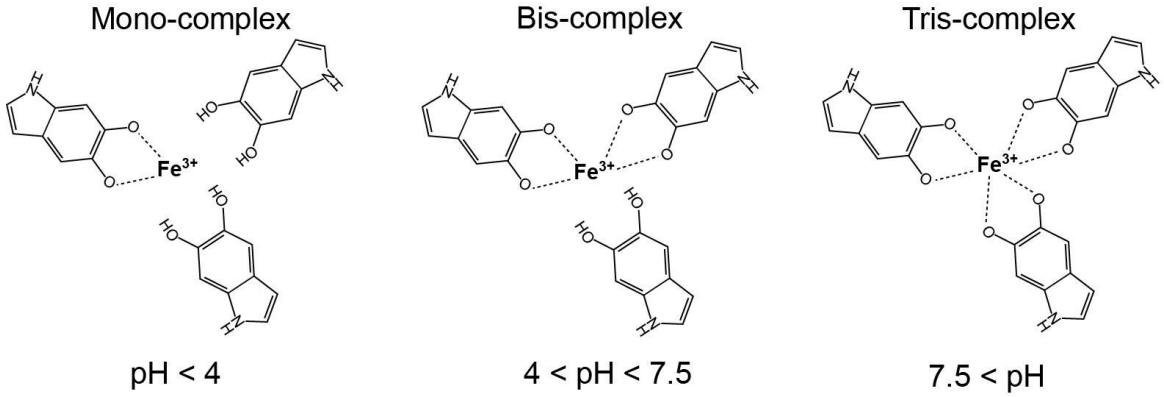

Figure 1.17: Fe^{+3} chelation to catechol groups in melanin molecules as the pH is raised from acidic values to basic (left to right). Adapted from [113] and [88].

In summary, the chemistry and structure of melanins such as PDA are dominated by their many catechol groups. The oxidative synthesis of PDA is controlled by the deprotonation and oxidation of dopamine's catechol group. Intramolecular cyclization by the amine in dopamine creates a heterocyclic compound more susceptible to oxidation than PDA, and di-radical coupling between the various catechol-containing molecules produces oligomers. The aggregation of these oligomers into amorphous/π-stacked nanoparticles can be controlled by reaction conditions and choice of buffer. The latent intrinsic reactivity of PDA is due to the various redox and acid-base equilibria of catechols and also residual amines within the films (to be discussed more in Chapters 4 and 5).

1.3 Applications

The facile synthesis and versatile adhesion of PDA have prompted its exploration for numerous applications as an adhesive primer, surface energy modifier, and ion exchange material. Extensive reviews have catalogued the hundreds of reports on PDA's potential functions for biomedical[11] and other technologies.[16,114]

The abundant catechols in PDA can serve as anchoring points for primary amines or thiols and their attached functional groups. Biomolecules such as trypsin[7] or cellular growth

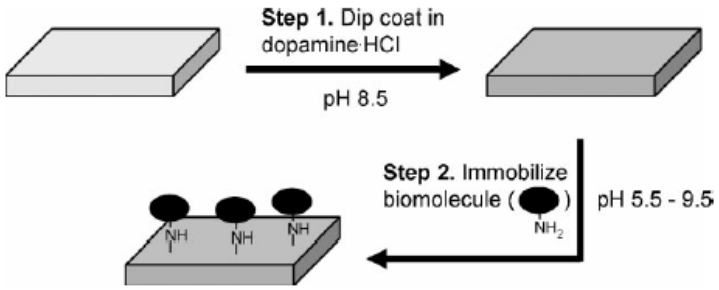

Figure 1.18: Illustration of PDA coating and biomolecule attachment. Reproduced from [7]

factors[115] can be covalently attached to PDA and modulate cells' interactions with the surfaces of implants (Fig. 1.18). For example, DM films were coated on common bio-electrode surfaces, bonded with poly-D-lysine, and then neuronal networks formed on them from which neural signals could be recorded.[116] Polyethylene glycol polymers can be grafted onto PDA coatings and lessen non-specific protein or fibroblast adsorption to the substrate material.[2] PDA coatings themselves can improve cell adhesion and proliferation on otherwise cytophobic surfaces such as PTFE and PDMS.[117] PDA can also function as an adhesive primer for the biomineral hydroxyapatite by chelating and concentrating Ca^{+2} ions at the surface of implant materials (Fig. 1.13).[9]

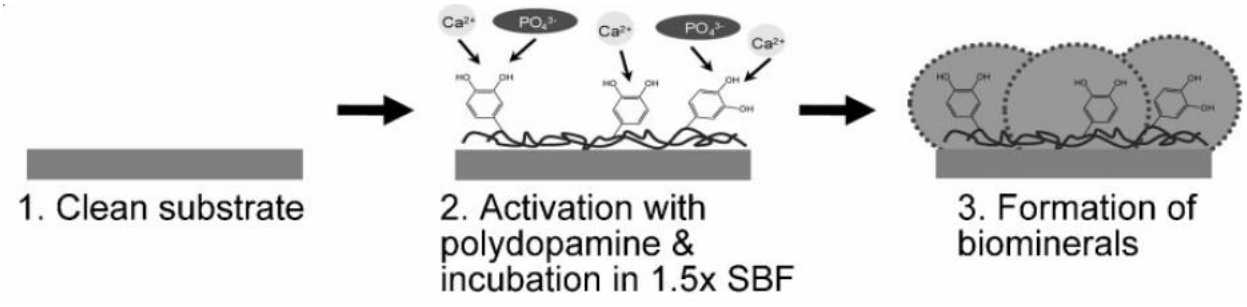

Figure 1.19: Formation of the biomineral hydroxyapatite on a surface is facilitated by Ca^{+2} adsorption by a PDA coating. Reproduced from [9].

PDA coatings can be used to modulate the hydrophobicity/surface energy of substrates. Polyethylene separators in Li-ion batteries were coated with PDA in order to improve power performance by increasing the hydrophilicity of the separator for the electrolyte (Fig. 1.20).[12] Fabrication of forward osmosis membranes was improved by PDA's ability to increase the hydrophilicity of a polysulfone substrate for subsequent interfacial polymerization of polyamide.[118] Low surface-energy substrates were also modified with PDA to improve block-copolymer lithography on those substrates.[119]

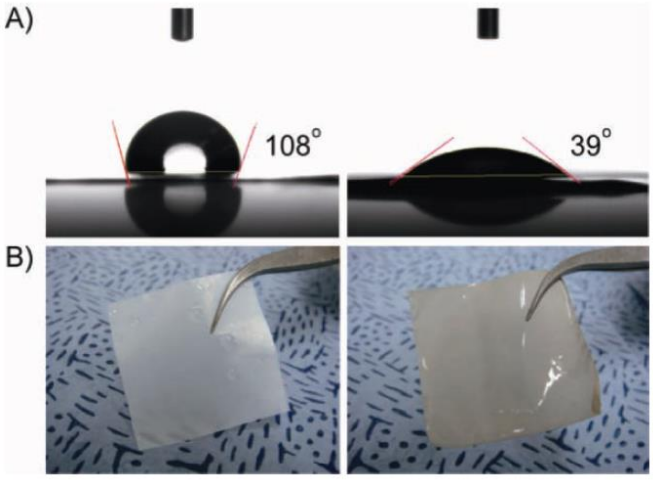

Figure 1.20. Contact angles for a Li-ion battery electrolyte on the polyethylene separator before (left) and after (right) PDA coating. The PDA coating increases the hydrophilicity of the separator. Reproduced from [12].

The strong metal cation-chelating properties of catechols observed in bacterial siderophores,[120] mussel byssal threads,[121] and melanin[122] have inspired the use of PDA for water purification devices. The underwater adhesive coating ability of PDA enabled the fabrication of high surface area PDA adsorbents on glass microbeads (Figure 1.21).[13] These PDA-coated beads exhibited passive metal sorption capacities comparable to or better than a common activated carbon adsorbent. Additionally, the metal sorption capacity of PDA-coated beads could be regenerated by exposure to dilute acid or by simply removing and re-applying the PDA coating.

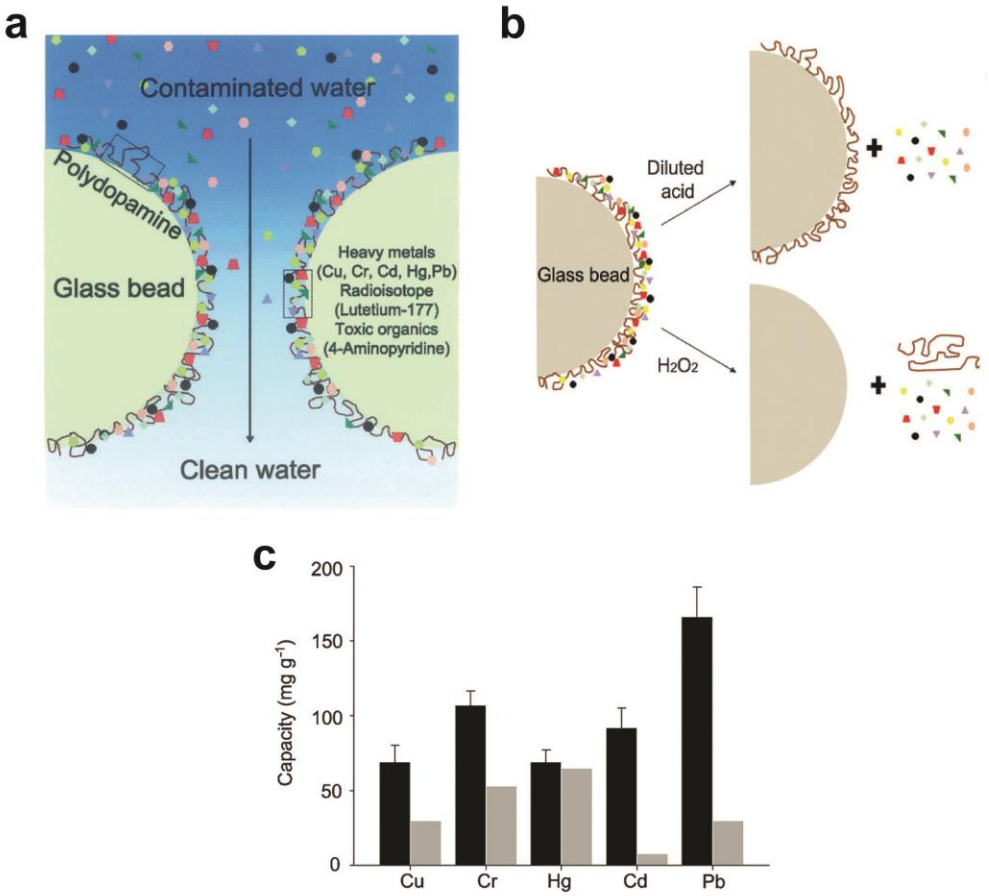

Figure 1.21: Water detoxification by PDA-coated glass beads. a) Contaminated water passes through a packed column of PDA-coated beads and metal cations are removed by catechol groups. b) Regeneration of PDA by dilute acid or regeneration of the beads by removal of PDA. c) Comparison of binding capacity of PDA (black) vs. activated carbon (gray) for different metals. Reproduced from [13]

The reversible redox cycling of catechols[123] and mixed ionic-electronic conduction of melanins[94] have also inspired the use of PDA for redox-active water purification. Coating PDA on stainless steel mesh allowed for electrical control over PDA's catechol redox states and therefore the anionic charge they presented (Figure 1.22).[14] Positive oxidizing potentials applied to PDA remove hydrogens and electrons from the catechol groups in the coating. Subsequent application of a negative reducing potential to the PDA injects electrons back into the catechols which are charged balanced by the influx of metal cations. This electrochemically mediated sorption process was rapid (~1 min for equilibration) and more than doubled the sorption capacity of the PDA coating for Mg^{2+} compared to passive sorption.

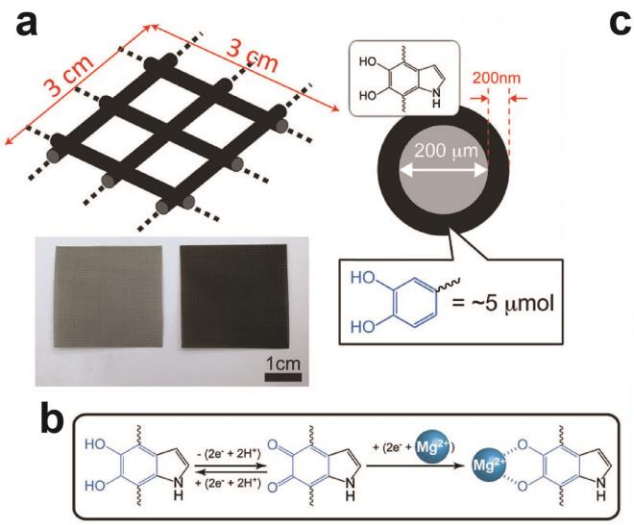

Table 4. Comparison of binding capacity of melanins to divalent ions

Material	Electrochemically mediated	Ion	Binding capacity (mmol g^{-1})	Ref.
Natural melanin[a]	No	Mg^{2+}	1.3	43
Natural melanin[a]	No	Ca^{2+}	1.4	43
Natural melanin[a]	No	Cu^{2+}	1.1	43
Natural melanin[a]	No	Zn^{2+}	1.5	43
Natural melanin[a]	Yes	Mg^{2+}	0.85	21
Synthetic melanin[b]	No	Mg^{2+}	1.91	This work
Synthetic melanin[b]	Yes	Mg^{2+}	4.61[c]	This work
Synthetic melanin[b]	Yes	Mg^{2+}	5.39[d]	This work

[a] Sourced from the ink sacs of *Sepia officinalis*.
[b] Synthesized through oxidative polymerization of dopamine in aqueous solutions.
[c] First cycle.
[d] 100th cycle.

Figure 1.22: Electrochemically-mediated removal of divalent cations from water. a) PDA coated onto stainless steel mesh. b) Proposed ion exchange of hydrogens with magnesium by first electrochemically oxidizing the catechols then reducing them. c) Comparisons of binding capacity via passive sorption in natural melanins, PDA, and electrochemically-mediated sorption in PDA. Reproduced from [14].

1.4 Summary and Objectives

Polydopamine belongs to a class of catecholamine materials that mimic the versatile underwater adhesion of mussels and the rich catechol chemistry of melanins. The combination of these properties makes PDA a promising coating for extensively modifying the surface functionality of numerous materials, or acting as a functional material in its own right (e.g. water purification). However, the facile and versatile coating of PDA belies its complex chemistry and composition.[79] PDA coatings are applied in widely varying contexts yet there is no established framework for understanding their synthesis, composition, microstructure, and stability.

The aim of this thesis is to develop the fundamental structure-processing-property relationships of PDA coatings in order to improve their performance in practical technologies and inform the design of derivative materials. The deposition, oxidation, and adhesive/cohesive mechanisms of PDA are reported and discussed. Special attention is paid to the role of metal

cations on the compositional and adhesive stability of PDA coatings in light of prospective water purification applications.

1.5 References

(1) Lee, B. P.; Messersmith, P. B.; Israelachvili, J. N.; Waite, J. H. Mussel-Inspired Adhesives and Coatings. *Annu. Rev. Mater. Res.* **2011**, *41*, 99–132.

(2) Lee, H.; Dellatore, S.M; Miller, W.M; Messersmith, P. B. Mussel-Inspired Surface Chemistry for Multifunctional Coatings. *Science* **2007**, *318*, 426–430.

(3) Sung, M. K.; Rho, J.; Choi, I. S.; Messersmith, P. B.; Lee, H. Norepinephrine: Material-Independent, Multifunctional Surface Modification Reagent. *J. Am. Chem. Soc.* **2009**, *131*, 13224–13225.

(4) Kuang, J.; Guo, J. L.; Messersmith, P. B. High Ionic Strength Formation of DOPA-Melanin Coating for Loading and Release of Cationic Antimicrobial Compounds. *Adv. Mater. Interfaces* **2014**, *1*, 1–6.

(5) Ham, H. O.; Liu, Z.; Lau, K. H. A.; Lee, H.; Messersmith, P. B. Facile DNA Immobilization on Surfaces through a Catecholamine Polymer. *Angew. Chemie - Int. Ed.* **2011**, *50*, 732–736.

(6) Kuang, J.; Messersmith, P. B. Universal Surface-Initiated Polymerization of Antifouling Zwitterionic Brushes Using a Mussel-Mimetic Peptide Initiator. *Langmuir* **2012**, *28*, 7258–7266.

(7) Lee, H.; Rho, J.; Messersmith, P. B. Facile Conjugation of Biomolecules onto Surfaces via Mussel Adhesive Protein Inspired Coatings. *Adv. Mater.* **2009**, *21*, 431–434.

(8) Sileika, T. S.; Kim, H. Do; Maniak, P.; Messersmith, P. B. Antibacterial Performance of Polydopamine-Modified Polymer Surfaces Containing Passive and Active Components. *ACS Appl. Mater. Interfaces* **2011**, *3*, 4602–4610.

(9) Ryu, J.; Ku, S. H.; Lee, H.; Park, C. B. Mussel-Inspired Polydopamine Coating as a Universal Route to Hydroxyapatite Crystallization. *Adv. Funct. Mater.* **2010**, *20*, 2132–2139.

(10) Pop-Georgievski, O.; Popelka, Š.; Houska, M.; Chvostová, D.; Proks, V.; Rypáček, F. Poly(ethylene Oxide) Layers Grafted to Dopamine-Melanin Anchoring Layer: Stability and Resistance to Protein Adsorption. *Biomacromolecules* **2011**, *12*, 3232–3242.

(11) Lynge, M. E.; van der Westen, R.; Postma, A.; Städler, B. Polydopamine--a Nature-Inspired Polymer Coating for Biomedical Science. *Nanoscale* **2011**, *3*, 4916–4928.

(12) Ryou, M.-H.; Lee, Y. M.; Park, J.-K.; Choi, J. W. Mussel-Inspired Polydopamine-Treated Polyethylene Separators for High-Power Li-Ion Batteries. *Adv. Mater.* **2011**, *23*, 3066–3070.

(13) Lee, M.; Rho, J.; Lee, D. E.; Hong, S.; Choi, S. J.; Messersmith, P. B.; Lee, H. Water Detoxification by a Substrate-Bound Catecholamine Adsorbent. *Chempluschem* **2012**, *77*, 987–990.

(14) Park, Hang-Ah; Kim, Young Jo; Kwon, Ik Soo; Klosterman, Luke; Bettinger, C. J. Lithium Purification from Aqueous Solutions Using Bioinspired Redox Active Melanin Membranes.

Polym. Int. **2016**.

(15) Farnad, N.; Farhadi, K.; Voelcker, N. H. Polydopamine Nanoparticles as a New and Highly Selective Biosorbent for the Removal of Copper (II) Ions from Aqueous Solutions. *Water, Air, Soil Pollut.* **2012**, *223*, 3535–3544.

(16) Liu, Yanlan; Ai, Kelong; Lu, L. Polydopamine and Its Derivative Materials: Synthesis and Promising Applications in Energy, Environmental, and Biomedical Fields. *Chem. Rev.* **2014**, *114*, 5057–5115.

(17) Ju, K.; Lee, Y.; Lee, S.; Park, S. B.; Lee, J. Bioinspired Polymerization of Dopamine to Generate Melanin-Like Nanoparticles Having an Excellent Free-Radical-Scavenging Property. **2011**, 625–632.

(18) Israelachvili, J. N. *Intermolecular and Surface Forces*; 3rd ed.; Academic Press: Burlington, MA, 2011.

(19) Wei, Q.; Haag, R. Universal Polymer Coatings and Their Representative Biomedical Applications. *Mater. Horizons* **2015**, *2*, 567–577.

(20) Love, J. C.; Estroff, L. A.; Kriebel, J. K.; Nuzzo, R. G.; Whitesides, G. M. *Self-Assembled Monolayers of Thiolates on Metals as a Form of Nanotechnology*; 2005; Vol. 105.

(21) Delamarche, E.; Michel, B. Structure and Stability of Self-Assembled Monolayers. *Thin Solid Films* **1996**, *273*, 54–60.

(22) Decher, G. Fuzzy Nanoassemblies: Toward Layered Polymeric Multicomposites. *Science* **1997**, *277*, 1232–1237.

(23) Shepard, K. B.; Priestley, R. D. MAPLE Deposition of Macromolecules. *Macromol. Chem. Phys.* **2013**, *214*, 862–872.

(24) Zasadzinski, J. A.; Viswanathan, R.; Madsen, L.; Garnaes, J.; Schwartz, D. K. Langmuir-Blodgett Films. *Science* **1994**, *263*, 1726–1733.

(25) Shim, B. S.; Podsiadlo, P.; Lilly, D. G.; Agarwal, a; Leet, J.; Tang, Z.; Ho, S.; Ingle, P.; Paterson, D.; Lu, W.; et al. Nanostructured Thin Films Made by Diewetting Method of Layer-by-Layer Assembly. *Nano Lett.* **2007**, *7*, 3266–3273.

(26) Ryu, D. Y.; Shin, K.; Drockenmuller, E.; Hawker, C. J.; Russel, T. P. A Generalized Approach to the Modifiction of Solid Surfaces. *Science* **2004**, *308*, 236–238.

(27) Kessler, D.; Metz, N.; Theato, P. Substrate-Independent Stable and Adherent Reactive Surface Coatings and Their Conversion with Amines. *Macromol. Symp.* **2007**, *254*, 34–41.

(28) Jiang, X.; Chen, H. Y.; Galvan, G.; Yoshida, M.; Lahann, J. Vapor-Based Initiator Coatings for Atom Transfer Radical Polymerization. *Adv. Funct. Mater.* **2008**, *18*, 27–35.

(29) Chen, H. Y.; Hirtz, M.; Deng, X.; Laue, T.; Fuchs, H.; Lahann, J. Substrate-Independent Dip-Pen Nanolithography Based on Reactive Coatings. *J. Am. Chem. Soc.* **2010**, *132*, 18023–18025.

(30) Chrisey, D. B.; Piqué, A.; McGill, R. A.; Horwitz, J. S.; Ringeisen, B. R.; Bubb, D. M.; Wu, P. K. Laser Deposition of Polymer and Biomaterial Films. *Chem. Rev.* **2003**, *103*, 553–576.

(31) Kinloch, A. J. The Science of Adhesion - Part 1 Surface and Interfacial Aspects. *J. Mater. Sci.* **1980**, *15*, 2141–2166.

(32) Waite, J. H. Nature's Underwater Adhesive Specialist. *Int. J. Adhes. Adhes.* **1987**, *7*, 9–14.

(33) Waite, J. H.; Qin, X. Polyphosphoprotein from the Adhesive Pads of Mytilus Edulis. *Biochemistry* **2001**, *40*, 2887–2893.

(34) Yu, M.; Deming, T. Synthetic Polypeptide Mimics of Marine Adhesives. *Macromolecules* **1998**, *31*, 4739–4745.

(35) Yamada, K.; Chen, T.; Kumar, G.; Vesnovsky, O.; Topoleski, L. D.; Payne, G. F. Chitosan Based Water-Resistant Adhesive. Analogy to Mussel Glue. *Biomacromolecules* **2000**, *1*, 252–258.

(36) Dalsin, J. L.; Hu, B. H.; Lee, B. P.; Messersmith, P. B. Mussel Adhesive Protein Mimetic Polymers for the Preparation of Nonfouling Surfaces. *J. Am. Chem. Soc.* **2003**, *125*, 4253–4258.

(37) Statz, A. R.; Meagher, R. J.; Barron, A. E.; Messersmith, P. B. New Peptidomimetic Polymers for Antifouling Surfaces. *J. Am. Chem. Soc.* **2005**, *127*, 7972–7973.

(38) Lee, H.; Scherer, N. F.; Messersmith, P. B. Single-Molecule Mechanics of Mussel Adhesion. *Proc. Natl. Acad. Sci.* **2006**, *103*, 12999–13003.

(39) Grandbois, M.; Beyer, M.; Rief, M.; Clausen-Schaumann, H.; Gaub, H. E. How Strong Is a Covalent Bond? *Science* **1999**, *283*, 1727–1730.

(40) Lee, B. P.; Chao, C.; Nunalee, F. N.; Motan, E.; Shull, K. R.; Messersmith, P. B.; Lee, B. P.; Chao, C.; Nunalee, F. N.; Motan, E.; et al. Rapid Gel Formation and Adhesion in Photocurable and Biodegradable Block Copolymers with High DOPA Content Rapid Gel Formation and Adhesion in Photocurable and Biodegradable Block Copolymers with High DOPA Content. *Macromolecules* **2006**, *39*, 1740–1748.

(41) Rodruiguez, R.; Blesa, M. A.; Regazzoni, A. E. Surface Complexation at the TiO 2 (Anatase)/ Aqueous Solution Interface : Chemisorption of Catechol. *J. Colloid Interface Sci.* **1996**, *177*, 122–131.

(42) Yu, J.; Wei, W.; Menyo, M. S.; Masic, A.; Waite, J. H.; Israelachvili, J. N. Adhesion of Mussel Foot Protein-3 to TiO2 Surfaces: The Effect of pH. *Biomacromolecules* **2013**, *14*, 1072–1077.

(43) Syres, K.; Thomas, A.; Bondino, F.; Malvestuto, M.; Grätzel, M. Dopamine Adsorption on Anatase TiO2(101): A Photoemission and NEXAFS Spectroscopy Study. *Langmuir* **2010**, *26*, 14548–14555.

(44) Martin, S. T.; Kesselman, J. M.; Park, D. S.; Lewis, N. S.; Hoffmann, M. R. Surface Structures of 4-Chlorocatechol Adsorbed on Titanium Dioxide. *Environ. Sci. Technol.* **1996**, *30*, 2535–2542.

(45) Gulley-Stahl, H.; Hogan, P. A.; Schmidt, W. L.; Wall, S. J.; Buhrlage, A.; Bullen, H. A. Surface Complexation of Catechol to Metal Oxides: An ATR-FTIR, Adsorption, and Dissolution Study. *Environ. Sci. Technol.* **2010**, *44*, 4116–4121.

(46) Mcbrlde, M. B.; Wessellnk, L. G. Chemisorpton of Catechol on Gibbsite, Boehmite, and Noncrystalline Alumina Surfaces. *Environ. Sci. Technol.* **1988**, *22*, 703–708.

(47) Qin, Z.; Buehler, M. Molecular Mechanics of Dihydroxyphenylalanine at a Silica Interface. *Appl.*

Phys. Lett. **2012**, *101*, 1–5.

(48) Mian, S. A.; Yang, L. M.; Saha, L. C.; Ahmed, E.; Ajmal, M.; Ganz, E. A Fundamental Understanding of Catechol and Water Adsorption on a Hydrophilic Silica Surface: Exploring the Underwater Adhesion Mechanism of Mussels on an Atomic Scale. *Langmuir* **2014**, *30*, 6906–6914.

(49) Anderson, T. H.; Yu, J.; Estrada, A.; Hammer, M. U.; Waite, J. H.; Israelachvili, J. N. The Contribution of DOPA to Substrate-Peptide Adhesion and Internal Cohesion of Mussel-Inspired Synthetic Peptide Films. *Adv. Funct. Mater.* **2010**, *20*, 4196–4205.

(50) Maier, G. P.; Rapp, M. V.; Waite, J. H.; Israelachvili, J. N.; Butler, A. Adaptive Synergy between Catechol and Lysine Promotes Wet Adhesion by Surface Salt Displacement. *Science* **2015**, *349*, 628–632.

(51) Rapp, M. V.; Maier, G. P.; Dobbs, H. A.; Higdon, N. J.; Waite, J. H.; Butler, A.; Israelachvili, J. N. Defining the Catechol–Cation Synergy for Enhanced Wet Adhesion to Mineral Surfaces. *J. Am. Chem. Soc.* **2016**

(52) Lim, C.; Huang, J.; Kim, S.; Lee, H.; Zeng, H.; Hwang, D. S. Nanomechanics of Poly(catecholamine) Coatings in Aqueous Solutions. *Angew. Chemie - Int. Ed.* **2016**, *55*, 3342–3346.

(53) Yu, J.; Kan, Y.; Rapp, M.; Danner, E.; Wei, W.; Das, S.; Miller, D. R.; Chen, Y.; Waite, J. H.; Israelachvili, J. N. Adaptive Hydrophobic and Hydrophilic Interactions of Mussel Foot Proteins with Organic Thin Films. *Proc. Natl. Acad. Sci. U. S. A.* **2013**, *110*, 15680–15685.

(54) Levine, Z. A.; Rapp, M. V; Wei, W.; Mullen, R. G.; Wu, C.; Zerze, G. H.; Mittal, J.; Waite, J. H.; Israelachvili, J. N.; Shea, J.-E. Surface Force Measurements and Simulations of Mussel-Derived Peptide Adhesives on Wet Organic Surfaces. *Proc. Natl. Acad. Sci. U. S. A.* **2016**, *113*, 4332–4337.

(55) Lu, Q. Y.; Danner, E.; Waite, J. H.; Israelachvili, J. N.; Zeng, H. B.; Hwang, D. S. Adhesion of Mussel Foot Proteins to Different Substrate Surfaces. *J. R. Soc. Interface* **2013**, *10*, 11.

(56) Li, Y.; Qin, M.; Li, Y.; Cao, Y.; Wang, W. Single Molecule Evidence for the Adaptive Binding of DOPA to Different Wet Surfaces. *Langmuir* **2014**, *30*, 4358–4366.

(57) Zucca, F. A.; Segura-Aguilar, J.; Ferrari, E.; Muñoz, P.; Paris, I.; Sulzer, D.; Sarna, T.; Casella, L.; Zecca, L. Interactions of Iron, Dopamine and Neuromelanin Pathways in Brain Aging and Parkinson's Disease. *Prog. Neurobiol.* **2015**.

(58) Ito, S. A Chemist's View of Melanogenesis. *Pigment Cells Res* **2003**, *16*, 230–236.

(59) García-Borrón, J. C.; Olivares Sánchez, M. C. Biosynthesis of Melanins. In *Melanins and Melanosomes: Biosynthesis, Biogenesis, Physiological, and Pathological Functions*; 2011; pp. 87–116.

(60) Raper, H. S. The Tyrosinase-Tyrosine Reaction. VI. Production from Tyrosine of 5:6-Dihydroxyindole and 5:6-Dihydroxyindole-2-Carboxylic Acid - The Precursors of Melanin. *Biochem J.* **1926**, *21*, 89–96.

(61) Pezzella, A.; Crescenzi, O.; Panzella, L.; Napolitano, A.; Land, E. J.; Barone, V.; D'Ischia, M. Free Radical Coupling of O-Semiquinones Uncovered. *J. Am. Chem. Soc.* **2013**, *135*, 12142–

12149.

(62) Burzio, L. A.; Waite, J. H. Cross-Linking in Adhesive Quinoproteins: Studies with Model Decapeptides. *Biochemistry* **2000**, *39*, 11147–11153.

(63) Mason, H. S. The Chemistry of Melanin; Mechanism of the Oxidation of Dihydroxyphenylalanine by Tyrosinase. *J. Biol. Chem.* **1948**, *172*, 83–99.

(64) Munoz-Munoz, J. L.; García-Molina, F.; Varón, R.; Tudela, J.; García-Cánovas, F.; Rodríguez-López, J. N. Generation of Hydrogen Peroxide in the Melanin Biosynthesis Pathway. *Biochim. Biophys. Acta* **2009**, *1794*, 1017–1029.

(65) Pezzella, A.; Napolitano, A.; D'Ischia, M.; Prota, G.; Seraglia, R.; Traldi, P. Identification of Partially Degraded Oligomers of 5,6-Dihydroxyindole-2-Carboxylic Acid in Sepia Melanin by Matrix-Assisted Laser Desorption/ionization Mass Spectrometry. *Rapid Commun. Mass Spectrom.* **1997**, *11*, 368–372.

(66) Della Vecchia, N. F.; Avolio, R.; Alfè, M.; Errico, M. E.; Napolitano, A.; d'Ischia, M. Building-Block Diversity in Polydopamine Underpins a Multifunctional Eumelanin-Type Platform Tunable Through a Quinone Control Point. *Adv. Funct. Mater.* **2013**, *23*, 1331–1340.

(67) D'Ischia, M.; Napolitano, A.; Pezzella, A.; Meredith, P.; Sarna, T. Chemical and Structural Diversity in Eumelanins: Unexplored Bio-Optoelectronic Materials. *Angew. Chemie - Int. Ed.* **2009**, *48*, 3914–3921.

(68) Liebscher, J.; Mrówczyński, R.; Scheidt, H. a; Filip, C.; Hădade, N. D.; Turcu, R.; Bende, A.; Beck, S. Structure of Polydopamine: A Never-Ending Story? *Langmuir* **2013**, *29*, 10539–10548.

(69) Hong, S.; Na, Y. S.; Choi, S.; Song, I. T.; Kim, W. Y.; Lee, H. Non-Covalent Self-Assembly and Covalent Polymerization Co-Contribute to Polydopamine Formation. *Adv. Funct. Mater.* **2012**, *22*, 4711–4717.

(70) d'Ischia, M.; Napolitano, A.; Ball, V.; Chen, C.; Buehler, M. J. Polydopamine and Eumelanin: From Structure − Property Relationships to a Unified Tailoring Strategy. *Acc. Chem. Res.* **2014**.

(71) Herlinger, Erwin; Jameson, Reginald F.; Linert, W. Spontaneous Autoxidation of Dopamine. *J. Chem. Soc., Perkin Trans. 2* **1995**, 259–263.

(72) Bernsmann, F.; Ball, V.; Ponche, A.; Michel, M.; Gracio, D. A.; Ruch, D. Dopamine - Melanin Film Deposition Depends on the Used Oxidant and Buffer Solution. *Langmuir* **2011**, *27*, 2819–2825.

(73) Wei, Q.; Zhang, F.; Li, J.; Li, B.; Zhao, C. Oxidant-Induced Dopamine Polymerization for Multifunctional Coatings. *Polym. Chem.* **2010**, *1*, 1430.

(74) Ponzio, F.; Barthes, J.; Bour, J.; Michel, M.; Bertani, P.; Hemmerlé, J.; D'Ischia, M.; Ball, V. Oxidant Control of Polydopamine Surface Chemistry in Acids: A Mechanism-Based Entry to Superhydrophilic-Superoleophobic Coatings. *Chem. Mater.* **2016**, *28*, 4697–4705.

(75) Gracio, J. D. A.; Singh, Â. M. K.; Ruch, D.; Buehler, M. J.; Al, C. E. T.; Ball, V. Self-Assembly of Tetramers of 5,6-Dihydroxyindole Explains the Primary Physical Properties of Eumelanin: Experiment, Simulation, and Design. *ACS Nano* **2013**, 1524–1532.

(76) Palumbo, A.; Cosmo, A. D. I.; Gesualdo, I.; Hearing, V. J. Subcellular Localization and Function

of Melanogenic Enzymes in the Ink Gland of Sepia Officinalis. *Biochem. J.* **1997**, *323*, 749–756.

(77) Palumbo, A. Melanogenesis in the Ink Gland of Sepia Officinalis. *Pigment Cell Res.* **2003**, *16*, 517–522.

(78) Raposo, G.; Marks, M. S. Melanosomes--Dark Organelles Enlighten Endosomal Membrane Transport. *Nat. Rev. Mol. Cell Biol.* **2007**, *8*, 786–797.

(79) Liebscher, J.; Mrówczyński, R.; Scheidt, H. a; Filip, C.; Hădade, N. D.; Turcu, R.; Bende, A.; Beck, S. Structure of Polydopamine: A Never Ending Story? *Langmuir* **2013**, *29*, 10539–10548.

(80) Cheng, Jin; Moss, Simon C.; Eisner, Melvin; Zschack, P. X-Ray Characterization of Melanins - I. *Pigment Cell Res.* **1994**, *7*, 255–262.

(81) Cheng, J.; Moss, S. C.; Eisner, M. X-Ray Characterization of Melanins - II. *Pigment Cell Res.* **1994**, *7*, 263–273.

(82) Zajac, G. W.; Gallas, J. M.; Cheng, J.; Eisner, M.; Moss, S. C.; Alvarado-Swaisgood, A. E. The Fundamental Unit of Synthetic Melanin: A Verification by Tunneling Microscopy of X-Ray Scattering Results. *Biochim. Biophys. Acta* **1994**, *1199*, 271–278.

(83) Littrell, K. C.; Gallas, J. M.; Zajac, G. W.; Thiyagarajan, P. Structural Studies of Bleached Melanin by Synchrotron Small-Angle X-Ray Scattering. *Photochem. Photobiol.* **2003**, *77*, 115–120.

(84) Watt, A. a. R.; Bothma, J. P.; Meredith, P. The Supramolecular Structure of Melanin. *Soft Matter* **2009**, *5*, 3754.

(85) Della Vecchia, Nicola Fyodor; Luchini, Alessandra; Napolitano, Alessandra; D'Errico, Gerardino; Vitiello, Giuseppe; Szekely, Noemi; d'Ischia, Marco; Paduano, L. Tris Buffer Modulates Polydopamine Growth, Aggregation, and Paramagnetic Properties. *Langmuir* **2014**, *30*, 9811–9818.

(86) Szpoganicz, B.; Gidanian, S.; Kong, P.; Farmer, P. Metal Binding by Melanins: Studies of Colloidal Dihydroxyindole-Melanin, and Its Complexation by Cu(II) and Zn(II) Ions. *J. Inorg. Biochem.* **2002**, *89*, 45–53.

(87) Ishimitsu, T.; Hirose, S.; Sakurai, H. Microscopic Acid Dissociation Constants of 3,4-Dihydroxyphenethylamine (Dopamine). *Chem. Pharm. Bull.* **1978**, *26*, 74–78.

(88) Charkoudian, L. K.; Franz, K. J. Fe (III) -Coordination Properties of Neuromelanin Components : 5,6-Dihydroxyindole and 5,6-Dihydroxyindole-2-Carboxylic Acid. *Inorg. Chem.* **2006**, *45*, 3657–3664.

(89) Rao, P. S.; Hayon, E. Ionization Constants and Spectral Characteristics of Some Semiquinone Radicals in Aqueous Solution. *J. Phys. Chem.* **1973**, *77*, 2274–2276.

(90) Steenken, S.; Peter, O. Demethoxylation of Methoxylated Phenols and Hydroxybenzoic Acids. *J. Phys. Chem.* **1977**, *81*, 505–508.

(91) AI-Kazwini, A. T.; et al. One-Electron Oxidation of Methoxylated and Hydroxylated Indoles by N3'. 1. Characterization of the Primary Indolic Radicals. *J Phys Chem-US* **1990**, *94*, 6666–6670.

(92) Zhang, F.; Dryhurst, G. Oxidation Chemistry of Dopamine: Possible Insights into the Age-

Dependent Loss of Dopaminergic Nigrostriatal Neurons. *Bioorg. Chem.* **1993**, *21*, 392–410.

(93) Mrówczyński, R.; Coy, L. E.; Scheibe, B.; Czechowski, T.; Augustyniak-Jabłokow, M.; Jurga, S.; Tadyszak, K. Electron Paramagnetic Resonance Imaging and Spectroscopy of Polydopamine Radicals. *J. Phys. Chem. B* **2015**, *119*, 10341–10347.

(94) Mostert, a. B.; Powell, B. J.; Pratt, F. L.; Hanson, G. R.; Sarna, T.; Gentle, I. R.; Meredith, P. Role of Semiconductivity and Ion Transport in the Electrical Conduction of Melanin. *Proc. Natl. Acad. Sci.* **2012**, *109*, 8943–8947.

(95) Felix, C. C.; Hyde, J. S.; Sarna, T.; Sealy, R. C. Interactions of Melanin with Metal Ions. Electron Spin Resonance Evidence for Chelate Complexes of Metal Ions with Free Radicals. *J. Am. Chem. Soc.* **1978**, *100*, 3922–3926.

(96) Chio, S. S.; Hyde, J. S.; Sealy, R. C. Paramagnetism in Melanins: pH Dependence. *Arch. Biochem. Biophys.* **1982**, *215*, 100–106.

(97) Cope, F. W.; Sever, R. J.; Polis, B. D. Reversible Free Radical Generation in the Melanin Granules of the Eye by Visible Light. *Arch. Biochem. Biophys.* **1963**, *100*, 171–177.

(98) Stratton, K.; Pathak, M. A. Photoenhancement Resonance Signal of the Electron from Melanins. *Arch. Biochem. Biophys.* **1968**, *123*, 477–483.

(99) Mostert, a. B.; Hanson, G. R.; Sarna, T.; Gentle, I. R.; Powell, B. J.; Meredith, P. Hydration-Controlled X-Band EPR Spectroscopy: A Tool for Unravelling the Complexities of the Solid-State Free Radical in Eumelanin. *J. Phys. Chem. B* **2013**, *117*, 4965–4972.

(100) Bernardus Mostert, a.; Powell, B. J.; Gentle, I. R.; Meredith, P. On the Origin of Electrical Conductivity in the Bio-Electronic Material Melanin. *Appl. Phys. Lett.* **2012**, *100*, 24–27.

(101) Wünsche, J.; Deng, Y.; Kumar, P.; Di Mauro, E.; Josberger, E.; Sayago, J.; Pezzella, A.; Soavi, F.; Cicoira, F.; Rolandi, M.; et al. Protonic and Electronic Transport in Hydrated Thin Films of the Pigment Eumelanin. *Chem. Mater.* **2015**, *27*, 436–442.

(102) Bernardus Mostert, a.; Davy, K. J. P.; Ruggles, J. L.; Powell, B. J.; Gentle, I. R.; Meredith, P. Gaseous Adsorption in Melanins: Hydrophilic Biomacromolecules with High Electrical Conductivities. *Langmuir* **2010**, *26*, 412–416.

(103) Ponzio, F.; Ball, V. Persistence of Dopamine and Small Oxidation Products Thereof in Oxygenated Dopamine Solutions and in “polydopamine” Films. *Colloids Surfaces A Physicochem. Eng. Asp.* **2014**, *443*, 540–543.

(104) Yang, J.; Niu, L.; Zhang, Z.; Zhao, J.; Chou, L. Electrochemical Behavior of a Polydopamine Nanofilm. *Anal. Lett.* **2015**, *48*, 2031–2039.

(105) Zecca, L.; Bellei, C.; Costi, P.; Albertini, A.; Monzani, E.; Casella, L.; Gallorini, M.; Bergamaschi, L.; Moscatelli, A.; Turro, N. J.; et al. New Melanic Pigments in the Human Brain That Accumulate in Aging and Block Environmental Toxic Metals. *Proc. Natl. Acad. Sci. U. S. A.* **2008**, *105*, 17567–17572.

(106) Zecca, L.; Tampellini, D.; Gerlach, M.; Riederer, P.; Fariello, R. G.; Sulzer, D. Substantia Nigra Neuromelanin: Structure, Synthesis, and Molecular Behaviour. *Mol. Pathol.* **2001**, *54*, 414–418.

(107) Bridelli, M. G.; Tampellini, D.; Zecca, L. The Structure of Neuromelanin and Its Iron Binding Site

Studied by Infrared Spectroscopy. *FEBS Lett.* **1999**, *457*, 18–22.

(108) Gadd, G.; Rome, L. Biosorption of Copper by Fungal Melanin. *Appl. Microbiol. Biotechnol.* **1988**, *29*, 610–617.

(109) Rizzo, D. M.; Blanchette, R. A.; Palmer, M. A. Biosorption of Metal Ions by Armillaria Rhizomorphs. *Can. J. Bot.* **1992**, *70*, 1515–1520.

(110) Baldrian, P. Interactions of Heavy Metals with White-Rot Fungi. *Enzyme Microb. Technol.* **2003**, *32*, 78–91.

(111) Potts, A. M.; Au, P. C. The Affinity of Melanin for Inorganic Ions. *Exp. Eye. Res.* **1976**, *22*, 487–491.

(112) Liu, Y.; Hong, L.; Kempf, V. R.; Wakamatsu, K.; Ito, S.; Simon, J. D. Ion-Exchange and Adsorption of Fe(III) by Sepia Melanin. *Pigment Cell Res.* **2004**, *17*, 262–269.

(113) Holten-Andersen, N.; Harrington, M. J.; Birkedal, H.; Lee, B. P.; Messersmith, P. B.; Lee, K. Y. C.; Waite, J. H. pH-Induced Metal-Ligand Cross-Links Inspired by Mussel Yield Self-Healing Polymer Networks with near-Covalent Elastic Moduli. *Proc. Natl. Acad. Sci. U. S. A.* **2011**, *108*, 2651–2655.

(114) Sedõ, J.; Saiz-Poseu, J.; Busqué, F.; Ruiz-Molina, D. Catechol-Based Biomimetic Functional Materials. *Adv. Mater.* **2013**, *25*, 653–701.

(115) Poh, C. K.; Shi, Z.; Lim, T. Y.; Neoh, K. G.; Wang, W. The Effect of VEGF Functionalization of Titanium on Endothelial Cells in Vitro. *Biomaterials* **2010**, *31*, 1578–1585.

(116) Kang, K.; Choi, I. S.; Nam, Y. A Biofunctionalization Scheme for Neural Interfaces Using Polydopamine Polymer. *Biomaterials* **2011**, *32*, 6374–6380.

(117) Ku, S. H.; Ryu, J.; Hong, S. K.; Lee, H.; Park, C. B. General Functionalization Route for Cell Adhesion on Non-Wetting Surfaces. *Biomaterials* **2010**, *31*, 2535–2541.

(118) Han, G.; Zhang, S.; Li, X.; Widjojo, N.; Chung, T.-S. Thin Film Composite Forward Osmosis Membranes Based on Polydopamine Modified Polysulfone Substrates with Enhancements in Both Water Flux and Salt Rejection. *Chem. Eng. Sci.* **2012**, *80*, 219–231.

(119) Kim, B. H.; Lee, D. H.; Kim, J. Y.; Shin, D. O.; Jeong, H. Y.; Hong, S.; Yun, J. M.; Koo, C. M.; Lee, H.; Kim, S. O. Mussel-Inspired Block Copolymer Lithography for Low Surface Energy Materials of Teflon, Graphene, and Gold. *Adv. Mater.* **2011**, *23*, 5618–5622.

(120) Hider, R. C.; Kong, X. Chemistry and Biology of Siderophores. *Nat. Prod. Rep.* **2010**, *27*, 637.

(121) Harrington, M. J.; Masic, A.; Holten-andersen, N.; Waite, J. H.; Fratzl, P. Iron-Clad Fibers : A Metal-Based Biological Strategy for Hard Flexible Coatings. *Science* **2010**, 216–220.

(122) Hong, L.; Simon, J. D. Current Understanding of the Binding Sites, Capacity, Affinity, and Biological Significance of Metals in Melanin. *J. Phys. Chem. B* **2007**, *111*, 7938–7947.

(123) Kim, E.; Liu, Y.; Leverage, W. T.; Yin, J.-J.; White, I. M.; Bentley, W. E.; Payne, G. F. Context-Dependent Redox Properties of Natural Phenolic Materials. *Biomacromolecules* **2014**, *15*, 1653–1662.

Chapter 2

Mechanisms of Polydopamine Film Formation

2.1 Abstract

Polydopamine (PDA) can be deposited on virtually any substrate from solution through oxidation of dopamine. The versatility of this process has enabled surface mediated assembly of PDA for a wide variety of functional thin film coatings. Chapter 2 discusses the impact of well-defined surface chemistries on the nucleation and growth of such films.

PDA was deposited on silicon dioxide (SiO_2) and SiO_2 substrates modified with self-assembled monolayers (SAM) bearing octadecyl (C18), phenethyl, and aminopropyl functional groups. Atomic force microscopy (AFM) revealed three-dimensional islands whose areal density and surface coverage is lowest on bare SiO_2 substrates, and highest on the aromatic and aliphatic substrates. Increasing the pH of the solution from 8.2 –10 ionizes catechol moieties in PDA and inhibits adsorption on negatively charged SiO_2 substrates. The growth rate of PDA films on SAM-modified SiO_2 is maximized at pH = 9.5 and almost completely abolished at pH = 10 due to increased PDA solubility.

The initial rates of PDA adsorption were measured using quartz crystal microbalance with dissipation (QCM-D) measurements. The initial adsorption rate is proportional to the nucleation density, which increases as the hydrophobicity of the substrate increases. Taken together, these data provide insight into the rates of heterogeneous nucleation and growth of PDA on substrates with well-defined chemistries.

2.2 Introduction

Several studies have been done investigating PDA film formation on silicon dioxide. The thickness of PDA films formed on SiO_2 substrates plateaus when using oxygenated tris(hydroxymethyl)aminomethane (Tris) buffer, but grows continuously when formed using phosphate buffer or Cu^{+2} as an oxidant.[1,2] The inhibited growth in Tris buffer may be attributed to the incorporation of Tris into PDA.[3] Increasing the pH or dopamine concentration increases the rate of film deposition and maximum thickness, which in turn is correlated with greater RMS roughness.[4] The dopamine reaction rate also greatly increases with increasing P_{O2} of the solution, along with a significant decrease in roughness compared to stirring with ambient oxygenation.[5] Additionally, the deposition kinetics can be fit with an exponential decay function.[4] The decay in deposition rate over time is likely due to aggregation of oligomers in solution and a concomitant decrease in depositing monomers over time.

Nanometer scale granule structures have been observed to form rapidly on the surface during deposition from solution (Figure 2.1).[6] Reaction times >10 min are required to form coherent films in stirred 1 mg/ml dopamine solutions at pH = 8.5, and reaction times >60 min are required for pinhole-free films.[7]

However, in contrast to reaction conditions, the impact of substrate composition on PDA film formation has not been examined explicitly. PDA deposition on polyvinylidene fluoride (PVDF) substrates produces films with greater thicknesses compared to SiO_2 substrates (Figure 2.2).[8] Oxidative degradation of PDA by sodium hypochlorite is more rapid on indium tin oxide (ITO) than glassy carbon, which may be due to a higher porosity and lower adhesion of the film on ITO than carbon.[9]

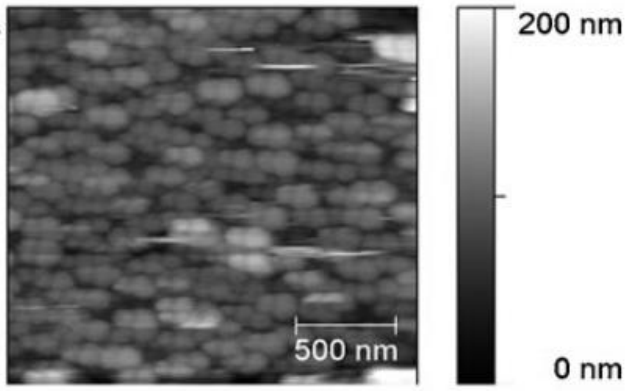

Figure 2.1: Morphology of PDA film deposited from 2 mg/ml dopamine solution in 50 mM Tris buffer. There appears to be contamination on the AFM tip resulting in doubling of features. Reproduced from [6].

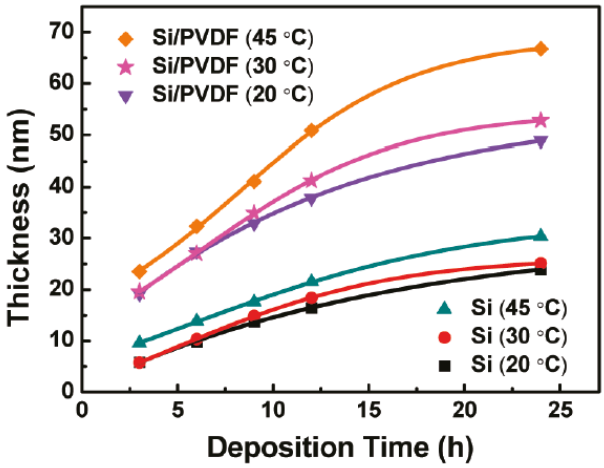

Figure 2.2: PDA film thickness vs. deposition time on polyvinylidene fluorid (PVDF) and SiO_2. The film thickness is greater on the hydrophobic PVDF. Reproduced from [8].

None of the existing studies on PDA film formation have clearly resolved the relationships between film morphology, deposition mechanisms, and substrate chemistry. Better data and experimental design is required in order to optimally engineer PDA film devices. In order to accomplish this, PDA films were deposited from solution on different surfaces with controlled chemistries. The surfaces studied were bare silicon dioxide and self-assembled monolayers with amino, phenyl, or aliphatic functional groups. Atomic force microscopy

(AFM) and quartz crystal microbalance (QCM) measurements revealed the 3-D island growth mechanisms and their dependency on surface chemistry, pH, and deposition rate.

2.3 Methods

2.3.1 Materials

Dopamine hydrochloride (98%), sodium bicarbonate (99%), and anhydrous trichloroethylene (99%) were purchased from Sigma-Aldrich (St. Louis, MO USA) and used as received. Sodium carbonate (99%) was purchased from Fisher Scientific and used as received. Water was purified (Type 3) using Direct-Q 3 UV-R system. The following reagents for surface modification were used as received (Gelest, Morrisville, PA USA): 3-aminopropyltrimethoxysilane, phenethyltrichlorosilane, and octadecyltrichlorosilane. Silicon wafers with 1 μm thermal oxide were used for PDA deposition and were purchased from Silicon Quest International (San Jose, CA USA; 4" diameter, phosphorus doped). QCM-D sensors (Q-Sense, QSX 303; Linthicum Heights, MD USA) are finished with SiO_2 layers and exhibit a fundamental frequency of 5 MHz.

2.3.2 Preparation of Self-Assembled Monolayers

Silicon substrates (0.8 x 2.8 cm^2) and QCM-D sensors were cleaned by sonication in acetone, followed by isopropyl alcohol (IPA) and then rinsed with de-ionized H_2O. Substrates were then cleaned by UV-ozone. (30 mW/cm^2, 5 min; Jelight, Irvine, CA). Coating solutions were prepared by combining 12 μL of either 3-aminopropyltrimethoxysilane, octadecyltrichlorosilane, or phenethyltrichlorosilane with 10 ml trichloroethylene. Substrates were incubated in the SAM precursor solution for 16 hr followed by sonication in acetone, IPA, then water and finally rinsed with methanol and dried with N_2 stream. Surface modification via self-assembled monolayers (SAM) was verified by water-in-air contact angles using the sessile

drop method (Figure 2.3). Measurements were repeated in triplicate at different locations on the surface.

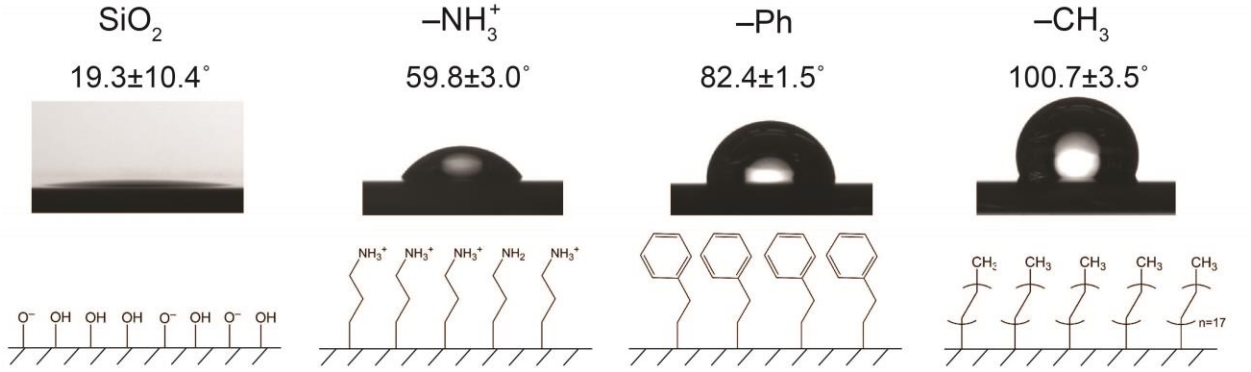

Figure 2.3: Average contact angles and example drops for the different substrate chemistries. Contact angles are the average of 45 measurements on each surface across 15 samples each.

2.3.3 Polydopamine Film Deposition

Polydopamine films were prepared on the SiO_2 and SAM surfaces by dissolving 2 mg/ml dopamine hydrochloride in 12 ml of 50 mM carbonate/bicarbonate buffer contained in a sealed 20 ml vial. PDA deposition proceeded for 24 hr after which samples were rinsed with H_2O and dried under an N_2 stream. The pH values of sample solutions were measured using an Ag/AgCl electrode (Hach, model 5014T; Loveland, CO USA).

2.3.4 Quartz-Crystal Microbalance with Dissipation Measurements (QCM-D)

The carbonate buffer for QCM-D (Q-Sense E4 system, QSoft401software) measurements was 40 ml at 50 mM, prepared at pH = 9.09. The QCM-D flow cell and tubing were cleaned prior to each experiment using 2% w/w sodium dodecyl sulfate and extensive de-ionized water rinsing. Functionalized QCM-D sensors were installed, the cell filled with carbonate buffer, and the temperature equilibrated at 25°C. Another buffer of the same volume, concentration and pH was prepared, and upon addition of 2 mg/ml dopamine, the pH drops to pH 8.5. Immediately after dissolving the dopamine, this solution was flowed through the system at 50 μL/min for

approximately four hours, and the frequency and dissipation shifts monitored. The sensors were then rinsed with H_2O and dried under an N_2 stream. New sensors were used for each measurement.

2.3.5 Morphological Characterization of PDA Films

Film thicknesses and areal island densities were measured using atomic force microscopy (NT-MDT NTegra AFM; Tempe, AZ) in tapping mode. Island areal density scans were 0.83x0.83 μm^2 at 2 Hz using tips of reported radius <1 nm (Budget Sensors; k = 5 N/m). Island densities were quantified by calculating the number of maxima using NIH ImageJ software. The "Find Maxima" function was used, which works by using a noise tolerance value to analyze how many contiguous pixels should be considered one maximum. Figure 2.4 shows the process for finding maxima and choosing the tolerance value.

Thickness scans on SAM substrates were 10x10 μm^2 at 0.8 Hz using tips of reported radius <10 nm (k = 40 N/m; Budget Sensors, Sofia, Bulgaria). The PDA film was scratched away using a disposable syringe needle, and the AFM scan was performed at the edge of the scratch (Figure 2.5). Three scratches and measurements were performed on each individual SAM sample, for a total of 9 measurements for each data point in Figure 2.9. The thickness of the SiO_2 films in chapter 3 were determined from the island density AFM scans. This is because the coverage was incomplete, and it was possible to measure the island heights directly against the background. Using ImageJ, a threshold pixel value was manually selected that just barely covered the islands, as shown in Figure 2.6. This separates the background pixels from the island pixels. Taking the difference in the averages of each of these two pixel distributions gives the thickness once the pixel value is converted to height value.

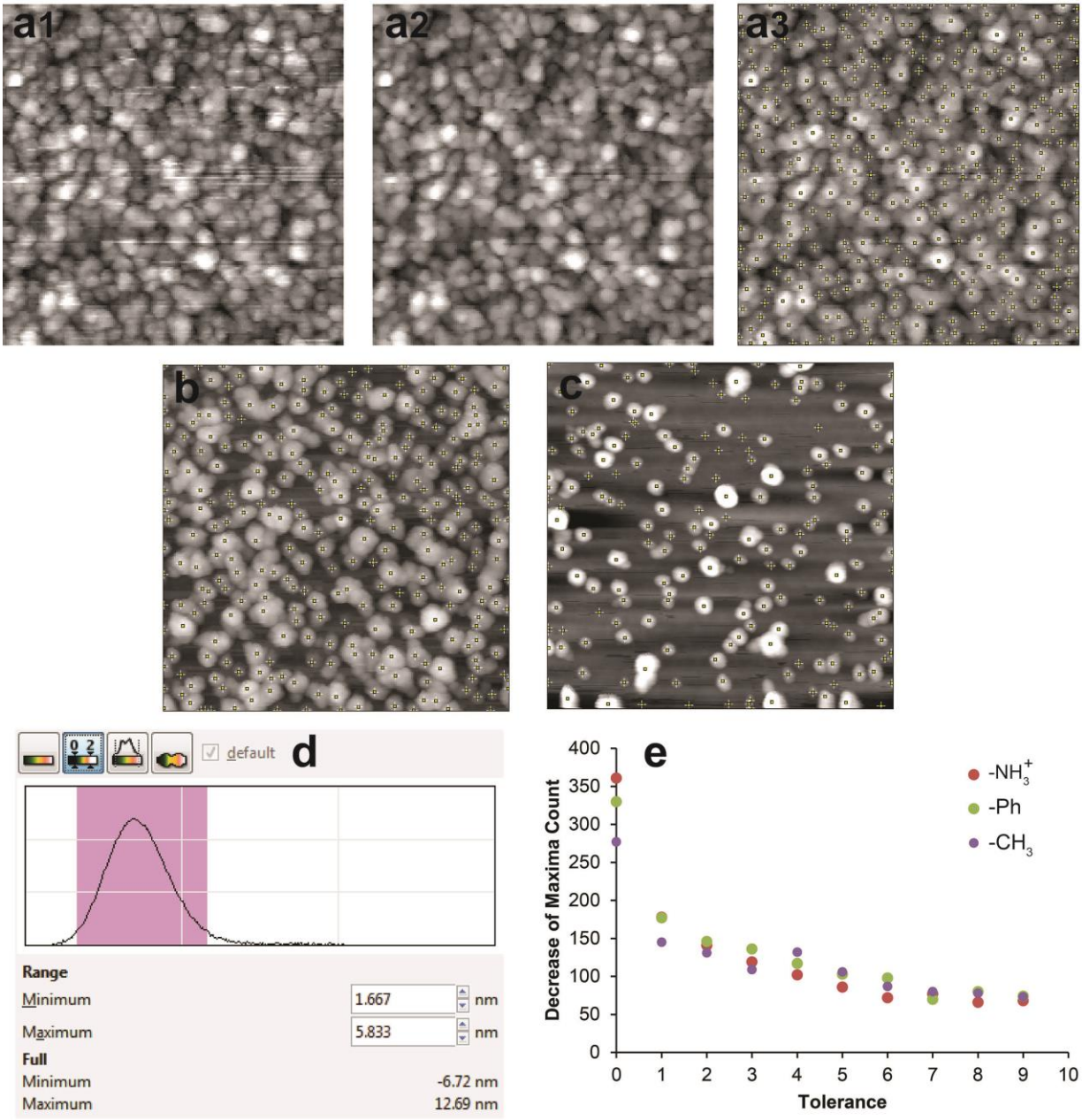

Figure 2.4: Method for determining the island areal density. a1) Original uncorrected scan. a2) Corrected scan using the "Remove outlier" function in ImageJ with radius and tolerance set at 1. a3) Maxima output at a tolerance of 1, which was used for surfaces with full coverage. b) Output at tolerance of 6 for SiO_2 samples prepared at pH < 9.5. c) Output at tolerance of 9 for SiO_2 at pH = 9.5. d) Example of typical contrast range in the pixel value distribution for the AFM scans. e) Decrease in maxima count as the tolerance value is increased to the next higher value. Results from one representative scan is shown for each substrate. There is a large drop in maxima count as the tolerance value is increased from 0 to 1 (shown as the data points at 0 in the plot). Therefore a tolerance of 1 was chosen to balance noise reduction and retention of real islands in the areal density calculations.

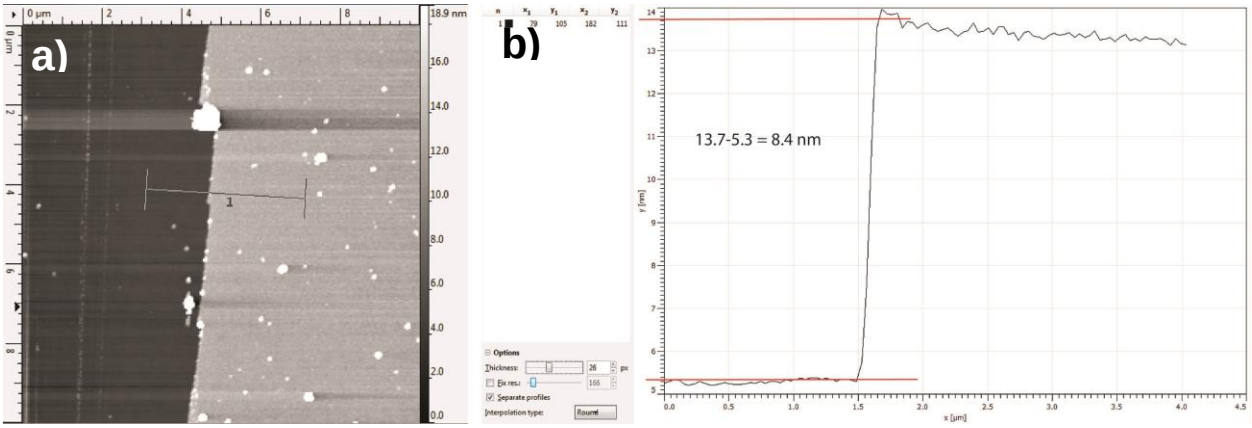

Figure 2.5: a) Example AFM scan done on the boundary of the scratch on the PDA film. b) The height profile (average of 1μm of pixels in the direction parallel to the scratch) is shown, as taken from line 1 in (a).

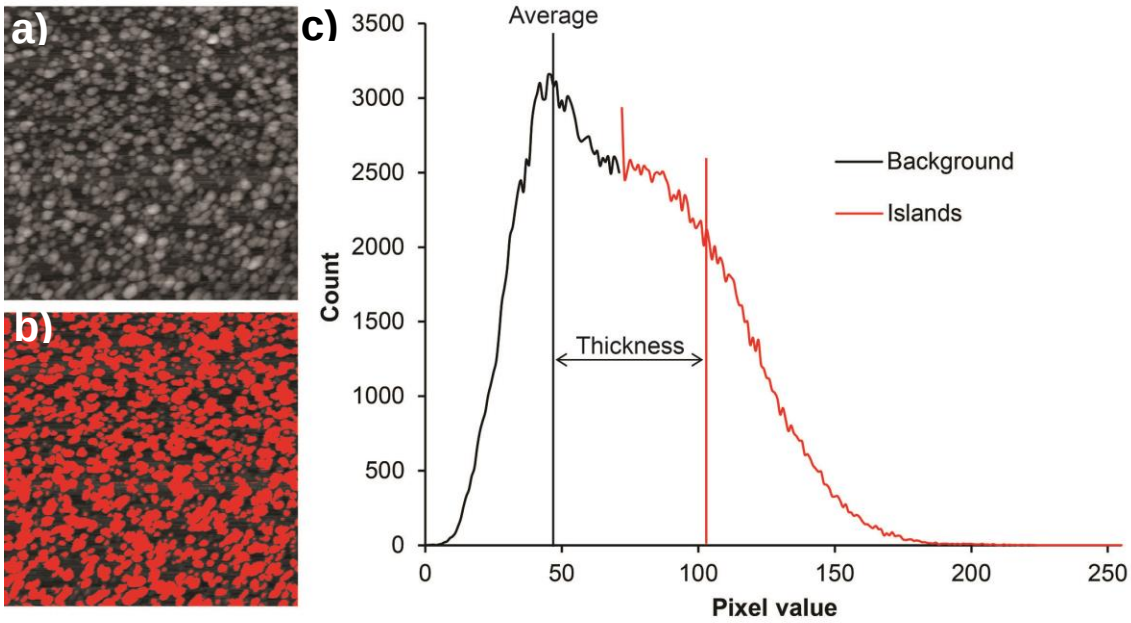

Figure 2.6: a) Example AFM scan on the SiO_2 substrate. b) The scan from (a) the after a threshold pixel value was chosen that just barely covered the islands. c) The pixel value distribution showing the two different distributions as divided by the threshold pixel value. The respective averages of these two distributions are shown as vertical lines.

2.4 Results and Discussion

2.4.1 Polydopamine films exhibit island growth that is modulated by each surface

The substrate compositions were chosen in order to probe a range of likely interactions between PDA precursors and surfaces during heterogeneous nucleation. Catechol moieties present in PDA are capable of hydrogen bonding, Michael-type additions between the quinone and amines, π-π interactions, and electrostatic interactions.[10] Therefore SAMs were prepared with primary amine (positively charged), aromatic phenyl, or aliphatic groups. Additionally, unmodified SiO_2 substrates exhibit terminal –SiOH or $–SiO^-$ groups and serve as a comparison to previous studies. Water-in-air contact angles and AFM scans of the substrates before PDA deposition are given in Figures 2.3 and A1. An increase in contact angle is observed for all substrates compared to bare SiO_2, and the contact angles are in agreement with previous reports utilizing these surface chemistries[11]: SiO_2 = 19.3±10.2°, NH_3^+ = 59.8±3.0°, Ph = 82.4±1.5°, CH_3 = 100.7±3.5°.

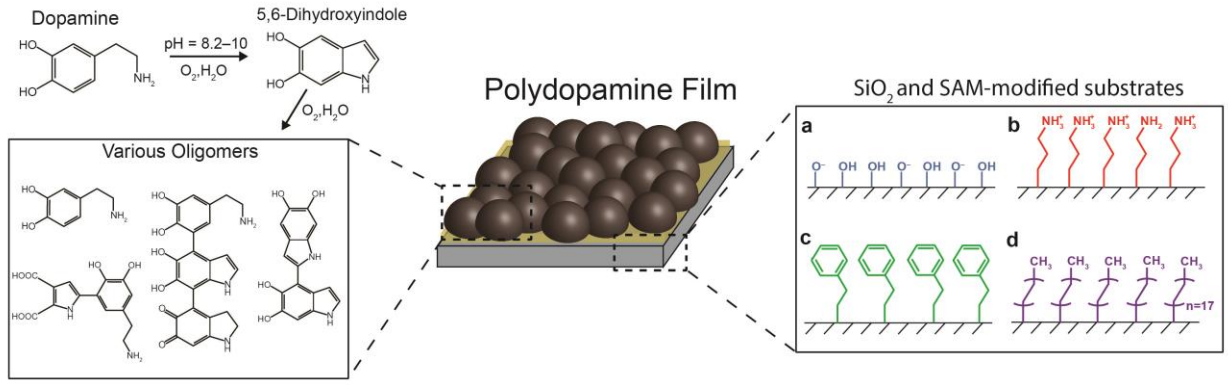

Scheme 2.1: Proposed synthesis scheme of polydopamine (PDA) on surface chemistries prepared in this study. PDA film formation proceeds via oxidation and subsequent cyclization to form oligomers that nucleate and growth on the surface. The substrate chemistries are a) silicon dioxide, and self-assembled monolayers of b) 3-aminopropyltrimethoxysilane, c) phenethyltrichlorosilane, and d) octadecyltrichlorosilane.

Scheme 2.1 illustrates substrate compositions and a typical evolution of PDA from dopamine in aqueous solution. As the reaction proceeds, intramolecular cyclization occurs and interactions

among these species results in visible black precipitation.[12–15] A film deposits simultaneously on the substrate which contains molecules and intermediates likely from all stages in the reaction.[7,16]

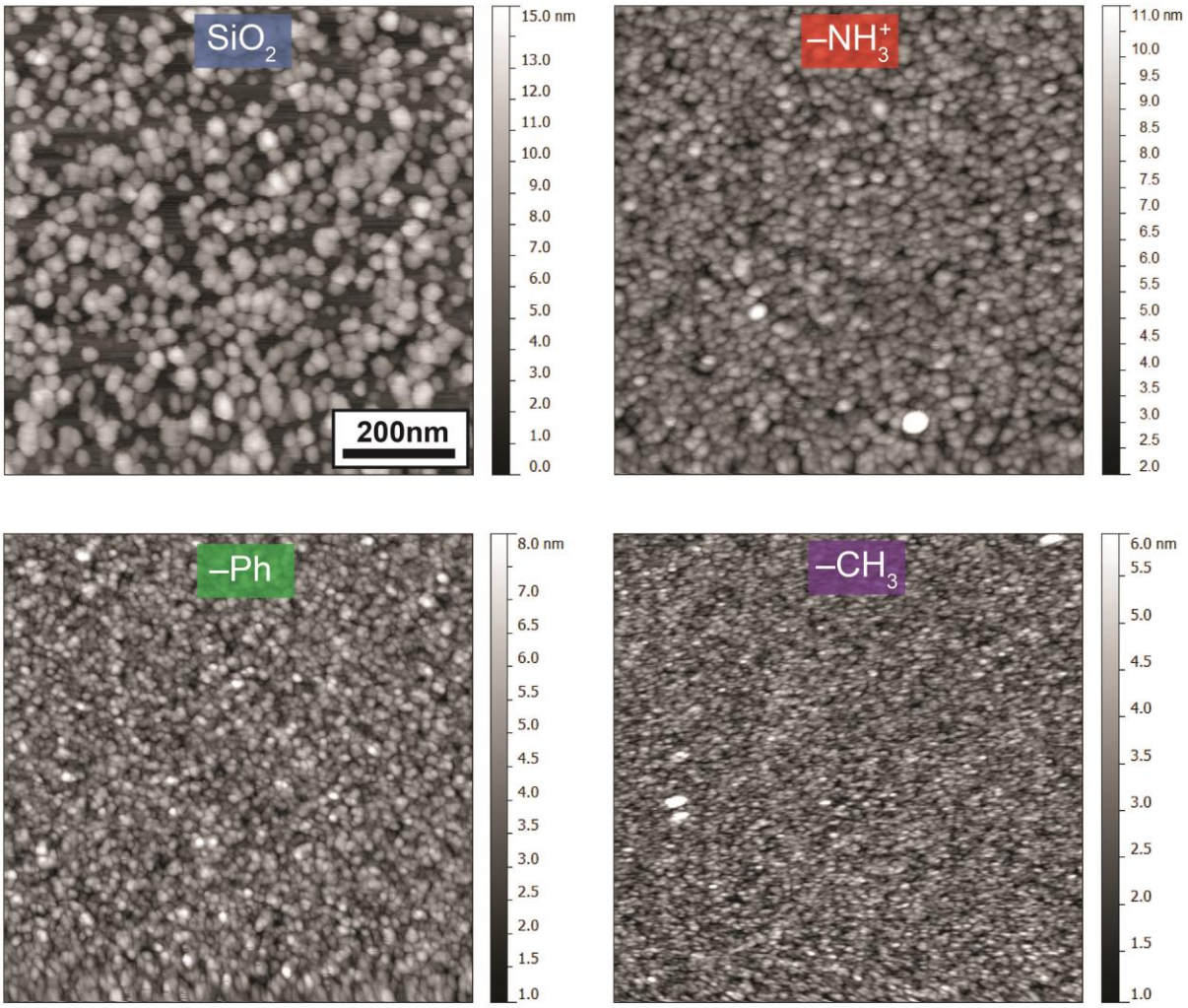

Figure 2.7: Representative AFM scans of PDA films labeled with the four terminal moieties of the substrates studied. Films were deposited in 50 mM carbonate/bicarbonate buffer with 2 mg/ml dopamine at pH = 8.5 for 24 hr. The areal density and coverage of islands are observed to depend on the substrate. All AFM images are 0.83 x 0.83 μm^2.

The morphology of the films after 24 hr was examined using AFM. The surface chemistry impacts the areal density and coverage of granules in PDA films produced at pH = 8.5 (Figure 2.7). This granule morphology has been observed previously.[6,17] Herein I distinguish granules (<1 μm distinct round structures in general) from islands (mound-like structures protruding from the surface). While the profiles of the granules are mound-like, preformed

particles deposited from solution may produce a comparable profile due to convolution of the tip as it moves over the particle. Granules formed on SiO_2 surfaces are on the order of ≥20 nm in diameter while only being ~4 nm in thickness. Considering that convolution of the 1 nm radius carbon spike tip would minimally affect a ≥20 nm diameter feature, these dimensions strongly favor an island morphology that is formed by direct nucleation on the surface. This dimensional argument is slightly more ambiguous for the other surface compositions. However, the average surface roughness of <1 nm for the 8 nm thick films and the uniformity of the granules make it implausible that PDA particles would nucleate and grow in the solution and only deposit in a packed monolayer after reaching a certain size. Thus PDA appears to exhibit 3-dimensional island growth similar to that observed, for example, in pthalocyanine[18] or poly(*p*-xylylene)[19] films in contrast to pentacene,[20] para-hexaphenyl,[21] or polyethylene films.[22]

One might expect the amino terminated surface to covalently bond with the PDA,[23] or that the aromatic phenyl groups might participate in π-π interactions and significantly affect the morphology. In general, the amino and aromatic phenyl groups produce PDA films with comparable nanoscale morphologies.

2.4.2 Surface-specific morphology depends on catechol ionization

The morphology and film thicknesses were measured as a function of pH in order to assess the coupled effect of both reaction rate and dissociation of hydrogens from catechol groups. The addition of dopamine hydrochloride to the 50 mM carbonate buffer in the initial pH range 8.5–10.5 causes the pH to drop by ~0.5 immediately, and then drop ≤0.1 over the subsequent 24 hr. This pH value after dopamine addition is what is reported throughout this chapter.

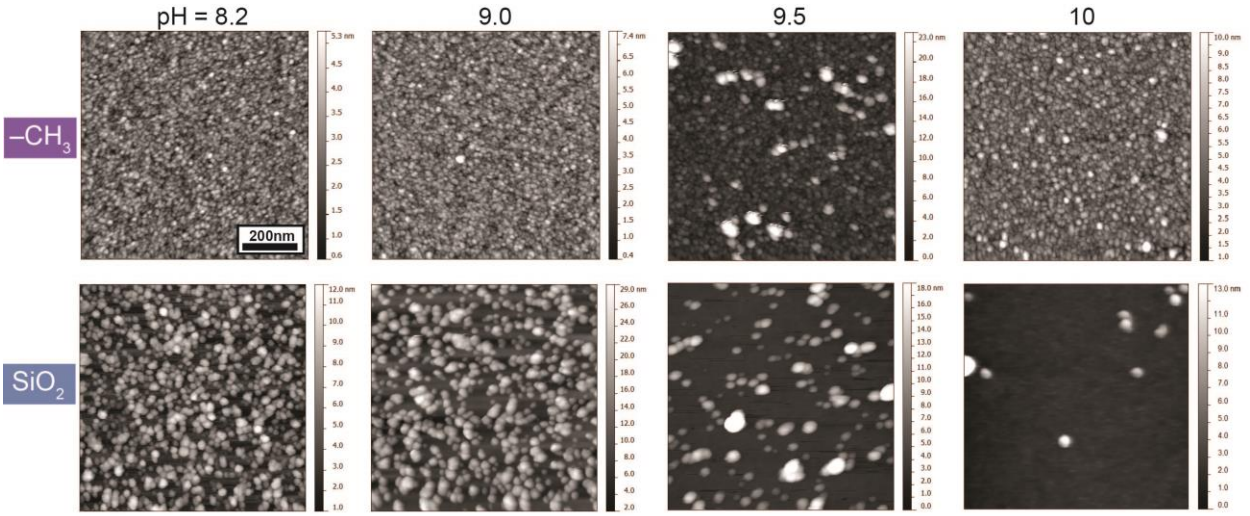

Figure 2.8: AFM scans of PDA films grown on the aliphatic and silicon dioxide substrates as a function of pH. Substrates modified with–Ph and $–NH_3^+$ SAMs exhibit a comparable pH-dependence relative to substrates modified with $–CH_3$ SAMs. See Figure A2 for morphology of PDA on $–NH_3^+$ SAMs at pH = 10. All AFM images are 0.83 x 0.83 μm^2.

SiO_2 surfaces exhibit a drop in fractional coverage ϕ from ϕ_{SiO2} = 55% for pH = 8.2–8.9, to 24% at pH = 9.5 and 1% at pH = 10. This observation is unique to SiO_2 compared to the SAM-modified surfaces (Fig. 2.8). A small decrease in ϕ_{NH3+} is observed at pH = 10 (see Fig. A2). The AFM thickness measurements reveal a linear increase in thickness *d* with pH up to 9.5,

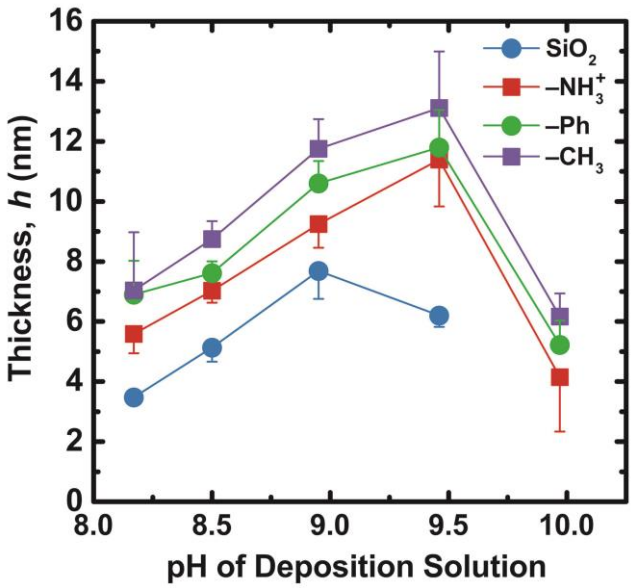

Figure 2.9: Film thickness vs. pH for each substrate, as determined by AFM scratches. The SiO_2 thickness was measured by analyzing the pixel value distributions in high resolution AFM scans. Thickness data on SiO_2 substrates at pH = 10 was unavailable due to low surface coverage (ϕ_{Si} < 1%) and resulting high variance in the data. Error bars represent one standard deviation.

and then a sharp drop-off at pH = 10 for the SAM-modified surfaces (Fig. 2.9). The thicknesses of PDA films prepared on SiO_2 substrates exhibit a linear increase from pH values of 8.2 to 8.9, but decreases at pH = 9.5 in contrast to the other surfaces. PDA films prepared on SiO_2 substrates at pH values of 10 exhibit limited surface coverage (~1%). The thickness of the PDA films on various substrate compositions d_i exhibits the following trend: $d_{SiO2} < d_{NH3+} < d_{Ph} < d_{CH3}$. This correlates with the relative hydrophobicities of the SAM chemistries and agrees with the observation that PDA films deposited on PVDF are thicker compared to PDA films prepared on bare SiO_2 (see Fig. 2.1).[8]

These results may be interpreted in light of the acid dissociation constants of dopamine and DHI. The pKa for the first hydroxyl deprotonation in dopamine and DHI is approximately 9.5–9.6.[24–26] Catechols likely serve as the primary adhesive mechanism of the PDA molecules to the surface.[27] Additionally, the solubility of the molecules would increase upon ionization,[28] thus shifting the adsorption/desorption equilibrium from the surface to the solution. Combined with this increased solubility effect is the increased reaction rate at elevated pH.[12] Therefore, values of d_i should increase with increasing pH until ionization of catechols becomes a dominant effect favoring dissolution rather than adsorption. The trends shown in Figure 2.9 support this mechanistic explanation. Ball and coworkers observed an increase in PDA film thickness as the pH increased from 5 –10.2, but did not observe a drop in thickness at pH = 10.2.[4] This potential discrepancy could be related to the different pH values reported before and after dopamine addition. These previous observations used reaction conditions with agitation and external supply of oxygen, which could also accelerate the reaction rate and PDA film growth compared to the reaction system reported herein.

Lower values of ϕ_{SiO2} and d_{SiO2} compared to ϕ_i and d_i of SAM-modified substrates is attributed to the negative surface charge on SiO_2, which inhibits adsorption of the ionized catechol groups of PDA. Rodriguez et al. quantified the adsorption of catechols to TiO_2 and observed a comparable reduction in adsorption between pH 9–10 compared to pH 8.5.[29] Electrostatic repulsion of SiO_2 substrates is attenuated when substrates are modified with SAMs. Thus, the observed decrease in d_i for SAM-modified substrates at pH >9.5 is attributed to increased PDA solubility.

PDA films formed on SAM-modified substrates at pH = 9.5 exhibit many apparently second-layer granules that are larger than the surrounding islands (Figure 2.10), an observation that is unique to this pH value. This morphological phenomenon may indicate a critical point in PDA precipitation. The trends in PDA film thickness vs. pH (Figure 2.9) suggest that pH value of 9.5 corresponds to the most rapid reaction rate in which adsorption is preferred compared to dissolution.

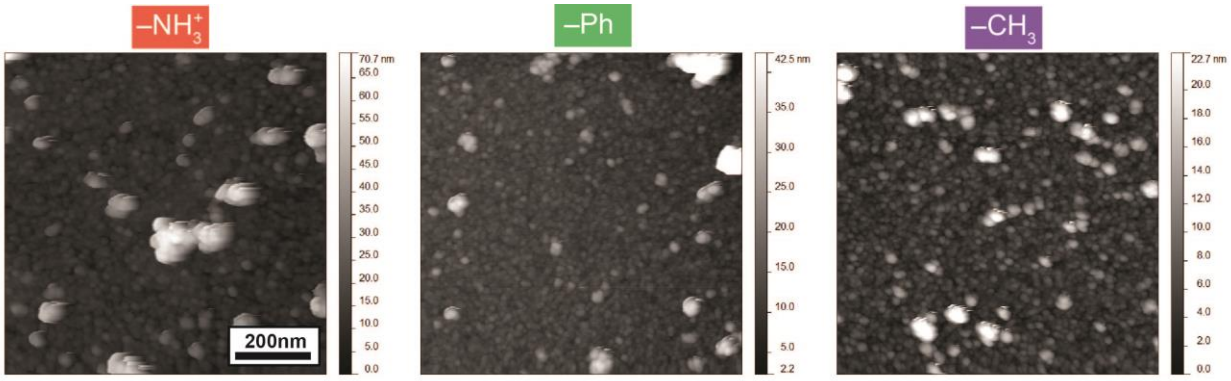

Figure 2.10: AFM scans at pH = 9.5 exhibiting the apparent second-layer granules. These PDA morphologies are not observed at any other pH value.

Overall, these results highlight the importance of the catechol's hydrogen dissociation equilibrium, and the resulting interactions with different surfaces and already-deposited PDA. The maximum PDA growth rate occurs at pH values of 9.5 and 9 for neutral/cationic and anionic

substrates, respectively. Also, larger maximum thicknesses are possible on neutral or positively charged surfaces compared to negatively charged surfaces.

2.4.3 Island areal density depends on surface-influenced initial deposition rate

Trends in areal island density (N = # of islands per μm^2) as a function of pH are as follows: $N_{SiO2} < N_{NH3} < N_{Ph} \leq N_{CH3}$ (Figure 2.11). The island density on bare SiO_2 substrates decreases linearly with the pH value. This observation is consistent with increasing catechol ionization and charge repulsion between the SiO_2 substrates and PDA. Values of N_i for SAM-modified substrates are lower at solutions of pH = 10 compared to solutions with pH value ranging from 8.2–8.9. The smallest values of N_i are observed when PDA films are formed at pH = 9.5 which is attributed to the unique heterogeneous second-layer granules discussed previously.

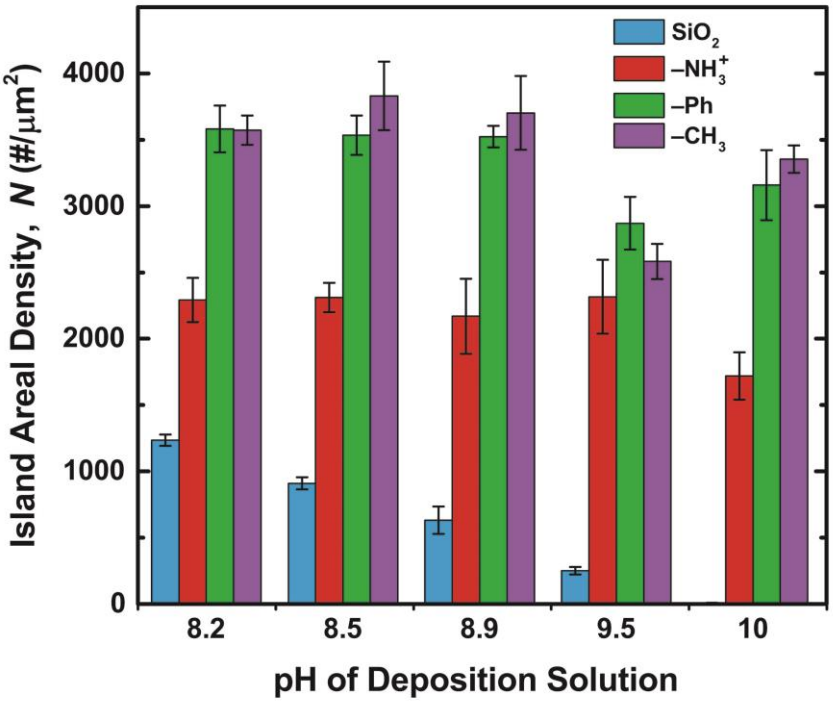

Figure 2.11: Areal density of PDA islands on substrates as a function of substrate composition and pH. Error bars represent the standard error of the mean.

The aqueous nucleation and growth of PDA films may be analyzed in comparison to vapor phase deposition of pentacene, for which much work has been done regarding the substrate and deposition-dependence of nucleation density.[30–33] Different rates of heterogeneous nucleation on different substrates are attributed to differences in activation energies for several processes including surface diffusion, evaporation, and binding energy of molecules with the surface (Fig. 2.12). These factors likely play a role in PDA nucleation and growth on the substrates discussed here.

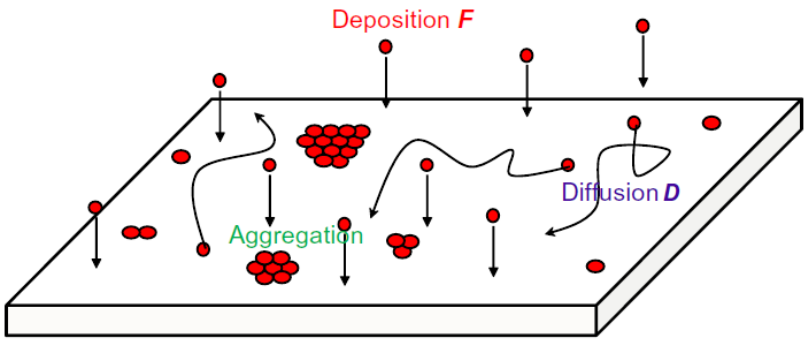

Figure 2.12: Schematic of island formation processes in vapor deposition. Reproduced from [34].

The theoretical basis for this dependency is a rate-equation formalism developed by Venebles and others.[35] A result of this model is Eqn. 3.1:

$$N \propto R^{\delta} \exp\left(\frac{E_{nucl}}{kT_s}\right) \qquad \text{Eqn. 3.1}$$

where N is the nucleation density, R is the deposition rate, δ relates to the critical nucleus size, T_s is the substrate temperature, and k is Boltzmann's constant. E_{nucl} is the overall activation energy for nucleation incorporating the activation energies for surface diffusion, evaporation, and cohesive binding. Thus, increasing the deposition rate increases the nucleation density, as previously observed in pentacene deposition (Fig. 2.13).[30,31] This observation is anticipated

based on increased nucleation frequency given enhanced local monomer concentrations on the substrate.

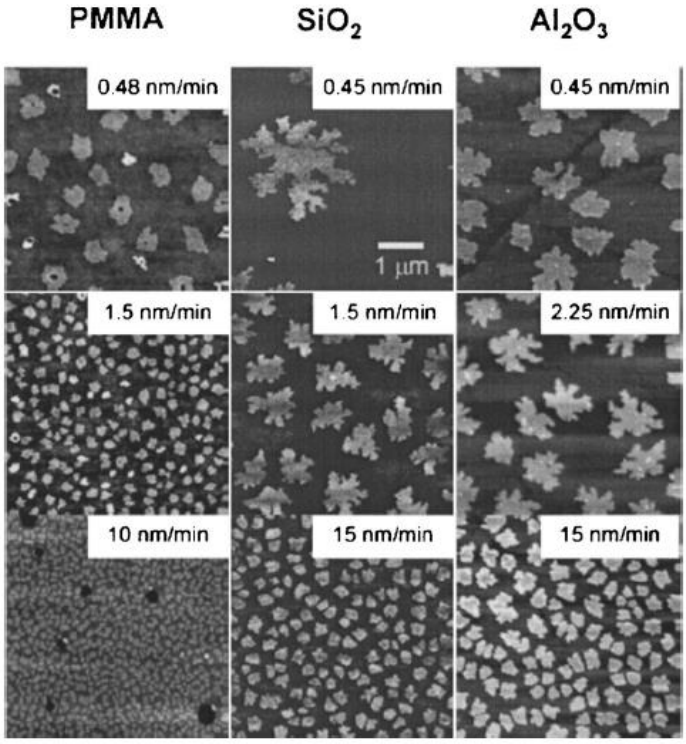

Figure 2.13: Effect of substrate chemistry and vapor deposition rate on the island density and coverage of pentacene. Reproduced from [30].

Upon first examination, the nucleation density appears to be independent of the deposition rate in the PDA system. The thickness of PDA islands on SiO_2 substrates increases for pH values from 8.2 to 8.9 even though the number of islands decreases. Also, the thickness of PDA films formed on SAMs increases from pH = 8.2 to 8.9 while the island density remains relatively constant. This paradox can be explained by the competing factors of solubility and relative surface attraction as discussed below.

The analogy of condensed phase PDA deposition to vapor phase deposition of organic small molecules is imperfect, although these two kinds of systems have been shown to be comparable.[36,37] It is difficult to control the rate of PDA deposition independently because PDA

precursor formation, polymerization, and deposition are inextricably coupled. For example, increasing the pH increases the formation rate of PDA oligomers, but it also increases catechol ionization. This enhances the solubility of PDA and favors desorption. However, the observed Volmer-Weber growth mechanism of PDA suggests that the PDA molecules have a stronger interaction with each other than the surface.[38] Additionally, covalent bonding may occur between soluble nascent PDA precursors and insoluble PDA films. Therefore, increasing the pH of the solution likely increases the rate of desorption from the bare portions of the substrate compared to portions of the substrate that are covered by PDA.

For the bare surfaces, the increased rate of monomer generation as the pH is increased may be balanced by the increased desorption of the depositing monomers. For PDA-coated regions of the substrate, cohesive interactions with the depositing monomers may supercede monomer dissolution from pH = 8.2–9.5. This observation could explain the apparent paradox in the thickness-nucleation density relationship mentioned previously. Also, the distribution of molecule types adsorbing on the substrate at early reaction times, which would determine the nucleation density, might be different as those that deposit at later times on top of the PDA film.

QCM-D measurements were performed in order to investigate the relationship of island density to the deposition rate of the PDA film. The QCM-D technique can track the mass deposited on a substrate by relating it to the shift in resonant frequency of an underlying quartz crystal.[39] Figure 2.14 shows the frequency ($\Delta f_5/5$, t = 0 to 240 min) shifts. The curves are offset to the beginning of the frequency drop, and Figures A3-4 show the raw frequency and dissipation curves for overtones n = 3–9 with the same offset. The frequency shifts exhibit the same linear decrease for all samples between 10-120 min, after which there is some flattening of the curves and deviations between samples. The sudden horizontal segments at 240 min correspond to

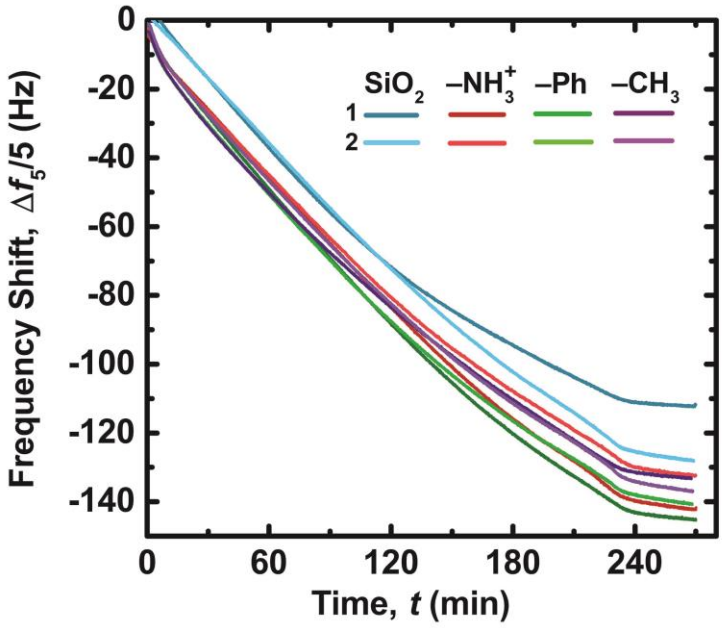

Figure 2.14: QCM-D frequency shifts with time for the fifth overtone for two samples on each substrate. The flow of dopamine precursor solutions was stopped at approximately 240 min.

when solution flow was stopped, and indicate that continuous deposition requires continuous flow of the reaction solution. Final frequency shifts are $\Delta f_5/5$ = -110 to -140 Hz after 4 hr solution flow.

The Sauerbrey relationship can describe the adsorbed mass (*m)* as a function of observed frequency shift (Δf_n) and overtone (n) at early times via the following relationship[39]:

$$m = -C\frac{\Delta f_n}{n} \qquad \text{Eqn. 3.2}$$

where C = 17.7 ng cm^{-2} Hz^{-1}. This relationship is justified at very early times (<10 min) by the small differences in overtones (~1 Hz; 3 and 5 Hz for –NH_3^+ 1 and 2) and small dissipation values (Figure A3–4). As the PDA film becomes thicker, the Sauerbrey relationship becomes less accurate, but still represents approximate deposition rates for the time period plotted in Figure 2.15a.

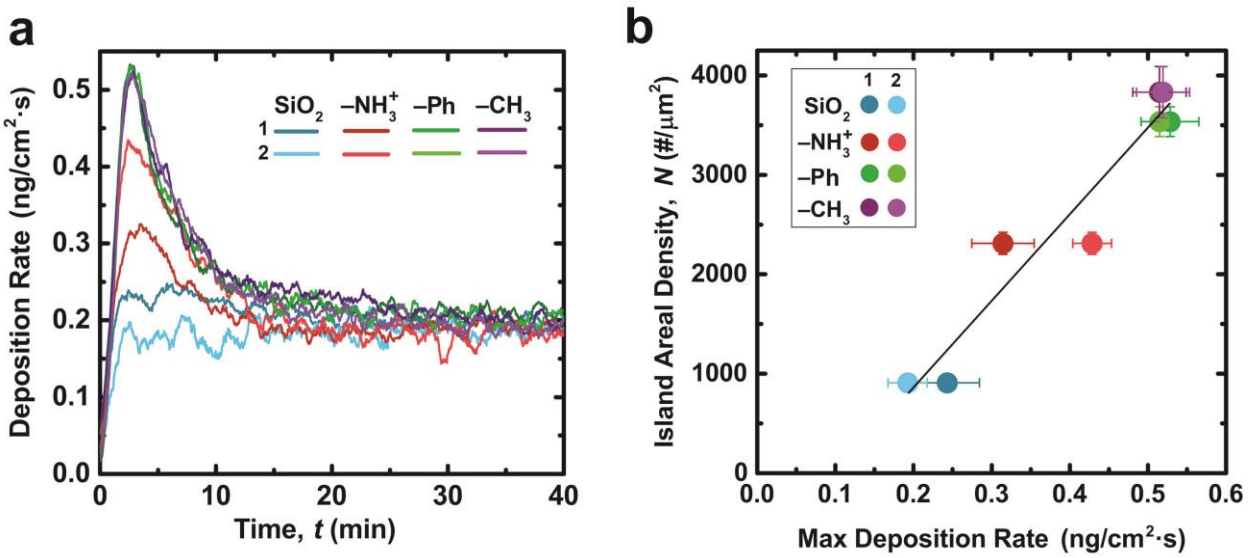

Figure 2.15: a) Approximate PDA deposition rates at early times, as calculated from the time derivative of the data in Fig. 2.15 and Eqn. 3.2. b) Areal island density as a function of maximum observed adsorption rate as recorded from the peaks in (a).

The approximate deposition rates (Figure 2.15) were calculated from the derivative of the frequency shifts. The deposition rates exhibit similarly shaped peaks at early times (t < 10 min) which then converge to a constant value at t > 15 min. This convergence of deposition rates is likely due to the bare substrate chemistries becoming obscured as PDA progressively deposits and covers the substrates. The deposition rate on SiO_2 reaches a steady state value more rapidly compared to the SAM-modified substrates. Substrates modified with –Ph and $–CH_3$ terminal SAM groups produce derivative curves that all peak at comparable values, while substrates with $–NH_3^+$ groups exhibit intermediate peaks.

Figure 2.15b shows a plot of the average areal island density (measured from the static vial depositions as shown in Figure 2.11) vs. the maximum adsorption rates averaged from overtones 3-9. A linear correlation is observed, which is expected considering that a greater flux of PDA monomers to the surface would increase the likelihood of a nucleation event.

The adsorption rates, besides being dependent on the substrate chemistry, can also be controlled by adjusting the dopamine concentration in the deposition solution (Figures 2.16 and 2.17). An increased dopamine concentration increases the reaction rate and flux of PDA molecules to the surface without affecting the ionization equilibrium of PDA molecules. This is in contrast to increasing the pH which, while increasing the reaction rate, also increases the solubility of the PDA molecules as discussed previously.

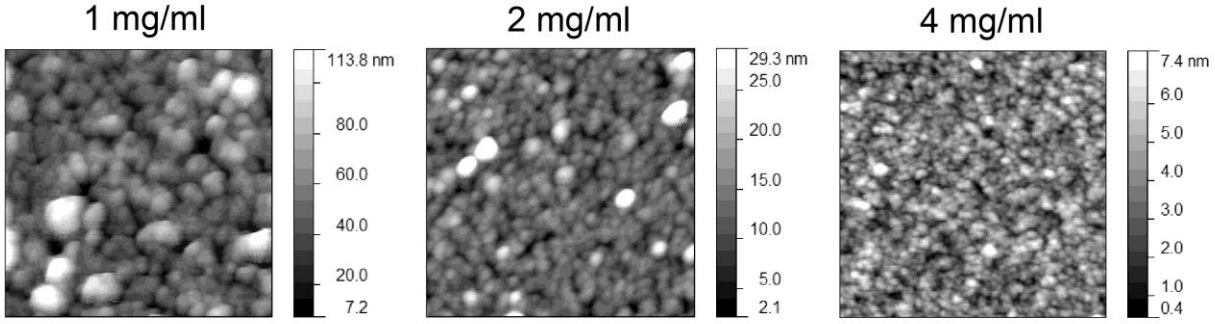

Figure 2.16. AFM scans of PDA films prepared on SiO_2 after two depositions at pH 8.5 in stirred, open solutions. Each scan shown is 1 x 1 μm^2.

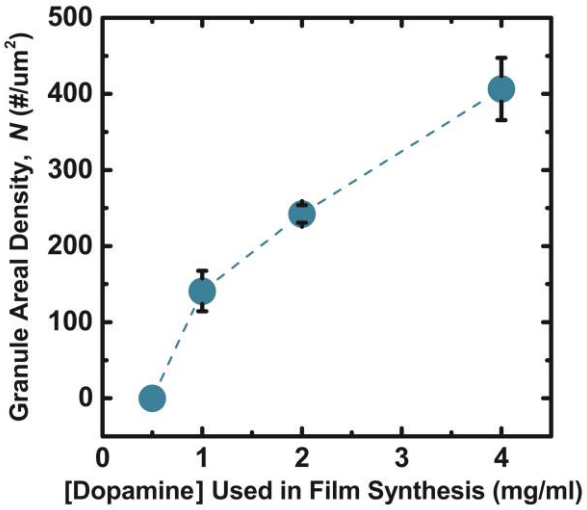

Figure 2.17: Granule densities of the PDA films shown in Figure 2.16. The term 'granule' instead of 'island' is used for these samples because they are the result of two depositions instead of one, and its unknown if a secondary nucleation event happened in the second deposition on top of the original islands. Three measurements were performed on each film. No film was observed at 0.5 mg/ml.

The range of deposition rates on different surface chemistries may be due to the differences in interfacial energies with water. The energy of PDA adsorption can be expressed as the difference in interfacial energies of the system before and after PDA deposition:

$$\Delta G_{Ads} = \gamma_{PDA/Sub} - \left(\gamma_{PDA/H_2O} + \gamma_{Sub/H_2O}\right) \quad \text{Eqn 3.3}$$

where ΔG_{Ads} is the work of adsorption, and γ is the interfacial energy for the respective interface (between PDA, H_2O, and the substrate as labeled). The interfacial energy values can be calculated from the dispersive and polar components of each isolated surface energy (in vapor) using the following equation[40]:

$$\gamma_{AB} = \gamma_A + \gamma_A - 2\sqrt{\gamma_A^D \gamma_B^D} - 2\sqrt{\gamma_A^P \gamma_B^P} \quad \text{Eqn 3.4}$$

where γ_{AB} is the interfacial energy, and γ^D and γ^P are the dispersive and polar surface energy components of each respective surface. Values of γ for the substrates were taken from [11] and for PDA from [8]. The results of this calculation are shown in Figure 2.18 relative to the max deposition rate observed. The deposition rate increases as ΔG_{Ads} decreases from SiO_2 to –Ph, as expected. However, a plateau past the –Ph surface suggests that there is a maximum surface-influenced deposition rate achievable under these reaction conditions (pH = 8.5, 2 mg/ml dopamine). The fact that deposition was still observed in the case of a positive ΔG_{Ads} for SiO_2 suggests that this simple interfacial energy model does not fully describe the system, but it is still qualitatively consistent with the incomplete surface coverage observed on SiO_2. In support of this interfacial energy interpretation, Sedeva et al. reported greater and faster adsorption of polyacrylamide with increasing hydrophobicity of SAM-modified QCM sensor surfaces.[41]

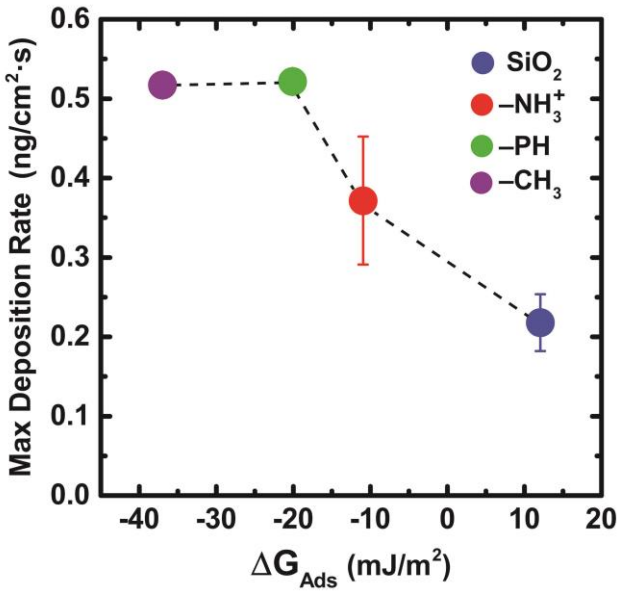

Figure 2.18: Max deposition rate observed via QCM-D vs. the Gibbs energy change (work) of adsorption. Points are the average of the data shown in Figure 2.15b with corresponding standard deviation for the 5th overtone only.

Overall, the QCM-D data suggests that PDA adsorption is promoted on hydrophobic substrates, and this is partly responsible for the differences in nucleation densities.

Finally, note that deposition continued over the entire 4 hr period for a single dopamine solution. This is in contrast to the observation that fresh dopamine solutions in Tris buffer are required every 20 min to continue film growth.[2] Tris contains primary amines that compete with intramolecular cyclization in ortho-quinone bearing dopamines, thereby scavenging PDA

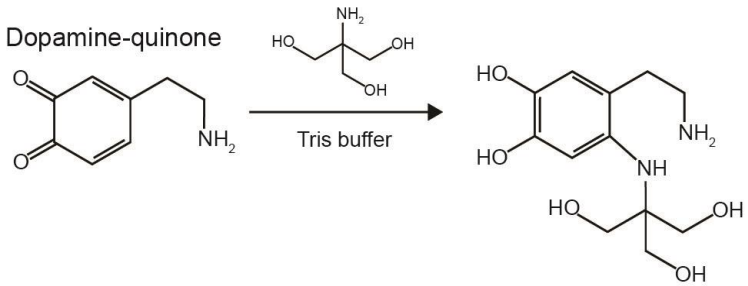

Figure 2.19: Tris buffer incorporation into dopamine-quinone preventing intramolecular cyclization.

precursors and preventing indole formation.[3,13] This observation is consistent with monotonically increasing PDA growth when using amine-free phosphate buffers.[1] Therefore, buffers without

primary amines appear to preserve the precursor evolution and aggregation processes necessary for film deposition and growth.

2.5 Conclusions

The nucleation and growth of PDA films in aqueous solution has been measured as a function of substrate composition. AFM scans indicate that PDA films consist of a granular morphology with 3-dimensional island growth. The coverage and density of the islands was smallest on SiO_2 surfaces and largest on neutral, hydrophobic surfaces. Increasing the pH of the deposition solution from 8.2 to 10 revealed the importance of catechol ionization on film deposition and morphology. Deposition of PDA from aqueous phases at pH = 9.5 represents a critical point for the SAM-modified substrates where the PDA precursor generation and film growth is maximized, yet the catechol ionization is not enough such that dissolution prevents adsorption, as is the case at pH = 10. Adsorption of PDA on charged surfaces composed of bare SiO_2 is inhibited by catechol ionization across pH values ranging from 8.2–10. QCM-D measurements suggest that the nucleation density is correlated with maximum adsorption rates at early deposition times. The correlation between increasing dopamine concentration and increased nucleation density supports this conclusion.

These data support the universal deposition capability of polydopamine while revealing that the substrate chemistry and deposition conditions affect the rate of nucleation and growth. This may have important implications in controlling the morphology of PDA films for applications as a functional coating.

2.6 References

(1) Bernsmann, F.; Ball, V.; Ponche, A.; Michel, M.; Gracio, D. A.; Ruch, D. Dopamine - Melanin Film Deposition Depends on the Used Oxidant and Buffer Solution. *Langmuir* **2011**, *27*, 2819–2825.

(2) Bernsmann, F.; Ponche, A.; Ringwald, C.; Hemmerlé, J.; Raya, J.; Bechinger, B.; Voegel, J.; Schaaf, P.; Ball, V. Characterization of Dopamine−Melanin Growth on Silicon Oxide. *J. Phys. Chem. C* **2009**, *113*, 8234–8242.

(3) Della Vecchia, Nicola Fyodor; Luchini, Alessandra; Napolitano, Alessandra; D'Errico, Gerardino; Vitiello, Giuseppe; Szekely, Noemi; d'Ischia, Marco; Paduano, L. Tris Buffer Modulates Polydopamine Growth, Aggregation, and Paramagnetic Properties. *Langmuir* **2014**, *30*, 9811–9818.

(4) Ball, V.; Frari, D. Del; Toniazzo, V.; Ruch, D. Kinetics of Polydopamine Film Deposition as a Function of pH and Dopamine Concentration: Insights in the Polydopamine Deposition Mechanism. *J. Colloid Interface Sci.* **2012**, *386*, 366–372.

(5) Kim, H. W.; McCloskey, B. D.; Choi, T. H.; Lee, C.; Kim, M. J.; Freeman, B. D.; Park, H. B. Oxygen Concentration Control of Dopamine-Induced High Uniformity Surface Coating Chemistry. *ACS Appl. Mater. Interfaces* **2013**, *5*, 233–238.

(6) Bernsmann, F.; Ersen, O.; Voegel, J.-C.; Jan, E.; Kotov, N. a; Ball, V. Melanin-Containing Films: Growth from Dopamine Solutions versus Layer-by-Layer Deposition. *ChemPhysChem* **2010**, *11*, 3299–3305.

(7) Zangmeister, R. a; Morris, T. a; Tarlov, M. J. Characterization of Polydopamine Thin Films Deposited at Short Times by Autoxidation of Dopamine. *Langmuir* **2013**, *29*, 8619–8628.

(8) Jiang, J.; Zhu, L.; Zhu, L.; Zhu, B.; Xu, Y. Surface Characteristics of a Self-Polymerized Dopamine Coating Deposited on Hydrophobic Polymer Films. *Langmuir* **2011**, *27*, 14180–14187.

(9) Del Frari, D.; Bour, J.; Ball, V.; Toniazzo, V.; Ruch, D. Degradation of Polydopamine Coatings by Sodium Hypochlorite: A Process Depending on the Substrate and the Film Synthesis Method. *Polym. Degrad. Stab.* **2012**, *97*, 1844–1849.

(10) Waite, J. H. Nature's Underwater Adhesive Specialist. *Int. J. Adhes. Adhes.* **1987**, *7*, 9–14.

(11) Janssen, D.; De Palma, R.; Verlaak, S.; Heremans, P.; Dehaen, W. Static Solvent Contact Angle Measurements, Surface Free Energy and Wettability Determination of Various Self-Assembled Monolayers on Silicon Dioxide. *Thin Solid Films* **2006**, *515*, 1433–1438.

(12) Herlinger, Erwin; Jameson, Reginald F.; Linert, W. Spontaneous Autoxidation of Dopamine. *J. Chem. Soc., Perkin Trans. 2* **1995**, 259–263.

(13) Della Vecchia, N. F.; Avolio, R.; Alfè, M.; Errico, M. E.; Napolitano, A.; D'Ischia, M. Building-Block Diversity in Polydopamine Underpins a Multifunctional Eumelanin-Type Platform Tunable through a Quinone Control Point. *Adv. Funct. Mater.* **2013**, *23*, 1331–1340.

(14) Liebscher, J.; Mrówczyński, R.; Scheidt, H. a; Filip, C.; Hădade, N. D.; Turcu, R.; Bende, A.; Beck, S. Structure of Polydopamine: A Never Ending Story? *Langmuir* **2013**, *29*, 10539–10548.

(15) Hong, S.; Na, Y. S.; Choi, S.; Song, I. T.; Kim, W. Y.; Lee, H. Non-Covalent Self-Assembly and Covalent Polymerization Co-Contribute to Polydopamine Formation. *Adv. Funct. Mater.* **2012**, *22*, 4711–4717.

(16) Ponzio, F.; Ball, V. Persistence of Dopamine and Small Oxidation Products Thereof in Oxygenated Dopamine Solutions and in "polydopamine" Films. *Colloids Surfaces A Physicochem. Eng. Asp.* **2014**, *443*, 540–543.

(17) Bernsmann, F.; Frisch, B.; Ringwald, C.; Ball, V. Protein Adsorption on Dopamine-Melanin Films: Role of Electrostatic Interactions Inferred from Zeta-Potential Measurements versus Chemisorption. *J. Colloid Interface Sci.* **2010**, *344*, 54–60.

(18) Yim, S.; Jones, T. Anomalous Scaling Behavior and Surface Roughening in Molecular Thin-Film Deposition. *Phys. Rev. B* **2006**, *73*, 161305.

(19) Strel'tsov, D. R.; Buzin, a. I.; Grigor'ev, E. I.; Dmitryakov, P. V.; Mailyan, K. a.; Pebalk, a. V.; Chvalun, S. N. Scaling Analysis of the Morphology of Nanostructured Poly(p-Xylylene) Films Synthesized by Vapor Deposition Polymerization. *Nanotechnologies Russ.* **2008**, *3*, 494–501.

(20) Ruiz, R.; Choudhary, D.; Nickel, B.; Toccoli, T.; Chang, K.; Mayer, A. C.; Clancy, P.; Blakely, J. M.; Headrick, R. L.; Iannotta, S.; et al. Pentacene Thin Film Growth. *Chem. Mater.* **2004**, *16*, 4497–4508.

(21) Tumbek, L.; Gleichweit, C.; Zojer, K.; Winkler, a. Origin of the Bimodal Island Size Distribution in Ultrathin Films of Para-Hexaphenyl on Mica. *Phys. Rev. B* **2012**, *86*, 085402.

(22) Choukourov, A.; Melnichuk, I.; Gordeev, I.; Kylián, O.; Hanuš, J.; Kousal, J.; Solař, P.; Hanyková, L.; Brus, J.; Slavínská, D.; et al. Dynamic Scaling and Kinetic Roughening of Poly(ethylene) Islands Grown by Vapor Phase Deposition. *Thin Solid Films* **2014**, *565*, 249–260.

(23) Lee, H.; Scherer, N. F.; Messersmith, P. B. Single-Molecule Mechanics of Mussel Adhesion. *Proc. Natl. Acad. Sci.* **2006**, *103*, 12999–13003.

(24) Ishimitsu, T.; Hirose, S.; Sakurai, H. Microscopic Acid Dissociation Constants of 3,4-Dihydroxyphenethylamine (Dopamine). *Chem. Pharm. Bull.* **1978**, *26*, 74–78.

(25) Charkoudian, L. K.; Franz, K. J. Fe (III) -Coordination Properties of Neuromelanin Components : 5,6-Dihydroxyindole and 5,6-Dihydroxyindole-2-Carboxylic Acid. *Inorg. Chem.* **2006**, *45*, 3657–3664.

(26) Szpoganicz, B.; Gidanian, S.; Kong, P.; Farmer, P. Metal Binding by Melanins: Studies of Colloidal Dihydroxyindole-Melanin, and Its Complexation by Cu(II) and Zn(II) Ions. *J. Inorg. Biochem.* **2002**, *89*, 45–53.

(27) Li, Y.; Qin, M.; Li, Y.; Cao, Y.; Wang, W. Single Molecule Evidence for the Adaptive Binding of DOPA to Different Wet Surfaces. *Langmuir* **2014**, *30*, 4358–4366.

(28) Bothma, J. P.; de Boor, J.; Divakar, U.; Schwenn, P. E.; Meredith, P. Device-Quality Electrically Conducting Melanin Thin Films. *Adv. Mater.* **2008**, *20*, 3539–3542.

(29) Rodruiguez, R.; Blesa, M. A.; Regazzoni, A. E. Surface Complexation at the TiO 2 (Anatase)/ Aqueous Solution Interface : Chemisorption of Catechol. *J. Colloid Interface Sci.* **1996**, *177*, 122–131.

(30) Pratontep, S.; Nüesch, F.; Zuppiroli, L.; Brinkmann, M. Comparison between Nucleation of Pentacene Monolayer Islands on Polymeric and Inorganic Substrates. *Phys. Rev. B* **2005**, *72*, 085211.

(31) Ribič, P.; Kalihari, V.; Frisbie, C.; Bratina, G. Growth of Ultrathin Pentacene Films on Polymeric Substrates. *Phys. Rev. B* **2009**, *80*, 115307.

(32) Yoshida, M.; Uemura, S.; Kodzasa, T.; Kamata, T.; Matsuzawa, M.; Kawai, T. Surface Potential Control of an Insulator Layer for the High Performance Organic FET. *Synth. Met.* **2003**, *137*, 967–968.

(33) Yang, S. Y.; Shin, K.; Park, C. E. The Effect of Gate-Dielectric Surface Energy on Pentacene Morphology and Organic Field-Effect Transistor Characteristics. *Adv. Funct. Mater.* **2005**, *15*, 1806–1814.

(34) Hader, a.; Achik, I.; Hajjaji, a.; Boughaleb, Y. The Ordering Islands Growth Kinetics during Self-Assembled Monolayer Formation. *Opt. Mater. (Amst).* **2012**, *34*, 1713–1716.

(35) Venables, J. a. Rate Equation Approaches to Thin Film Nucleation Kinetics. *Philos. Mag.* **1973**, *27*, 697–738.

(36) Doudevski, I.; Hayes, W.; Schwartz, D. Submonolayer Island Nucleation and Growth Kinetics during Self-Assembled Monolayer Formation. *Phys. Rev. Lett.* **1998**, *81*, 4927–4930.

(37) Doudevski, I.; Schwartz, D. Dynamic Scaling of the Submonolayer Island Size Distribution during Self-Assembled Monolayer Growth. *Phys. Rev. B* **1999**, *60*, 14–17.

(38) Venables, J. A.; Spiller, G. D. T.; Hanbuken, M. Nucleation and Growth of Thin Films. *Rep. Prog. Phys.* **1984**, *47*, 399–459.

(39) Reviakine, I.; Johannsmann, D.; Richter, R. P. Hearing What You Cannot See and Visualizing What You Hear : *Anal. Chem.* **2011**, *83*, 8838–8848.

(40) Kinloch, A. J. The Science of Adhesion - Part 1 Surface and Interfacial Aspects. *J. Mater. Sci.* **1980**, *15*, 2141–2166.

(41) Sedeva, I. G.; Fornasiero, D.; Ralston, J.; Beattie, D. A. The Influence of Surface Hydrophobicity on Polyacrylamide Adsorption. *Langmuir* **2009**, *25*, 4514–4521.

Chapter 3

Compositional Control of Polydopamine Films

3.1 Abstract

The facile preparation of conformal PDA films on broad classes of materials has prompted extensive research into a wide variety of potential applications for PDA. The constituent molecular species in PDA exhibit diverse chemical moieties, and therefore highly variable properties of PDA-based devices may evolve with post-processing conditions. Chapter 3 discusses the use of redox-inactive cations for oxidative post-processing of deposited PDA films. PDA films incubated in alkaline $CaCl_2$ solutions produce 5,6-dihydroxyindole (DHI) radicals in a dose-dependent manner. PDA films incubated in $CaCl_2$ solutions exhibit 53% of the oxidative charge transfer compared to pristine PDA films. Carboxylic acid groups generated from the oxidation process lower the isoelectric point of PDA films from pH = 4.0 ± 0.2 to pH 3.1 ± 0.3. PDA films exposed to $CaCl_2$ solutions during post-processing also enhance Fe^{2+}/Fe^{3+} chelation compared to pristine PDA films. These data illustrate that the molecular heterogeneity and non-equilibrium character of as-deposited PDA films afford control over the final composition by choosing post-processing conditions, but also demands forethought into how the performance of PDA-incorporated devices may change over time in salt solutions.

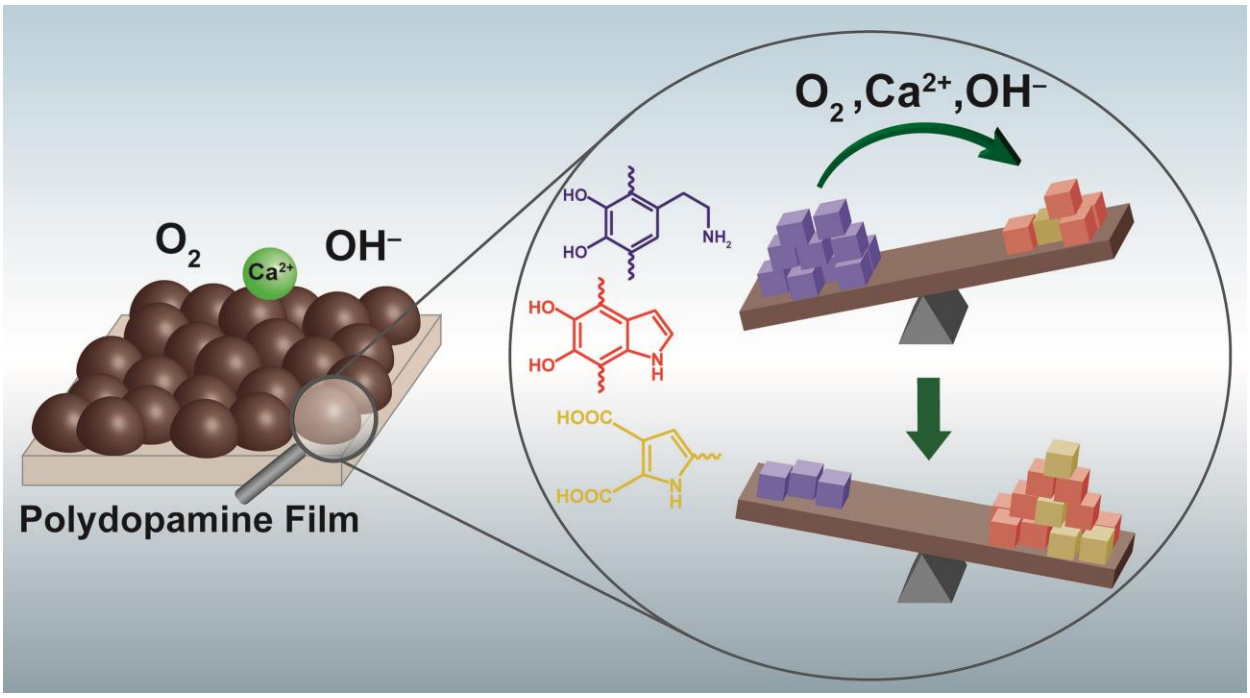

Scheme 3.1: Graphical summary of Chapter 3. Freshly-synthesized PDA films are partially oxidized and contain molecular species from all stages of the dopamine oxidation pathway. Alkaline solutions of redox-inactive cations can bias the composition of PDA towards downstream oxidative products and in doing so modulate the physical properties of PDA films.

3.2 Introduction

The primary means of controlling the intrinsic properties of PDA films thus far explored have been the conditions of the precursor solution. The intrinsic oxidation mechanism of dopamine is sensitive to dissolved O_2, dopamine, and hydronium concentration[1], however buffer composition and substrate chemistry also influence PDA film growth. The rate of PDA film growth is accelerated as pH values approach 9.5 above which (pH > 9.5) increased PDA solubility compromises film quality.[2,3] Copper ions and periodate oxidants, in contrast to dissolved O_2, can create PDA films in aqueous solutions at pH < 7.0.[4,5] Electrochemical oxidation of dopamine produces PDA films with increased ion permeability[6] and stability[7] compared to PDA films formed through auto-oxidation. Buffer composition and substrate

chemistry also influence the deposition rate and nanostructure of PDA films.[3,8,9] Post-synthesis treatments such as thermal annealing[10,11] or $FeCl_3$ treatments[12] of PDA films increases their stability in alkaline solutions compared to pristine PDA films. Taken together, these numerous strategies illustrate the use of PDA deposition conditions and post-processing to tune PDA composition and reactivity.

A comprehensive understanding of structure-processing-property relationships in PDA could accelerate the implementation of this material in many technologies. Devices incorporating PDA are most commonly applied in aqueous solutions of metal salts. Yet there is little knowledge regarding the temporal evolution of PDA properties in response to solutions of group I and II cations which are known to influence cohesive forces[13] and redox kinetics[14] in other catecholic materials. Chapter 3 discusses the influence of $CaCl_2$ solutions on oxidation of pre-deposited PDA films. The oxidation kinetics, redox state, and physicochemical properties of PDA films are reported. Functional properties of PDA films including catechol-cation chelation are also investigated.

3.3 Methods

3.3.1 Materials

Dopamine hydrochloride (98%), iron(III) chloride hexahydrate (>99%), iron(II) chloride tetrahydrate (>99%) sodium chloride (>99%) and citric acid (>99.5%) were purchased from Sigma-Aldrich (St. Louis, MO USA) and used as received. Sodium bicarbonate (>99%), sodium carbonate (>99%), tris(hydroxymethyl) aminomethane (Tris), sodium phosphate dibasic (99.2%) and magnesium chloride hexahydrate (>99%) were purchased from Fisher Scientific (Hampton, NH USA) and used as received. Calcium chloride dihydrate (>99%) was purchased from BDH

VWR International (Radnor, PA USA). Water was purified (18.2 MΩ-cm) using Direct-Q 3 UV-R system (Millipore). Silicon wafers with native oxide were purchased from Silicon Quest International (San Jose, CA USA; 1" diameter, phosphorus doped). Indium tin oxide (ITO) pieces were purchased from University Wafer (Boston, MA USA; 20 Ω/□; ITO on glass.

3.3.2 PDA Film Preparation and Iron Binding

Silicon and ITO substrates were cleaned by sonication in acetone, followed by isopropyl alcohol and then rinsed with de-ionized water (ddH_2O). Substrates were then cleaned by UV-ozone (30 mW/cm^2, 5 min; Jelight, Irvine, CA USA). PDA films were prepared by dissolving 2 mg/ml dopamine hydrochloride in 200 ml of 50 mM bicarbonate buffer at pH = 8.5. Pre-cleaned substrates were incubated in dopamine solutions in ambient air and rotational agitation (65 rpm). After 24 hr the substrates were rinsed and incubated in a refreshed deposition solution for another 24 hr and a total 48 hour deposition time. The substrates were then rinsed and placed in ddH_2O for 24 hr then dried under a stream of N_2.

PDA films were incubated in 3.2 mM HCl (pH = 2.5) for 15 min after exposure to post-processing solutions ($CaCl_2$ + Tris, Tris, ddH_2O only) and then washed with ddH_2O to remove precipitates and equilibrate the pH within the films. The pH values of all sample solutions were measured using an Ag/AgCl electrode (Hach, model 5014T; Loveland, CO USA).

For iron chelation assays, PDA films were incubated in either ddH_2O or 300 mM $CaCl_2$ (pH = 9.5) for 4 hr, then in pH = 2.5 HCl for 15 min, and finally 5 mM $FeCl_2$ or $FeCl_3$ solutions for 100 min. $FeCl_2$ was used to investigate iron chelation at pH > 4 where Fe^{3+} ions precipitate as hydroxide species.[15]

3.3.3 Spectroscopic and Electrochemical Characterization of PDA Films

Ultraviolet-Visible (UV-Vis) spectra of hydrated PDA films on 0.9 x 2.5 cm^2 ITO substrates were recorded (UV-2600, Shimadzu; Kyoto, JAPAN) in various buffered salt solutions with a pristine ITO substrate and solution in the reference cell. After incubating the PDA films for 3 min in the desired solution (to allow for solution permeation and pH equilibration), the spectra of the films were recorded every 83 seconds for several hours.

Fourier transform infrared (FTIR) spectra of the PDA films were recorded via attenuated total reflectance (ATR) technique (Frontier, PerkinElmer; Waltham, MA USA). Raman spectra (NTegra Spectra; Tempe, AZ) were recorded with a 532 nm laser. Each measurement was done at unique single point of spot size ~1 μm diameter at 1 mW power for 50-60 seconds. Peak deconvolution was performed with OriginLab software (Northampton, MA USA).

Zeta potentials of PDA films were calculated by measuring the streaming potential near a rotating disk[16] (PDA film on SiO_2) at different pH with a custom-built ZetaSpin apparatus.[17]

Cyclic voltammetry was performed in a conventional three-electrode setup with saturated Ag/AgCl reference electrodes (Koslow Scientific; Englewood, NJ USA) and platinum mesh as counter electrode. Tests were performed in 180 mM citric acid-sodium phosphate buffer (pH = 7.0) with 100 mM NaCl supporting electrolyte that had been purged for 1 hr N_2. Scans were swept between -0.4 V and 0.9 V at 30 mV/s using an Interface 1000 potentiostat (Gamry Instruments; Warminster, PA USA).

3.3.4 Morphological Characterization of PDA Films

Film thicknesses and morphology were measured using atomic force microscopy (NT-MDT NTegra AFM; Tempe, AZ) in tapping mode. Large range scans were 9 x 9 μm^2 at 0.8 Hz

(NT-MDT NTegra AFM; Tempe, AZ; k = 25-95 N/m, tip radius = 35 nm). High resolution scans were recorded at areas of 0.9 x 0.9 μm^2 at 2 Hz (Budget Sensors; k = 5 N/m, tip radius <1 nm). Film thickness was determined by scratching the films and measuring the height profile with AFM.[3]

3.4 Results and Discussion

3.4.1 Alkaline calcium solutions promote oxidation of PDA films and generation of DHI radicals

Oxidative chemical synthesis of PDA films from dopamine is a complex multi-step process (Scheme 3.2) that includes redox processes, cyclization, polymerization, and various cleavage reactions that may serve as control points for altering the composition of PDA.[1,8,18] Although the precursors are relatively simple, multiple different possible reaction pathways quickly increase the diversity of products. The rate limiting step is the first $1e^-$ oxidation of deprotonated catechol by molecular O_2 to produce dopamine-semiquinone and O_2^{-}.[1] The semiquinone is oxidized again by O_2 to produce dopamine-quinone, which can then undergo intramolecular cyclization. Subsequent oxidation steps and intramolecular rearrangements produce various heterocyclic species.[8,18,19] H_2O_2 generated upon oxidation of the catechol groups by O_2^- can also generate pyrrole-carboxylic acids by cleaving 5,6-dihydroxyindole units.[8,20] Reactive monomers produced during the dopamine oxidation pathway oligomerize (observed up to the octamer level[8,18]) and aggregate into disordered graphite-like nanostructures.[21] The resulting PDA has a stable population of free radicals (ca. 1 radical per 1700 monomers[22]) that depends on the buffer used during PDA synthesis.[9]

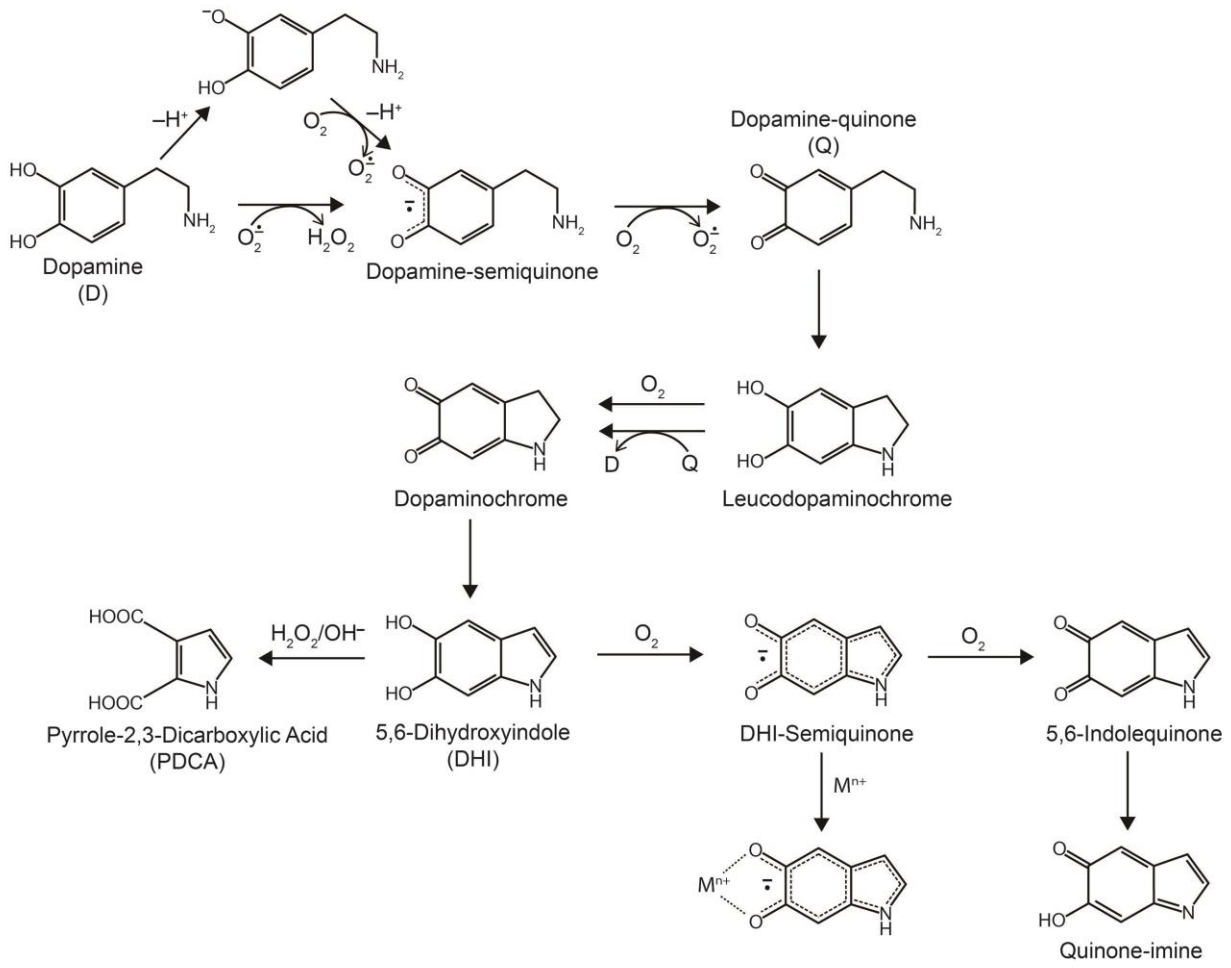

Scheme 3.2: Oxidation pathway of dopamine in alkaline solutions exposed to O_2. The proposed structure of PDA consists of oligomers of all species shown.

Freshly-synthesized PDA films and particles are partially oxidized and contain species from all stages of the dopamine oxidation pathway.[8,18] Although the microstructure of PDA is largely static, the chemical composition (and subsequent physical properties) of PDA films evolves continuously over their lifetime as constituent molecules are exposed to controlled conditions after film deposition or *de facto* post-processing conditions via the ambient environment. The *in situ* chemical evolution of PDA films incubated in $CaCl_2$ solutions was monitored via UV-Vis spectroscopy. The difference in the spectra of the PDA films from the initial recording (ΔA = Abs(t) – Abs(0 min); Figure 3.1) reveal two distinct peaks at λ_{Abs} = 337

nm and λ_{Abs} = 487 nm that develop over several hours (henceforth designated as ΔA_{337nm} and ΔA_{487nm}). The ΔA_{337nm} and ΔA_{487nm} peaks are assigned to DHI-semiquinone species based on

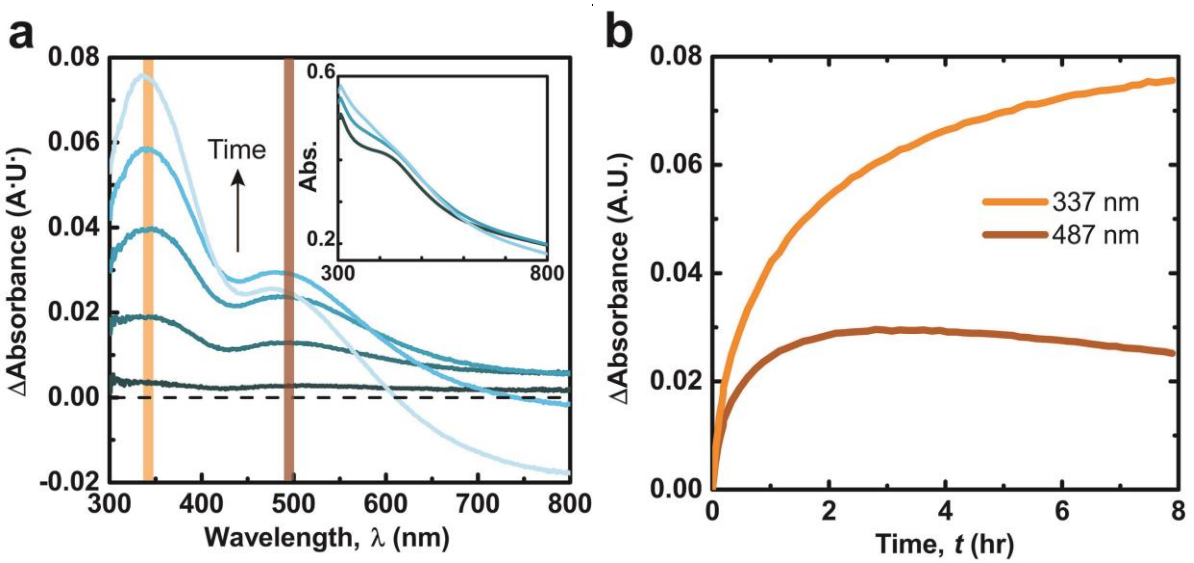

Figure 3.1: a) Subtracted UV-Vis spectra of PDA film in 300 mM $CaCl_2$, 50 mM Tris buffer pH = 9.5. Inset: Original spectra. b) Absorbance at the designated wavelengths over time (spectra recorded every 83 s).

peak positions and dependence on incubation conditions. While the positions of the two observed peaks are comparable to dopaminochrome (λ_{Abs} = 300 nm and λ_{Abs} = 476 nm),[23] they are in closer agreement to DHI-semiquinone (λ_{Abs} = 330 nm and λ_{Abs} = 490 nm).[24] Additionally, ΔA_{337nm} and ΔA_{487nm} increase when Ca^{2+} is present in the solution (Figure 2a). Ca^{2+} ions bias the comproportionation equilibrium towards greater radical concentration in catecholic systems.[14,25,26] Ca^{2+} ions also associate with and stabilize semiquinone radicals, as has been observed for various multivalent cations in DHI-rich[27] eumelanin.[28]

The temporal evolution of PDA film composition is likely due to altered oxidative mechanisms induced by Ca^{2+} cations. The hour long time scales for the DHI-semiquinone generation in $CaCl_2$-incubated PDA films (Figure 1b) suggest an oxygen kinetic limitation, considering that the autoxidation of dopamine solutions occurs on similar time scales.[1,2] Ca^{2+}

ions accelerate the oxygen consumption of solutions of pyrocatechol and dopamine,[14,25,26] which is attributed to Ca^{2+}-mediated deprotonation of the catechol group and subsequent $1e^-$ oxidation by O_2.[25] The proportional increase of ΔA_{337nm} and ΔA_{487nm} with [$CaCl_2$] and pH further support

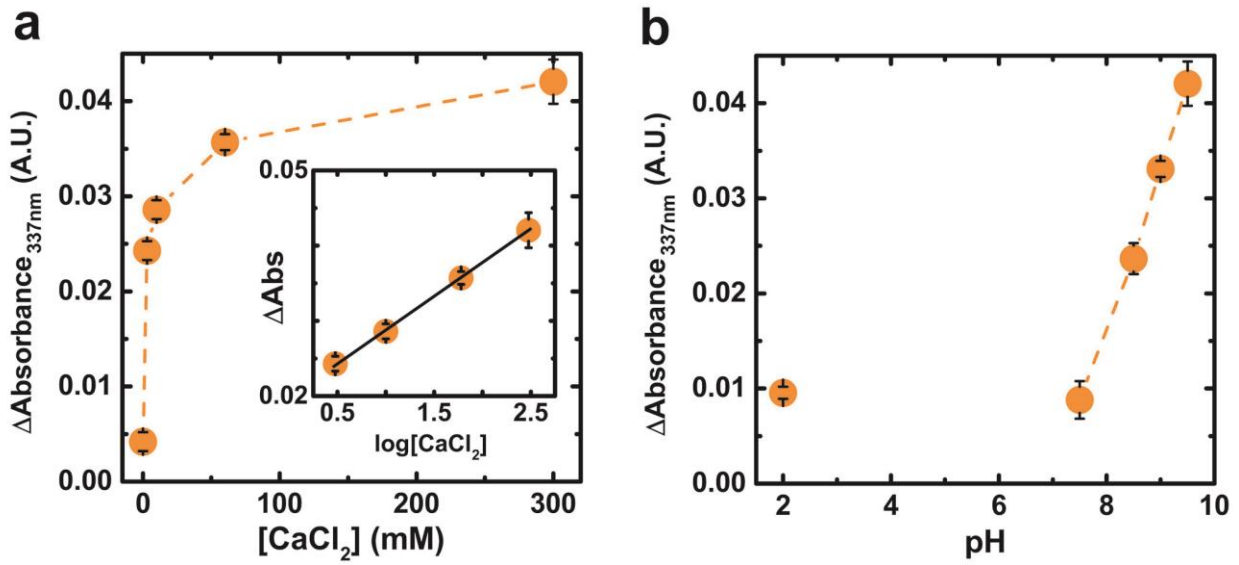

Figure 3.2: a) Subtracted spectra absorbance at λ_{Abs} = 337 nm after 1 hr as a function of [$CaCl_2$] in 50 mM Tris buffer pH = 9.5. b) Subtracted spectra absorbance after 1 hr as a function of pH in 300 mM $CaCl_2$, 50 mM Tris buffer. See Figure S4 for equivalent data at λ_{Abs} = 487 nm. Data are represented as the average ± std. dev. (n = 2).

this proposed catechol-cation interaction (Figure 3.2). The increase in ΔA_{337nm} between pH = 7.5 and 9.5 indicates an underlying mechanism dependent on catechol deprotonation (pK_a ~ 9).[29] Interestingly, the semiquinone population in melanins increases at pH > 7 in a similar manner to the absorbance behavior observed in Figure 3.2b[30,31] further supporting the assignment of ΔA_{337nm} and ΔA_{487nm} to DHI-semiquinone.

Aqueous solutions of redox-inactive cations can be used as post-processing buffers to control the composition of PDA films. Alkaline NaCl solutions accelerate oxidation of pre-deposited PDA films compared to Tris buffer alone (Figure 3.3a). The spectra recorded from films incubated in NaCl solutions exhibit suppressed absorbance values and less-defined peaks compared to PDA films incubated in $CaCl_2$, which is likely due to relatively weak bonding of

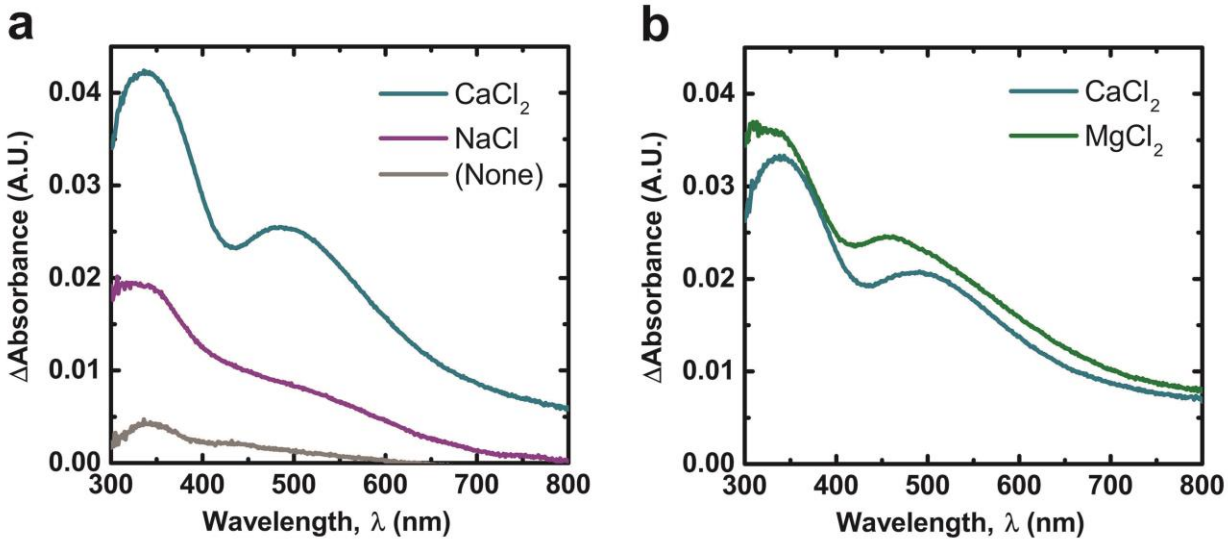

Figure 3.3: a) Subtracted spectra after 1 hr in 300 mM of indicated salt + 50mM Tris buffer pH 9.5. b) Subtracted spectra after 1 hr in 300 mM of indicated salt + 50mM Tris buffer pH 9.0. Spectra are averages of two samples.

monovalent cations with catechols compared to divalent cations. Films incubated in alkaline $MgCl_2$ solutions, in contrast to NaCl, do produce a spectrum of similar intensity to $CaCl_2$ (Figure 3.3b). There are two weak convoluted peaks at ca. λ_{Abs} = 458 nm and 310 nm which suggests a slightly different distribution of oxidation products compared to films in $CaCl_2$ solutions. Overall, the accelerated spectral evolution of PDA films in the presence of NaCl, $MgCl_2$, and $CaCl_2$ solutions show that redox-inactive cations modify the constituent molecules in PDA films.

Cation-mediated oxidation of PDA films is supported by cyclic voltammetry (Figure 3.4). The midpoint between the onset of the oxidation and reduction curves in the voltammogram is approximately 180 mV (vs Ag/AgCl), consistent with a dopamine/quinone redox couple at pH = 7.0.[23] The films incubated in 300 mM $CaCl_2$ solutions (pH = 9.5) exhibited a total oxidative charge transfer only 56% of that of films incubated in equivalent pH without $CaCl_2$ (4.85 mC vs. 8.70 mC, respectively). The decrease in reversible oxidation capacity could result from damage to the films and a corresponding reduction in film thickness. However, the thickness of PDA films is largely constant before and after $CaCl_2$ incubation (59 ± 3 nm before, 61 ± 6 nm after).

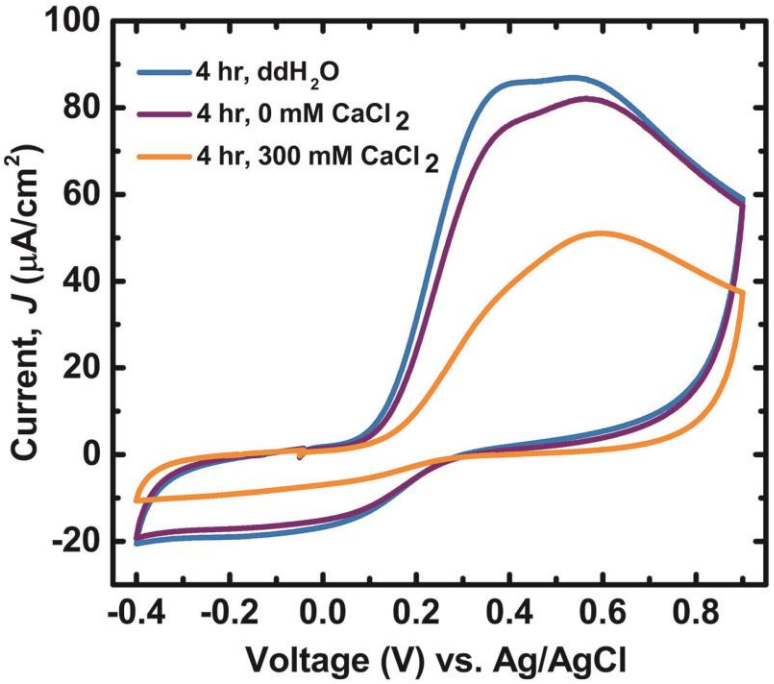

Figure 3.4: First cycle voltammograms of PDA films that were incubated for 4 hours in either ddH_2O, 0 mM $CaCl_2$ 50mM Tris buffer pH = 9.5, or 300 mM $CaCl_2$ 50mM Tris buffer pH = 9.5. Electrolyte consisted of 180 mM sodium diphosphate – citric acid buffer and 100 mM NaCl at pH = 7.0. Scan rate was 30 mV/s.

Therefore, the relative decrease in oxidative charge transfer in PDA films incubated in $CaCl_2$ solutions compared to those incubated without $CaCl_2$ is direct evidence that Ca^{2+} ions promote oxidation of PDA.

3.4.2 Alkaline calcium solutions generate carboxylic acid groups in PDA and lower the isoelectric point

The altered molecular composition of PDA exposed to redox-inactive cations has important implications for PDA's function as a metal sorption material.[10,11-13] The $2e^-$ oxidation of DHI produces 5,6-indolequinone which can tautomerize to quinone-imine or quinone-methide.[37,38] Also, H_2O_2 in alkaline solutions – generated during dopamine oxidation – can transform DHI species into pyrrole scaffolds with pendant carboxylates.[8] Quinone-imine and carboxylates may compete with catechols for metal cations[46] and increase binding capacity in

PDA since $pK_{a,quinone\text{-}imine,\ carboxylate} < pK_{a,dopamine}$. These species also contribute negative space charges in PDA films that can affect ion transport within the film.[39,40]

The Ca^{2+}-induced oxidation of PDA films generates carboxylic acid groups, as confirmed by ATR–FTIR spectroscopy (Figure 3.5). The two peaks in the 1600–1500 cm^{-1} region for PDA

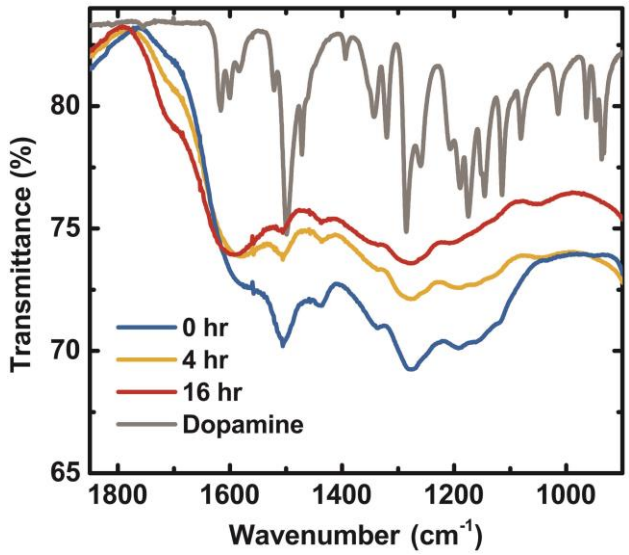

Figure 3.5: ATR-FTIR spectra of PDA films that were incubated in 300 mM $CaCl_2$ 50mM Tris buffer pH = 9.5 for the designated times. Also shown is the spectrum of dopamine hydrochloride stock powder, scaled and shifted for clarity.

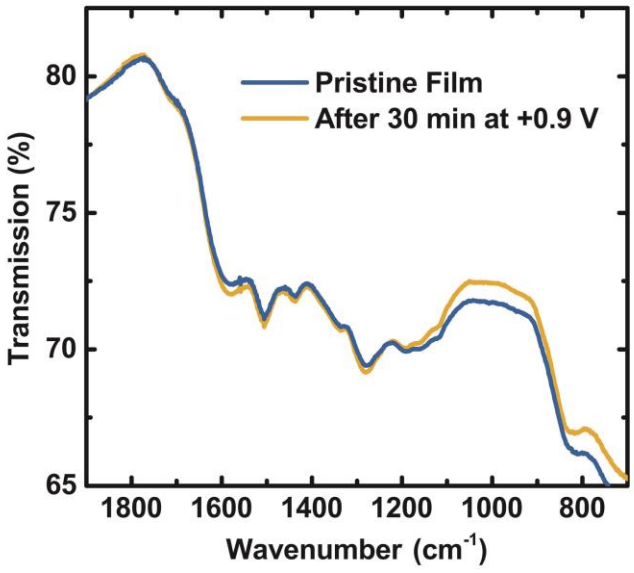

Figure 3.6: ATR-FTIR spectra of pristine PDA film before and after applied voltage of +0.9 V for 30 min at pH = 7.

are assigned to aromatic C=C vibrations.[41] The overlap of peaks in PDA and dopamine, centered about 1500 cm^{-1} and 1285 cm^{-1}, are attributed to uncyclized dopamine in PDA. Incubating PDA in $CaCl_2$ solutions lowers the relative intensity of the 1500 cm^{-1} and 1285 cm^{-1} peaks, which is consistent with oxidation and cyclization of residual dopamine. A shoulder at ca. 1700 cm^{-1} increases with increasing incubation time, which could be attributed to either pyrrole carboxylic acids or quinone moieties, both of which are oxidation products of dopamine. However, the intensity of the 1700 cm^{-1} shoulder was preserved after the electrochemical generation of quinone moieties (0.9 V vs Ag/AgCl for 30 min) (Figure 3.6). Unlike electrochemical oxidation, molecular O_2-induced oxidation of catechols produces H_2O_2 which can convert PDA into pyrrole carboxylic acids.[8] Therefore, the increase in intensity of this vibration in the alkaline $CaCl_2$-incubated films is attributed to pyrrole carboxylic acids. The aforementioned changes in features observed in IR spectra with increasing time in alkaline $CaCl_2$ solution are comparable to those observed in PDA created from dopamine with increasing concentrations of chemical oxidant.[5] This congruence further supports the interpretation that Ca^{2+} cations promote *in situ* oxidative maturation of PDA films.

The formation of pyrrole carboxylic acid groups as a mature oxidation product in $CaCl_2$-oxidized PDA films is further supported by zeta potential measurements. The zeta potential of pristine PDA is negative above pH = 4 and becomes less negative as the pH is decreased (Figure 3.7). Catechol and amine groups in the PDA films are fully protonated at pH = 7.[29] Therefore, the loss of negative surface charge below pH = 7.0 in pristine PDA is attributed to protonation of a variety of other species such as quinone imine (pK_a: 6.3), or pyrrole carboxylic acids. The primary amines on uncyclized dopamine incorporated in PDA films also contribute to the net positive ζ at pH < 4. The average isoelectric point of pH = 4.0 ± 0.2 for the three samples agrees

with a previous report.[42] The value of ζ becomes more negative as PDA films are incubated in 300 mM $CaCl_2$ solutions resulting in a lowered average isoelectric point of 3.1 ± 0.3. A new inflection point appears around pH = 4.5 below which ζ becomes less negative. The pH value of this inflection point suggests protonation of carboxylic acid moieties, while the absence of an

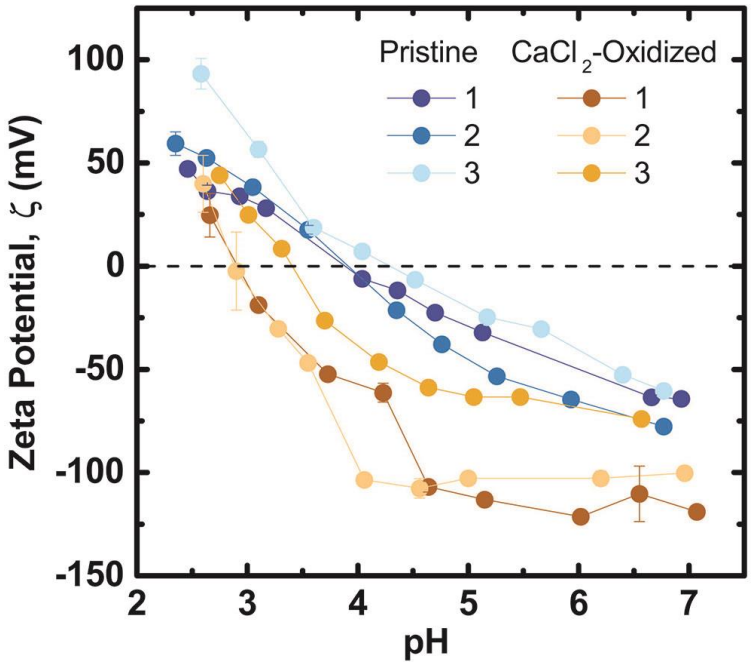

Figure 3.7: Zeta potential titrations of pristine PDA films and PDA films that were incubated in 300 mM $CaCl_2$ 50mM Tris buffer pH = 9.5 for 4 hours. Numbers 1-3 designate unique samples.

inflection point at pH = 6.3 suggests that quinone-imine species do not contribute significantly to ζ for $CaCl_2$-oxidized PDA films.[42] The more negative surface charge in oxidized PDA films is therefore attributed to pyrrole carboxylic acid groups, which are known downstream products of PDA oxidation.[8]

3.4.3 Films incubated in alkaline $CaCl_2$ solutions exhibit enhanced iron chelation

The altered molecular composition of $CaCl_2$-oxidized PDA films increases iron chelation as measured by Raman spectroscopy. Raman spectroscopy can identify iron-catechol chelates in *Sepia* melanin[43] and mussel byssal threads[44] which contain equivalent structural components

(dihydroxyindoles and catecholamines) to PDA. The spectrum of PDA (Figure 3.9) is dominated by two broad convoluted peaks at ca. 1360 cm^{-1} and 1570 cm^{-1} which are characteristic of disordered aromatic carbon materials.[45] Deconvolution of the region between 1050 – 1800 cm^{-1}

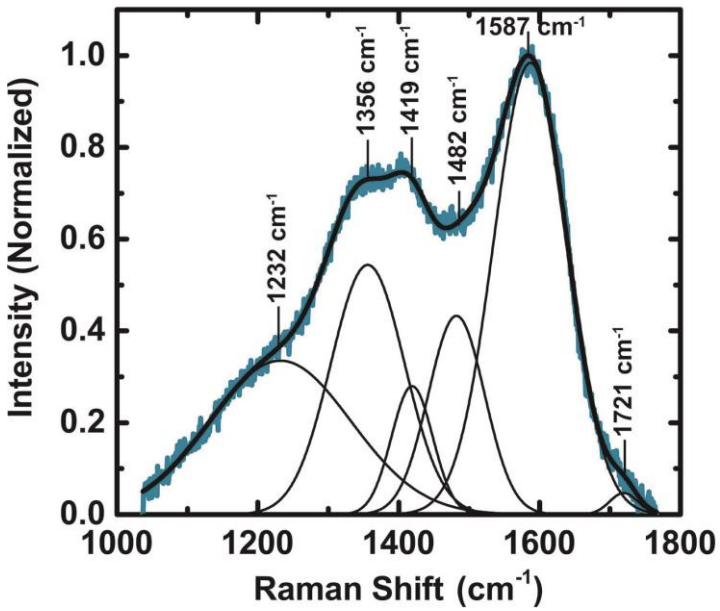

Figure 3.8: Deconvoluted Raman spectrum of PDA film.

revealed 6 component vibrational bands similar to that of eumelanin (Figure 3.8).[46,47] The two most prominent bands centered at 1587 cm^{-1} and 1356 cm^{-1} are assigned to the in-plane parallel displacement of sp^2-bonded carbons ("G band") and the breathing vibration of 6-carbon aromatic rings ("D band"), respectively.[45] The overall spectra and individual components of the deconvoluted spectra are observed in various disordered aromatic carbon materials such as humic acids and carbonized biopolymers.[48–51] Also present in the Raman spectrum of PDA is a low intensity band centered at 460 cm^{-1}, which is attributed to torsion of –OH groups in catechols.[43,52]

$CaCl_2$-oxidized PDA films exhibit clear enhanced iron chelation after incubation in iron solutions (Figures 3.9, 3.10). The Raman spectra of pristine films remain unchanged before and

after incubation in all iron solutions. Conversely, $CaCl_2$-oxidized PDA films generate two features: a new band at 555 cm^{-1}; an increase in intensity at 1482 cm^{-1}. These signatures observed in PDA are also detected in *Sepia* melanin.[43] When *Sepia* melanin is enriched with Fe^{3+} a new band appears at 570 cm^{-1} with similar intensity to the 460 cm^{-1} band, and the intensity increases in the convoluted 1470 cm^{-1} region.

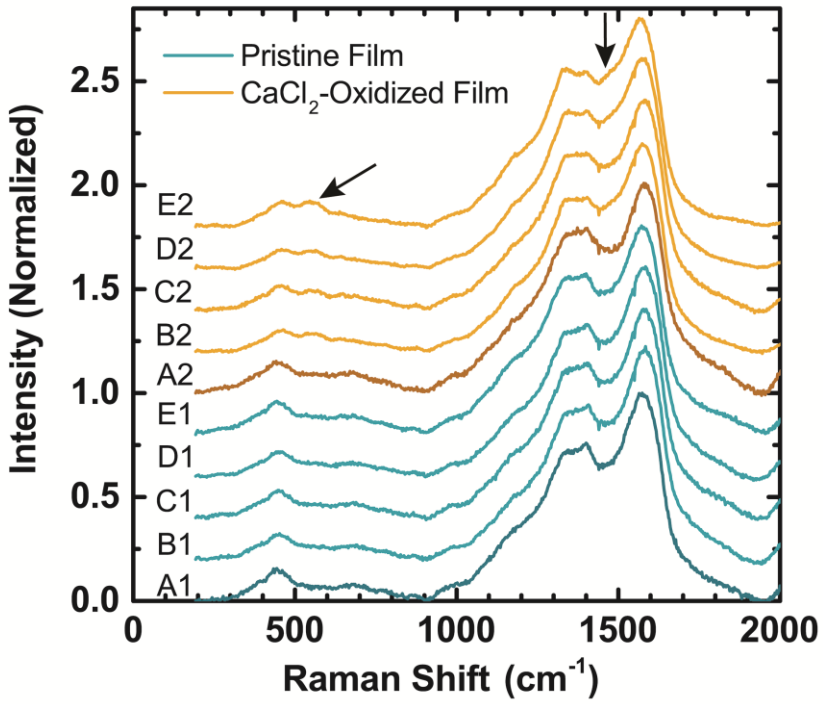

Figure 3.9: Raman spectra of PDA films before and after incubating in 5 mM iron solutions for 100 min. A) Films with no iron exposure. B) $FeCl_3$ pH = 2.6 C) $FeCl_2$ pH = 2.6 D) $FeCl_2$ pH = 4.1 E) $FeCl_2$ pH = 5.1

The two intensified bands imply that $CaCl_2$-oxidized PDA films exhibit increased iron chelation capacity compared to pristine counterparts. The chelate vibrations of Fe-enediolate complexes are observed in the 500 cm^{-1}– 600 cm^{-1} region in a variety of systems.[44,53–55] The 555 cm^{-1} band is assigned to the 5-membered chelate ring of catechol moieties bound to iron in PDA. Additionally, a band between 1480 – 1490 cm^{-1} is also indicative of catecholic chelates with iron in solution or nanoparticle surfaces. [55–58] The intensity of the 1482 cm^{-1} band (Figure 3.11)

follows the same trend with pH and film condition as the 555 cm^{-1} band (Figure 3.10), indicating that both bands serve as indicators of increased iron chelation capacity in $CaCl_2$-oxidized films compared to pristine PDA films.

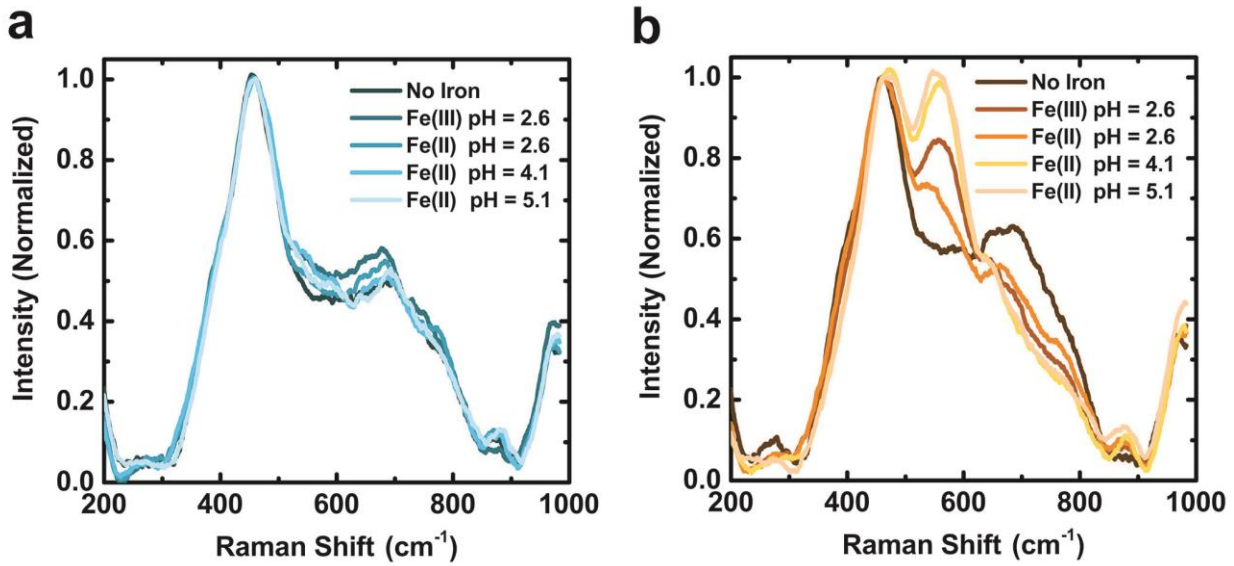

Figure 3.10: Raman spectra of PDA films before and after incubation in 5 mM iron chloride solutions for 100 min. a) Pristine PDA films. b) PDA films that were incubated in in 300 mM $CaCl_2$ 50mM Tris buffer pH = 9.5 for 4 hours. The band centered at 460 cm^{-1} corresponds to –OH torsion. The band at 555 cm^{-1} visible in (b) is due to vibration of the five-membered chelate ring of iron with catechol.

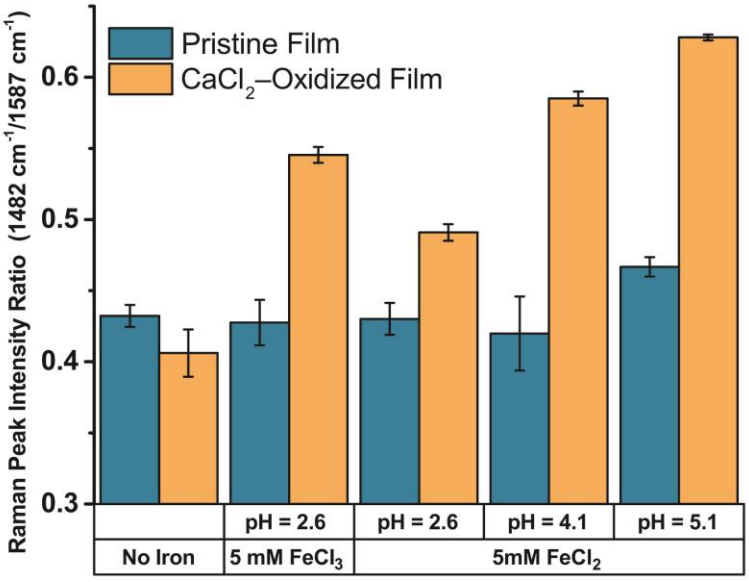

Figure 3.11: Ratio of the intensity of the 1482 cm^{-1} peak to the 1587 cm^{-1} peak for PDA films before and after incubating in 5 mM iron solutions for 100 min. Standard error bars are for 5 measurements on each sample.

Elevated iron chelation capacity in $CaCl_2$-oxidized films is attributed to several factors. Previous electrochemical studies on PDA films have revealed that at pH < 4, PDA films are impermeable to multivalent cations due to a net positive charge in the film.[39,40] Pristine films exhibit more positive zeta potentials compared to $CaCl_2$-oxidized films which could account for the lack of detectable iron chelation in pristine films. However, altered surface charges cannot fully account for the differences in iron chelation as iron chelation is observed in $CaCl_2$-oxidized films at pH = 2.6 where $\zeta > 0$, and not observed in pristine PDA films at pH = 5.1 where $\zeta < 0$. The most significant factor affecting iron chelation is likely the difference in iron-binding affinity between dopamine and DHI units. Alkaline solutions of $CaCl_2$ bias the products of the PDA synthetic pathway towards downstream products including DHI. Furthermore, DHI has a higher binding affinity for Fe^{3+} between pH 3 – 10 compared to free dopamine.[59] Finally, bis-coordinated catechol-Fe^{3+} species from catechol-bearing DHI are stable over a wider pH range for DHI compared to catechol-bearing dopamine. Taken together, the increase in Fe^{3+} binding affinity is therefore primarily attributed to increased concentrations of DHI in post-processed PDA films.

The evolution of both carboxylic acids and DHI as downstream oxidation products in $CaCl_2$-oxidized PDA suggests that the functional properties of PDA films can be controlled by post-processing. Ion exchange studies on *Sepia* melanin revealed that Mg^{2+} and Ca^{2+} cations have a greater passive affinity for carboxylic acid groups in melanin compared to catechol groups, and the converse for Fe^{3+}.[60] Therefore, $CaCl_2$-induced oxidation of PDA may increase PDA's passive affinity for group II/I cations while simultaneously enhancing binding of Fe^{3+} via DHI units. This is in contrast to a more actively-controlled (i.e. electrically biased) affinity for group II cations in pristine PDA films.[35] Additionally, cation transport through PDA films can be

enhanced by more carboxylic acid groups, as discussed previously in the context of more negative zeta potential of the films.[39,40] Therefore, post-processing of PDA films can potentially be used to modulate the metal sorption properties of PDA films for application specific coatings. Prospective applications include novel ion-exchange membranes or separation layers for electrochemical storage systems.[33–35,61]

3.5 Conclusions

Redox-inactive metal cations can bias oxidative dopamine pathways to produce downstream products in PDA films (e.g. DHI and pyrrole carboxylic acids as opposed to dopamine). The enhanced iron chelating ability of the oxidized PDA films is attributed to a more negative zeta potential and greater binding affinity for Fe^{3+} in catechols found in DHI compared to dopamine. These results emphasize the practical considerations and limitations associated with the non-equilibrium state and heterogeneity of pristine PDA films. Technological translation of PDA films must account for the evolution of PDA's chemical behavior over time in different environmental conditions. PDA's heterogeneity also enables a broad range of control over its properties, and group I/II cation solutions can act as a post-processing strategy to tune the chemical composition of PDA films. The balance between upstream products such as non-cyclized dopamine can be balanced with downstream products such as DHI. This technique could improve reproducibility and ultimately accelerate the use of PDA as a functional material.

3.6 References

(1) Herlinger, Erwin; Jameson, Reginald F.; Linert, W. Spontaneous Autoxidation of Dopamine. *J. Chem. Soc., Perkin Trans. 2* **1995**, 259–263.

(2) Ball, V.; Frari, D. Del; Toniazzo, V.; Ruch, D. Kinetics of Polydopamine Film Deposition as a Function of pH and Dopamine Concentration: Insights in the Polydopamine Deposition Mechanism. *J. Colloid Interface Sci.* **2012**, *386*, 366–372.

(3) Klosterman, L.; Riley, J. K.; Bettinger, C. J. Control of Heterogeneous Nucleation and Growth Kinetics of Dopamine-Melanin by Altering Substrate Chemistry. *Langmuir* **2015**, *31*, 3451–3458.

(4) Bernsmann, F.; Ball, V.; Ponche, A.; Michel, M.; Gracio, D. A.; Ruch, D. Dopamine - Melanin Film Deposition Depends on the Used Oxidant and Buffer Solution. *Langmuir* **2011**, *27*, 2819–2825.

(5) Ponzio, F.; Barthes, J.; Bour, J.; Michel, M.; Bertani, P.; Hemmerlé, J.; D'Ischia, M.; Ball, V. Oxidant Control of Polydopamine Surface Chemistry in Acids: A Mechanism-Based Entry to Superhydrophilic-Superoleophobic Coatings. *Chem. Mater.* **2016**, *28*, 4697–4705.

(6) Bernsmann, F.; Voegel, J. C.; Ball, V. Different Synthesis Methods Allow to Tune the Permeability and Permselectivity of Dopamine-Melanin Films to Electrochemical Probes. *Electrochim. Acta* **2011**, *56*, 3914–3919.

(7) Del Frari, D.; Bour, J.; Ball, V.; Toniazzo, V.; Ruch, D. Degradation of Polydopamine Coatings by Sodium Hypochlorite: A Process Depending on the Substrate and the Film Synthesis Method. *Polym. Degrad. Stab.* **2012**, *97*, 1844–1849.

(8) Della Vecchia, N. F.; Avolio, R.; Alfè, M.; Errico, M. E.; Napolitano, A.; D'Ischia, M. Building-Block Diversity in Polydopamine Underpins a Multifunctional Eumelanin-Type Platform Tunable through a Quinone Control Point. *Adv. Funct. Mater.* **2013**, *23*, 1331–1340.

(9) Della Vecchia, Nicola Fyodor; Luchini, Alessandra; Napolitano, Alessandra; D'Errico, Gerardino; Vitiello, Giuseppe; Szekely, Noemi; d'Ischia, Marco; Paduano, L. Tris Buffer Modulates Polydopamine Growth, Aggregation, and Paramagnetic Properties. *Langmuir* **2014**, *30*, 9811–9818.

(10) Ryu, J.; Ku, S. H.; Lee, H.; Park, C. B. Mussel-Inspired Polydopamine Coating as a Universal Route to Hydroxyapatite Crystallization. *Adv. Funct. Mater.* **2010**, *20*, 2132–2139.

(11) Proks, V.; Brus, J.; Pop-Georgievski, O.; Večerníková, E.; Wisniewski, W.; Kotek, J.; Urbanová, M.; Rypáček, F. Thermal-Induced Transformation of Polydopamine Structures: An Efficient Route for the Stabilization of the Polydopamine Surfaces. *Macromol. Chem. Phys.* **2013**, *214*, 499–507.

(12) Kim, S.; Gim, T.; Kang, S. M. Stability-Enhanced Polydopamine Coatings on Solid Substrates by iron(III) Coordination. *Prog. Org. Coatings* **2014**, *77*, 1336–1339.

(13) Lim, C.; Huang, J.; Kim, S.; Lee, H.; Zeng, H.; Hwang, D. S. Nanomechanics of Poly(catecholamine) Coatings in Aqueous Solutions. *Angew. Chemie - Int. Ed.* **2016**, *55*, 3342–3346.

(14) Lebedev, a. V.; Ivanova, M. V.; Ruuge, E. K. Calcium-Dioxolene Complexes: Rate Constants of Pyrocatechol Oxidation in the Presence of Ca2+. *Biophysics (Oxf).* **2011**, *56*, 188–193.

(15) Misawa, T. The Thermodynamic Consideration for Fe-H2O System at 25°C. *Corros. Sci.* **1973**, *13*, 659–676.

(16) Hoggard, J. D.; Sides, P. J.; Prieve, D. C. Measurement of the Streaming Potential and Streaming Current near a Rotating Disk to Determine Its Zeta Potential. *Langmuir* **2005**, *21*, 7433–7438.

(17) Aigen, Sam; Saiget, Tom; Sides, P. J. ZetaSpin: A Revolution in Zeta Potential Measurement https://www.andrew.cmu.edu/course/39-801/index.html (accessed Jul 20, 2016).

(18) Liebscher, J.; Mrówczyński, R.; Scheidt, H. a; Filip, C.; Hădade, N. D.; Turcu, R.; Bende, A.; Beck, S. Structure of Polydopamine: A Never Ending Story? *Langmuir* **2013**, *29*, 10539–10548.

(19) Hong, S.; Na, Y. S.; Choi, S.; Song, I. T.; Kim, W. Y.; Lee, H. Non-Covalent Self-Assembly and Covalent Polymerization Co-Contribute to Polydopamine Formation. *Adv. Funct. Mater.* **2012**, *22*, 4711–4717.

(20) Munoz-Munoz, J. L.; García-Molina, F.; Varón, R.; Tudela, J.; García-Cánovas, F.; Rodríguez-López, J. N. Generation of Hydrogen Peroxide in the Melanin Biosynthesis Pathway. *Biochim. Biophys. Acta* **2009**, *1794*, 1017–1029.

(21) Gracio, J. D. A.; Singh, Â. M. K.; Ruch, D.; Buehler, M. J.; Al, C. E. T.; Ball, V. Self-Assembly of Tetramers of 5,6-Dihydroxyindole Explains the Primary Physical Properties of Eumelanin: Experiment, Simulation, and Design. *ACS Nano* **2013**, 1524–1532.

(22) Mrówczyński, R.; Coy, L. E.; Scheibe, B.; Czechowski, T.; Augustyniak-Jabłokow, M.; Jurga, S.; Tadyszak, K. Electron Paramagnetic Resonance Imaging and Spectroscopy of Polydopamine Radicals. *J. Phys. Chem. B* **2015**, *119*, 10341–10347.

(23) Zhang, F.; Dryhurst, G. Oxidation Chemistry of Dopamine: Possible Insights into the Age-Dependent Loss of Dopaminergic Nigrostriatal Neurons. *Bioorg. Chem.* **1993**, *21*, 392–410.

(24) Lambert, C.; Chacon, J. N.; Chedekel, M. R.; Land, E. J.; Riley, P. A.; Thompson, A.; Truscott, T. G. A Pulse Radiolysis Investigation of the Oxidation of Indolic Melanin Precursors: Evidence for Indolequinones and Subsequent Intermediates. *Biochim. Biophys. Acta* **1989**, *993*, 12–20.

(25) Lebedev, A. V; Ivanova, M. V; Timoshin, A. a; Ruuge, E. K. Effect of Group II Metal Cations on Catecholate Oxidation. *Chemphyschem* **2007**, *8*, 1863–1869.

(26) Lebedev AV , Ivanova MV , Timoshin AA, R. E. Effect of Calcium Cations on Acid-Base Properties and Free Radical Oxidation of Dopamine and Pyrocatechol. *Biomed. Khim.* **2008**, *54*, 687–695.

(27) Meredith, P.; Sarna, T. The Physical and Chemical Properties of Eumelanin. *Pigment Cell Res.* **2006**, *19*, 572–594.

(28) Felix, C. C.; Hyde, J. S.; Sarna, T.; Sealy, R. C. Interactions of Melanin with Metal Ions. Electron Spin Resonance Evidence for Chelate Complexes of Metal Ions with Free Radicals. *J. Am. Chem. Soc.* **1978**, *100*, 3922–3926.

(29) Ishimitsu, T.; Hirose, S.; Sakurai, H. Microscopic Acid Dissociation Constants of 3,4-Dihydroxyphenethylamine (Dopamine). *Chem. Pharm. Bull.* **1978**, *26*, 74–78.

(30) Mostert, a. B.; Powell, B. J.; Pratt, F. L.; Hanson, G. R.; Sarna, T.; Gentle, I. R.; Meredith, P. Role of Semiconductivity and Ion Transport in the Electrical Conduction of Melanin. *Proc. Natl. Acad. Sci.* **2012**, *109*, 8943–8947.

(31) Chio, S. S.; Hyde, J. S.; Sealy, R. C. Paramagnetism in Melanins: pH Dependence. *Arch. Biochem. Biophys.* **1982**, *215*, 100–106.

(32) Ryu, J.; Ku, S. H.; Lee, H.; Park, C. B. Mussel-Inspired Polydopamine Coating as a Universal Route to Hydroxyapatite Crystallization. *Adv. Funct. Mater.* **2010**, *20*, 2132–2139.

(33) Lee, M.; Rho, J.; Lee, D. E.; Hong, S.; Choi, S. J.; Messersmith, P. B.; Lee, H. Water Detoxification by a Substrate-Bound Catecholamine Adsorbent. *Chempluschem* **2012**, *77*, 987–990.

(34) Farnad, N.; Farhadi, K.; Voelcker, N. H. Polydopamine Nanoparticles as a New and Highly Selective Biosorbent for the Removal of Copper (II) Ions from Aqueous Solutions. *Water, Air, Soil Pollut.* **2012**, *223*, 3535–3544.

(35) Park, Hang-Ah; Kim, Young Jo; Kwon, Ik Soo; Klosterman, Luke; Bettinger, C. J. Lithium Purification from Aqueous Solutions Using Bioinspired Redox Active Melanin Membranes. *Polym. Int.* **2016**.

(36) Gao, H.; Sun, Y.; Zhou, J.; Xu, R.; Duan, H. Mussel-Inspired Synthesis of Polydopamine-Functionalized Graphene Hydrogel as Reusable Adsorbents for Water Purification. *ACS Appl. Mater. Interfaces* **2013**, *5*, 425–432.

(37) Szpoganicz, B.; Gidanian, S.; Kong, P.; Farmer, P. Metal Binding by Melanins: Studies of Colloidal Dihydroxyindole-Melanin, and Its Complexation by Cu(II) and Zn(II) Ions. *J. Inorg. Biochem.* **2002**, *89*, 45–53.

(38) d'Ischia, M.; Napolitano, A.; Pezzella, A.; Land, E. J. . R.; C. A.; Riley, P. A. 5,6-Dihydroxyindoles and Indole-5,6-Diones. *Adv. Heterocycl. Chem.* **2005**, *89*, 1–63.

(39) Yu, B.; Liu, J.; Liu, S.; Zhou, F. Pdop Layer Exhibiting Zwitterionicity: A Simple Electrochemical Interface for Governing Ion Permeability. *Chem. Commun. (Camb).* **2010**, *46*, 5900–5902.

(40) Gao, B.; Su, L.; Tong, Y.; Guan, M.; Zhang, X. Ion Permeability of Polydopamine Films Revealed Using a Prussian Blue-Based Electrochemical Method. *J. Phys. Chem. B* **2014**, *118*, 12781–12787.

(41) Gunasekaran, S.; Kumar, R. T.; Ponnusamy, S. Vibrational Spectra and Normal Coordinate Analysis of Adrenaline and Dopamine. *Indian J. Pure Appl. Phys.* **2007**, *45*, 884–892.

(42) Ball, V. Impedance Spectroscopy and Zeta Potential Titration of Dopa-Melanin Films Produced by Oxidation of Dopamine. *Colloids Surfaces A Physicochem. Eng. Asp.* **2010**, *363*, 92–97.

(43) Samokhvalov, A.; Liu, Y.; Simon, J. D. Characterization of the Fe(III)-Binding Site in Sepia Eumelanin by Resonance Raman Confocal Microspectroscopy. *Photochem. Photobiol.* **2004**, *80*, 84–88.

(44) Harrington, M. J.; Masic, A.; Holten-andersen, N.; Waite, J. H.; Fratzl, P. Iron-Clad Fibers : A Metal-Based Biological Strategy for Hard Flexible Coatings. *Science* **2010**, 216–220.

(45) Ferrari, a.; Robertson, J. Interpretation of Raman Spectra of Disordered and Amorphous Carbon. *Phys. Rev. B* **2000**, *61*, 14095–14107.

(46) Capozzi, V.; Perna, G.; Gallone, a.; Biagi, P. F.; Carmone, P.; Fratello, a.; Guida, G.; Zanna, P.; Cicero, R. Raman and Optical Spectroscopy of Eumelanin Films. *J. Mol. Struct.* **2005**, *744-747*, 717–721.

(47) Albano, L. G. S.; Di Mauro, E.; Kumar, P.; Cicoira, F.; Graeff, C. F. O.; Santato, C. Novel Insights on the Physicochemical Properties of Eumelanins and Their DMSO Derivatives. *Polym. Int.* **2016**.

(48) Sevilla, M.; Fuertes, A. B. Chemical and Structural Properties of Carbonaceous Products Obtained by Hydrothermal Carbonization of Saccharides. *Chem. - A Eur. J.* **2009**, *15*, 4195–4203.

(49) John, K. J.; Manoj, B. Raman Spectroscopy Investigation of Camphor Soot : Spectral Analysis and Structural Information. *Int. J. Electrochem. Sci.* **2013**, *8*, 9421–9428.

(50) Sánchez-Cortés, S.; Francioso, O.; Ciavatta, C.; García-Ramos, J. V.; Gessa, C. pH-Dependent Adsorption of Fractionated Peat Humic Substances on Different Silver Colloids Studied by Surface-Enhanced Raman Spectroscopy. *J. Colloid Interface Sci.* **1998**, *198*, 308–318.

(51) Sevilla, M.; Fuertes, a. B. The Production of Carbon Materials by Hydrothermal Carbonization of Cellulose. *Carbon N. Y.* **2009**, *47*, 2281–2289.

(52) Tylli, H.; Konschin, H. A Raman Spectroscopic Study of the OH and OD Torsion in 1,2-Dihydroxybenzene. *J. Mol. Struct.* **1979**, *57*, 13–19.

(53) Fujita, J.; Martell, A. E.; Nakamoto, K. Infrared Spectra of Metal Chelate Compounds. VI. A Normal Coordinate Treatment of Oxalato Metal Complexes. *J. Chem. Phys.* **1962**, *36*, 324.

(54) Michaud-Soret, I.; Andersson, K. K.; Que, L.; Haavik, J. Resonance Raman Studies of Catecholate and Phenolate Complexes of Recombinant Human Tyrosine Hydroxylase. *Biochemistry* **1995**, *34*, 5504–5510.

(55) Salama, S.; Stong, J. D.; Neilands, J. B.; Spiro, T. G. Electronic and Resonance Raman Spectra of iron(III) Complexes of Enterobactin, Catechol, and N-Methyl-2,3-Dihydroxybenzamide. *Biochemistry* **1978**, *17*, 3781–3785.

(56) Que Jr., L.; Heistand II, R. H. Resonance Raman Studies on Pyrocatechase. *Am. Chem. Soc.* **1979**, *101*, 2219–2221.

(57) Hurst, S. J.; Fry, H. C.; Gosztola, D. J.; Rajh, T. Utilizing Chemical Raman Enhancement: A Route for Metal Oxide Support-Based Biodetection. *J. Phys. Chem. C* **2011**, *115*, 620–630.

(58) Musumeci, A.; Gosztola, D.; Schiller, T.; Dimitrijevic, N. M.; Mujica, V.; Martin, D.; Rajh, T. SERS of Semiconducting Nanoparticles (TiO(2) Hybrid Composites). *J. Am. Chem. Soc.* **2009**, *131*, 6040–6041.

(59) Charkoudian, L. K.; Franz, K. J. Fe (III) -Coordination Properties of Neuromelanin Components : 5,6-Dihydroxyindole and 5,6-Dihydroxyindole-2-Carboxylic Acid. *Inorg. Chem.* **2006**, *45*, 3657–3664.

(60) Liu, Y.; Hong, L.; Kempf, V. R.; Wakamatsu, K.; Ito, S.; Simon, J. D. Ion-Exchange and Adsorption of Fe(III) by Sepia Melanin. *Pigment Cell Res.* **2004**, *17*, 262–269.

(61) Ryou, M.-H.; Lee, Y. M.; Park, J.-K.; Choi, J. W. Mussel-Inspired Polydopamine-Treated Polyethylene Separators for High-Power Li-Ion Batteries. *Adv. Mater.* **2011**, *23*, 3066–3070.

Chapter 4

Bulk Adhesive and Cohesive Mechanics of Polydopamine Films

4.1 Abstract

The adhesive and cohesive interactions of polydopamine (PDA) are currently explained in terms of PDA's abundant catechol groups and microstructural similarity to melanins. Control over PDA's adhesive and structural stability requires a more comprehensive, material-specific understanding of PDA's bulk properties. Chapter 4 describes quantification of PDA film delamination kinetics and elastic modulus. Visual recording of PDA film delamination from SiO_2 substrates revealed accelerated delamination (spanning orders of magnitude from 12 hr to 1 min) with increasing pH and monovalent salt concentration. Delamination was retarded for films synthesized from higher dopamine concentrations, and it was completely prevented in the presence of Ca^{2+}. Films on indium tin oxide (ITO) did not spontaneously delaminate in alkaline salt solutions, but application of +0.9 V (vs. Ag/AgCl) for 20 min did cause coherent delamination. Delaminated films exhibited orientation-dependent adhesion to polydimethylsiloxane (PDMS) elastomer. Elastic moduli of PDA films were quantified by compressive thin film wrinkling, and the measured value of 2.0 ± 0.9 GPA agrees with simulations of PDA based on a monomeric aggregate model. Crosslinking of primary amines within the films by genipin was successful in increasing the modulus to 7.9 ± 2.5 GPA. These results demonstrate that the adhesive stability and elastic modulus of PDA films can be controlled by synthesis and post-processing techniques.

4.2 Introduction

The versatile and relatively strong underwater adhesion of catechols has been established in numerous contexts. Empirical and theoretical investigations of catechol-surface interactions have demonstrated the importance of the un-oxidized, bidentate catechol moiety in forming interfacial hydrogen bonds or metal-coordination bonds depending on the surface chemistry.[1–5] Recent studies have revealed the cooperative adhesive action of primary amines, which displace hydrated surface salts allowing for close approach of nearby catechol groups.[6,7] A more comprehensive understanding of how these two adhesive mechanisms manifest in bulk catecholamine coatings would help accelerate their practical implementation and the design of derivative materials.

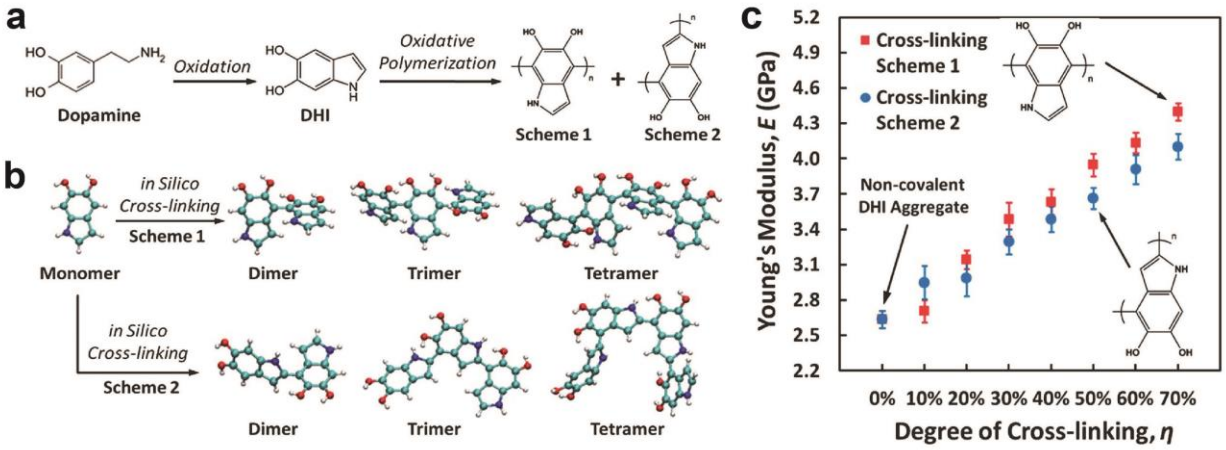

Figure 4.1: Simulations of aggregates of DHI monomers showed an increase in Young's modulus as the degree of bonding between the monomers increased. Reproduced from [8]

In addition to their adhesive properties, understanding the microstructure and internal cohesion of catecholamine films is important for controlling their mechanical stability. The most commonly used catecholamine film *polydopamine* is not an extended polymer in the traditional sense but likely rather a heterogeneous aggregate of small oligomers (observed up to the octamer level).[9–11] Computational modeling of PDA has been successful in reproducing fundamental

physical parameters of the bulk material, and has also revealed the positive role of interunit bonding in increasing the elastic modulus of PDA. (Figure 4.1).[8,12] Increasing the internal cohesion and robustness of PDA films could improve their long-term performance in mechanically agitated environments,[45-47] such as in the human body[13] or flowing liquids.[48-49]

Chapter 4 discusses the bulk adhesive and cohesive properties of polydopamine films and means for controlling them via synthesis conditions, salt valency, and chemical crosslinking. Delamination kinetics of films on SiO_2 and indium tin oxide (ITO) surfaces under selected solution conditions are reported, along with subsequent compressive buckling of these films.

4.3 Methods

4.3.1 Materials

Dopamine hydrochloride (98%), sodium chloride (>99%) iron(III) chloride hexahydrate (>99%) were purchased from Sigma-Aldrich (St. Louis, MO USA) and used as received. Sodium bicarbonate (>99%), sodium carbonate (>99%), tris(hydroxymethyl) aminomethane (Tris), sodium sulfate (>99%) and sodium phosphate dibasic (99.2%) were purchased from Fisher Scientific (Hampton, NH USA) and used as received. Calcium chloride dihydrate (>99%) was purchased from BDH VWR International (Radnor, PA USA). Water was purified (18.2 MΩ-cm) using Direct-Q 3 UV-R system (Millipore). Silicon wafers with 1 μm thermal oxide were purchased from Silicon Quest International (San Jose, CA USA; 4" diameter, phosphorus doped). Indium tin oxide (ITO) pieces were purchased from University Wafer (Boston, MA USA; 20 Ω/□; ITO on glass).

4.3.2 PDA Film Preparation

Silicon and ITO substrates were cleaned by sonication in acetone, followed by isopropyl alcohol and then rinsed with de-ionized water (ddH_2O). Substrates were then cleaned by UV-ozone (30 mW/cm^2, 5 min; Jelight, Irvine, CA USA). PDA films were prepared by dissolving 1, 2.5, or 4 mg/ml dopamine hydrochloride in 200 ml of 50 mM bicarbonate buffer at pH = 8.5. Pre-cleaned substrates were incubated in dopamine solutions in ambient air and rotational agitation (65 rpm). After 24 hr the substrates were rinsed and incubated in a refreshed deposition solution. This process was repeated as necessary to achieve a desired film thickness (24, 48, or 72 hr). The substrates were then rinsed and placed in ddH_2O for 24 hr then dried under a stream of N_2. The pH values of all sample solutions were measured using an Ag/AgCl electrode (Hach, model 5014T; Loveland, CO USA).

4.3.3 Delamination of PDA Films

Individual samples of PDA were cut from a larger parent sample and placed in ddH_2O for 14 hr before delamination. Samples were placed in petri dishes, the desired solution was poured in, and the delamination process was observed visually (see Figures 1b and SX-X). The buffered solutions were periodically partially refreshed during long tests (>30 min) in order to maintain the specified pH. The times until complete delamination were recorded. Optical images and video were taken with a Canon EOS Rebel T3i camera.

Electrochemical tests were performed in a conventional three-electrode setup with saturated Ag/AgCl reference electrodes (Koslow Scientific; Englewood, NJ USA) and platinum mesh as counter electrode. Tests were performed in 50 mM bicarbonate/carbonate buffer (pH = 10) with 122 mM NaCl supporting electrolyte (to attain [Na^+] = 200 mM) and in ambient atmosphere. PDA films on ITO were delaminated by applying +0.9 V for 20 min. Cyclic

voltammetry scans were swept between -0.4 V and 0.9 V at 30 mV/s using an Interface 1000 potentiostat (Gamry Instruments; Warminster, PA USA).

4.3.4 PDA Film Wrinkling and Crosslinking

Elastomeric substrates were prepared using polydimethylsiloxane (PDMS, Sylgard 184, Dow Corning, Midland, MI USA) cured in a 10:1 ratio at 75°C for 5 hr. Rectangular PDMS coupons (W × L × H = 1.3 cm × 4 cm × 0.9 cm) were mounted in a custom fixation device and strained by 8% on the long axis. ddH_2O drops were placed on the strained PDMS and free-floating PDA films were transferred into the drops and laminated onto the PDMS via applied pressure. The excess ddH_2O was then blown away by flowing N_2. After 10 min the strain on the PDMS was slowly released (~0.5 mm/s) in order to induce wrinkling on the PDA film.

Iron crosslinking was performed by first incubating delaminated films in 100 mM $CaCl_2$ (50 mM Tris buffer, pH = 10) for 100 min. This initial step acts to oxidize the films and was necessary to observe iron chelation in the Raman spectrum (see Chapter 3). Films were then dipped in ddH_2O and placed in 5 mM $FeCl_3$ solution for 100 min. Films were then placed in pH = 10 Tris buffer for 20 min to ensure the pH of the films was high enough (pH > 5) to ensure at least bis-coordination of catechols with Fe^{3+}.[15,16] Raman spectra of the pristine and iron-chelated films (NTegra Spectra; Tempe, AZ) were recorded with a 532 nm laser. Each measurement was done at unique single point of spot size ~1 μm diameter at 1 mW power for 30 seconds.

Genipin crosslinking was performed by placing delaminated films in solutions of 3 mg/ml genipin (pH = 7; 50 mM phosphate buffer) for 24 hr at 40°C. Films were then dipped in ddH_2O and placed in ddH_2O for 12 hours before wrinkling tests. Control samples were put through the same process except no genipin was present in the heated solution.

All PDA film samples used for wrinkling measurements were prepared in 1 mg/ml dopamine solution for a 24 + 24 hr deposition resulting in 59 nm thickness. PDA films used for crosslinking were delaminated from SiO_2 in 200 mM NaCl at pH = 10 (50 mM Tris buffer).

Uniaxial tensile tests (n = 4) on PDMS were conducted using a 10 N load cell at strain rates of 2 mm/min (Instron 5943 equipped with Bluehill 3 software, Norwood, MA)

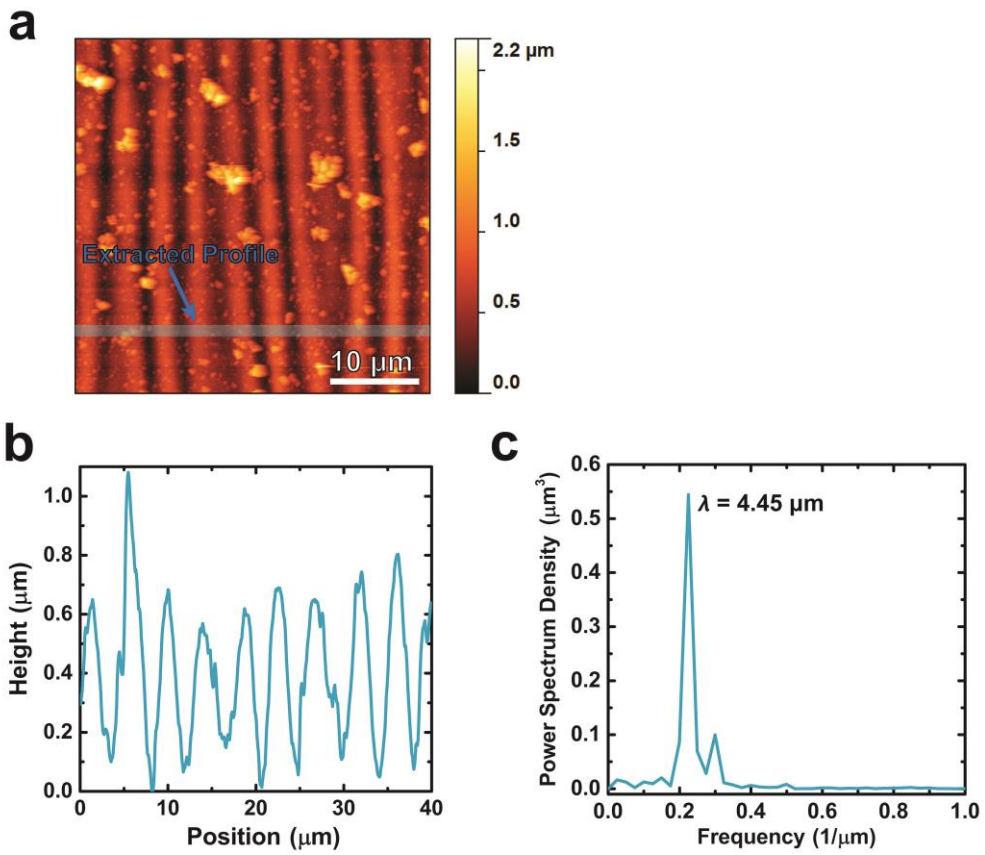

Figure 4.2: Quantification of wrinkling wavelengths: (a) AFM scan of a wrinkled genipin-crosslinked film. A height profile was extracted from the blue highlighted region. (b) Height profile illustrating periodic wrinkling (c) Fast Fourier transform of the height profile indicating a characteristic wavelength of λ = 4.45µm

4.3.5 Morphological Characterization of PDA Films

Film thicknesses and morphology were measured using atomic force microscopy (NT-MDT NTegra AFM; Tempe, AZ) in tapping mode. Scans for wrinkling measurements were performed with tips of radius = 35 nm and k = 25-95 N/m (NT-MDT NTegra AFM; Tempe, AZ).

Wrinkling wavelengths were quantified by fast Fourier transform of the transverse height profile (Figure 4.2). Small scale morphology scans were performed with tips of radius <1 nm and k = 5 N/m (Budget Sensors; Sofia, Bulgaria). Imaging of the PDA film-substrate surface was accomplished by draping a free-floating film over a small flat glass puck that was then lifted out of the liquid and subsequently dried in ambient atmosphere. Film thicknesses were determined by scratching the as-synthesized films and measuring the height profile with AFM.[17]

4.4 Results and Discussion

4.4.1 PDA film adhesion is multimodal and can be enhanced by multivalent cations, choice of substrate, and synthesis conditions

The adhesive stability of polydopamine films were characterized by their time to delamination in un-agitated alkaline salt solutions (Scheme 4.1).

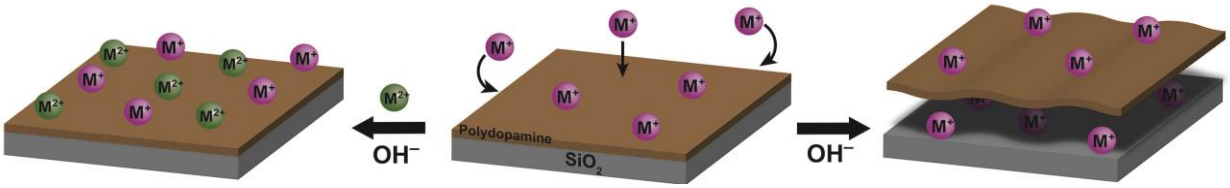

Scheme 4.1. Schematic of PDA film delamination process in alkaline monovalent salt solutions (right) or with the addition of multivalent cations (left).

Concentrated NaOH solutions are known to remove PDA from various substrates.[18–20] I separated the concomitant variables of pH and metal salt concentration through the use of an organic amine buffer and independent addition of metal salts. Delamination was observed visually via light scattering caused by the loss of conformal interface between the PDA film and SiO_2 and resulting deformation of the free-standing PDA film. Two kinds of delamination centers were observed: interfacial defects (edges and scratches; labeled by arrows 1 and 2 in

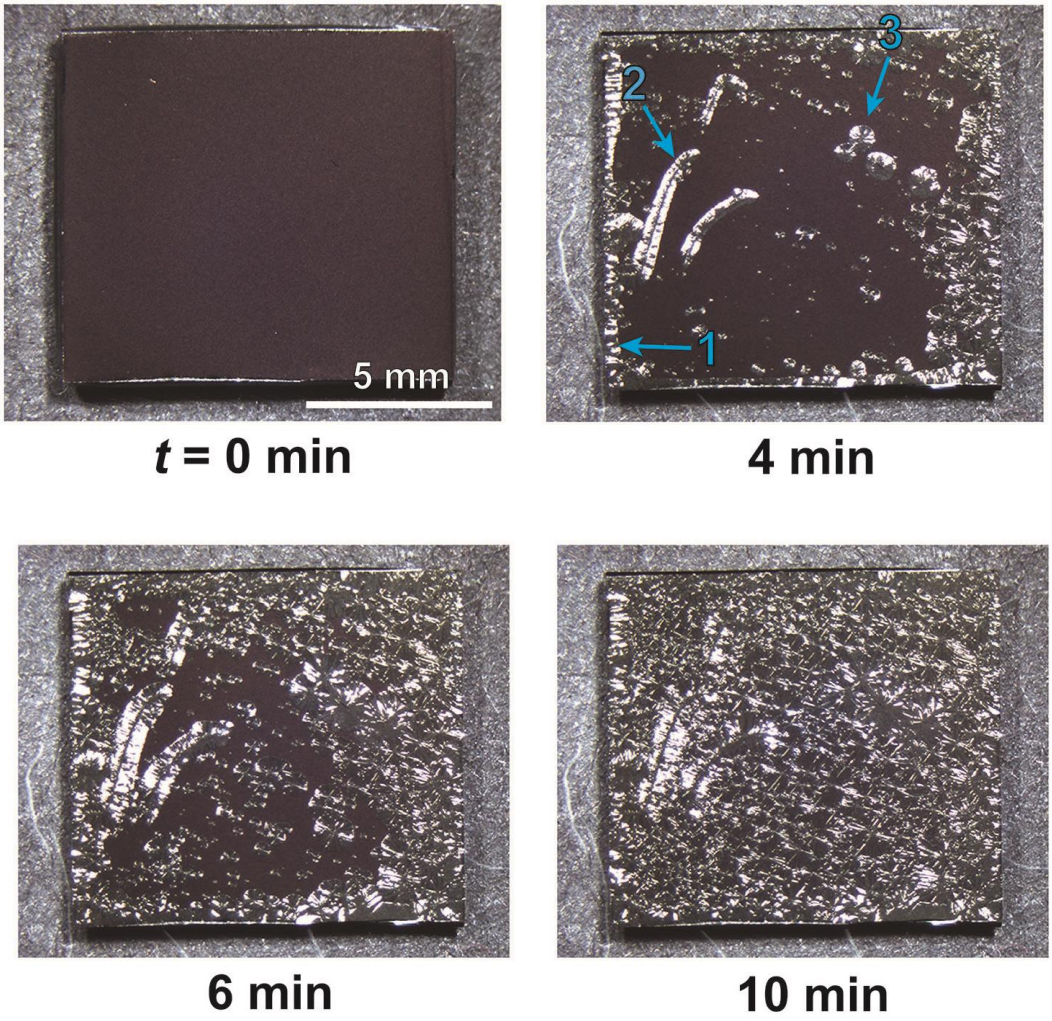

Figure 4.3: Time lapse of PDA film delamination in 200 mM NaCl + 50 mM Tris buffer at pH = 9.5. Arrows indicate delamination centers.

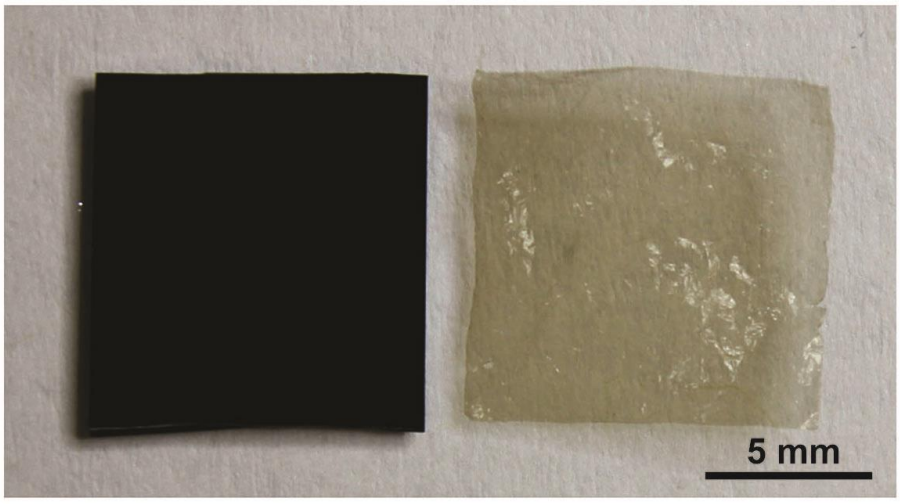

Figure 4.4: Image of a delaminated PDA film (h = 59 nm) along with a SiO_2 wafer from which its PDA film had been delaminated.

Figure 4.3) and points in the bulk of the film (arrow 3). The delamination propagates outwards from the different origins eventually delaminating the entire film (Figure 4.4).

PDA film delamination is greatly accelerated by solutions containing group I cations (Figure 4.5a), requiring t > 12 hr for complete delamination in the absence of NaCl to t = 1 min in 200 mM NaCl (pH = 10). This phenomenon may be explained in light of the catecholate

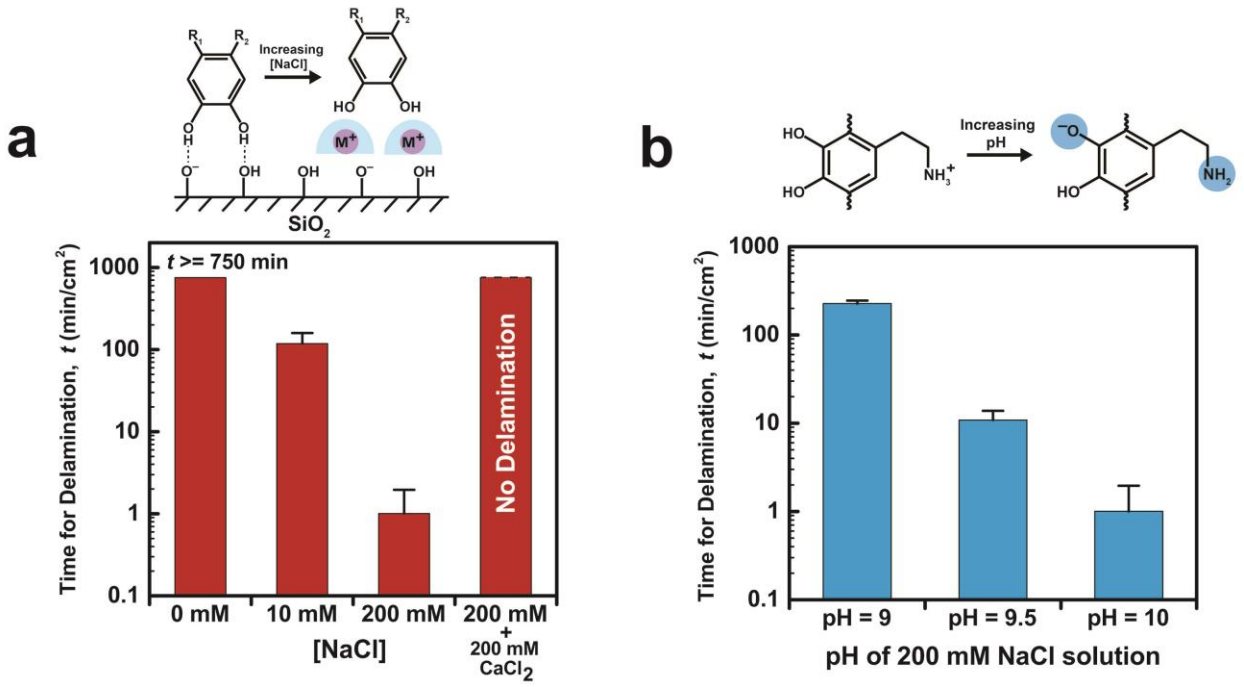

Figure 4.5. (a) Time to complete delamination in different salt solutions in 50 mM Tris buffer at pH = 10. All PDA films were 59 nm thick and synthesized from 1 mg/ml dopamine solutions. Films in 200 mM NaCl + 200 mM $CaCl_2$ solutions showed zero delamination initiation over the course of 12 hr. Associated graphic illustrates proposed disruption of catechol-SiO_2 hydrogen bonding by adsorption of cations. (b) Time to complete delamination at different pH in 200 mM NaCl + 50 mM Tris buffer. All PDA films were 59 nm thick and synthesized from 1 mg/ml dopamine solutions. Associated graphic illustrates ionization of catechol groups and deprotonation of primary amines on dopamine within the PDA film.

adhesion mode to SiO_2. Simulations of catechol interaction with silica surfaces showed direct hydrogen bonding between the catecholic hydroxyls and silica surfaces underwater.[3,4] Metal cations such as sodium may competitively adsorb to the silica surface[21] and disrupt this intimate hydrogen bond.[6,7] Raising the pH of the NaCl solution from pH = 9 to 10 also accelerates the

delamination (Figure 4.5b) due to a greater proportion of catechols existing in an ionized state and thus not contributing bidentate hydrogen bonding to the bulk film adhesion. Delamination was not inhibited by an increasing film thickness (Figure 4.6b) which is attributed to structural defects in the film (Figure 4.3) and the persistence of permeable pathways for monovalent cations in the bulk of the film.[22]

The cooperative adhesive action of primary amines in the PDA film is supported by the slower delamination of films that had been synthesized from more highly concentrated dopamine solutions (Figure 4.6a). Compositional characterization of PDA revealed that lower dopamine concentrations during PDA synthesis (e.g. 0.5 mM dopamine) produce PDA with lesser proportion of primary amines compared to more highly concentrated solutions (e.g. 10 mM dopamine).[10] A higher concentration of primary amines in PDA films may inhibit metal cation adsorption at the SiO_2 interface via a similar mechanism to that observed for catecholamine adsorption to mica.[6,7]

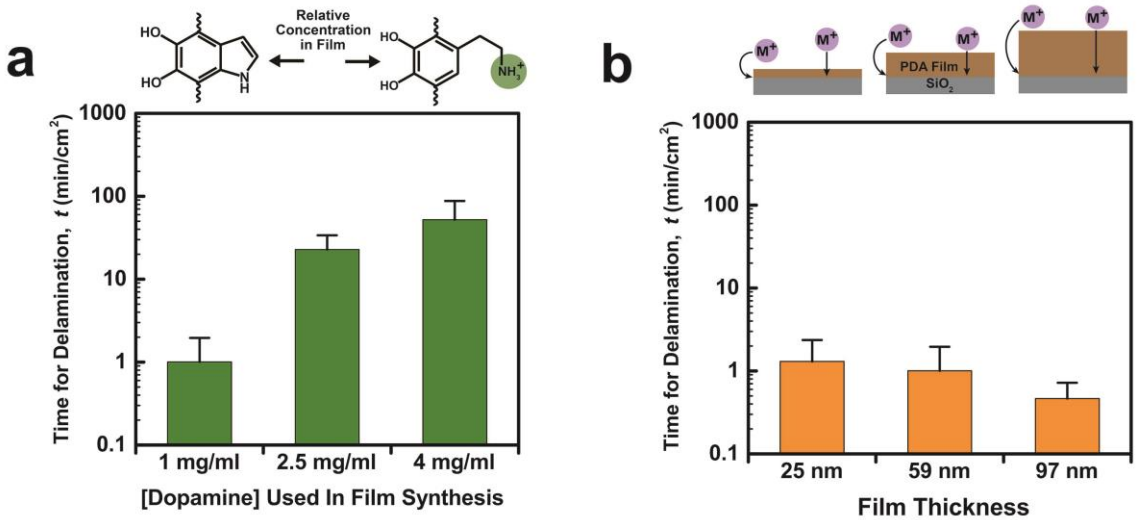

Figure 4.6: (a) Time to complete delamination for films synthesized in solutions of varying dopamine concentration. All solutions were 200 mM NaCl + 50 mM Tris buffer at pH = 10. Associated graphic illustrates the greater proportion of uncyclized dopamine and primary amines in the 2.5 and 4 mg/ml films. (b) Time to complete delamination for different film thicknesses. All solutions were 200 mM NaCl + 50 mM Tris buffer at pH = 10. Associated graphic illustrates the unaffected transport of cations to the film-substrate interface.

The simultaneous presence of the divalent cation Ca^{2+} in NaCl solutions prevented delamination of PDA (Figures 4.5a and A17). This enhanced stability persisted upon subsequently removing the Ca^{2+} component of the solution (Figure A18). This observation is strong evidence that the rapid delamination of PDA in alkaline salt solutions is not primarily attributed to catechol oxidation, since Ca^{2+} accelerates the oxidation of catechol moieties.[23–25] A definitive detailed explanation for the enhanced film stability in the presence of Ca^{2+} is not possible at this time. However, it may be related to attractive electrostatic interactions between negatively charged ionized catechols and divalent Ca^{2+} cations adsorbed at the SiO_2 surface.[26] Fe^{3+} cations have also been observed to enhance PDA film stability in strongly alkaline solutions, which corroborates the observation reported here.[20] Multivalent anions (e.g. in Na_2CO_3 and Na_2SO_4) did not prevent delamination.

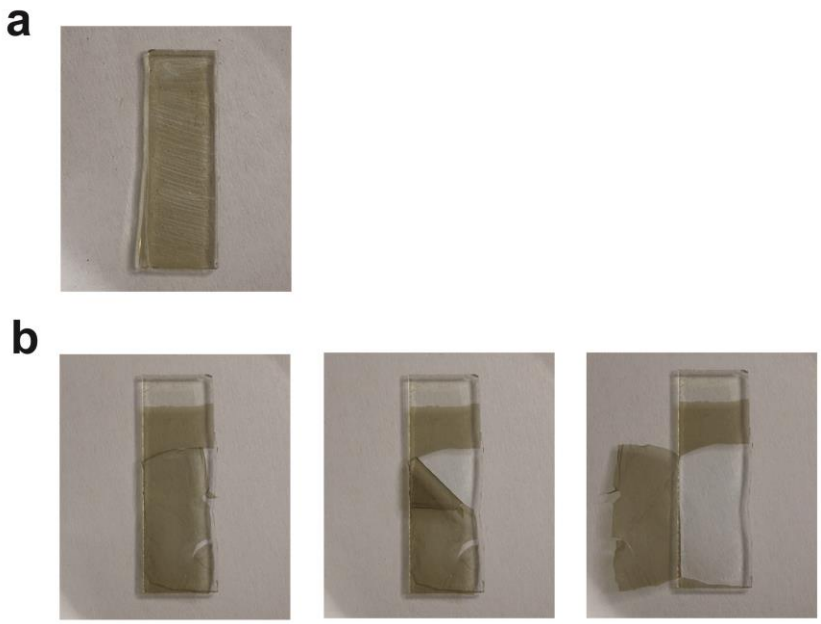

Figure 4.7: (a) PDA film (nominally 59 nm thickness; synthesized from 1 mg/ml dopamine) on indium tin oxide (ITO) that had sat for 12 hr in 50 mM bicarbonate/carbonate buffer at pH = 10 with added NaCl equivalent to 200 mM Na^+. Scratching the film did not disturb the surrounding film (seen in image) indicating lack of film delamination. This observation was consistent for all samples studied (n = 4) and the same effects were observed in 50 mM Tris buffer + 200 mM NaCl at pH = 10 (n = 4). (b) PDA film on ITO that had been electrically biased at +0.9 V (vs. Ag/Agcl) in 50 mM bicarbonate/carbonate buffer at pH = 10 with added NaCl equivalent to 200 mM Na^+. The series of images illustrate the delaminated character of the PDA film. Equivalent results were observed for a total of n = 4 samples.

PDA films on indium tin oxide substrates did not spontaneously delaminate in alkaline salt solution (Figure 4.7). However, electrically oxidizing the films at +0.9 V (vs. Ag/AgCl) for 20 min did result in delamination, which is attributed to oxidation of catechols.[1,27] This contrast of PDA film stability between SiO_2 and ITO emphasizes the multi-modality of catechol surface interactions.[5] For example, catechols participate in strong complexes with TiO_2 surfaces in contrast to weaker hydrogen bonds with mica, and a similar contrast could account for the greater stability of PDA on ITO vs. SiO_2.[2]

The delaminated PDA films (Figure 4.4 and Video 4.1) are structurally stable under gentle manipulation, including repeated transfer to different solutions. These films can be re-laminated on polydimethylsiloxane (PDMS) elastomer underwater via applied pressure in an orientation-dependent manner (Video 4.1). The surface of the film that originally interfaced with the parent SiO_2 substrate was readily adhesive to PDMS underwater, while the other PDA film surface was not. AFM images of the two surfaces (Figure 4.8) reveal a stark contrast in morphology. PDA films nucleate on SiO_2 via a 3-D island nucleation process, and this gives

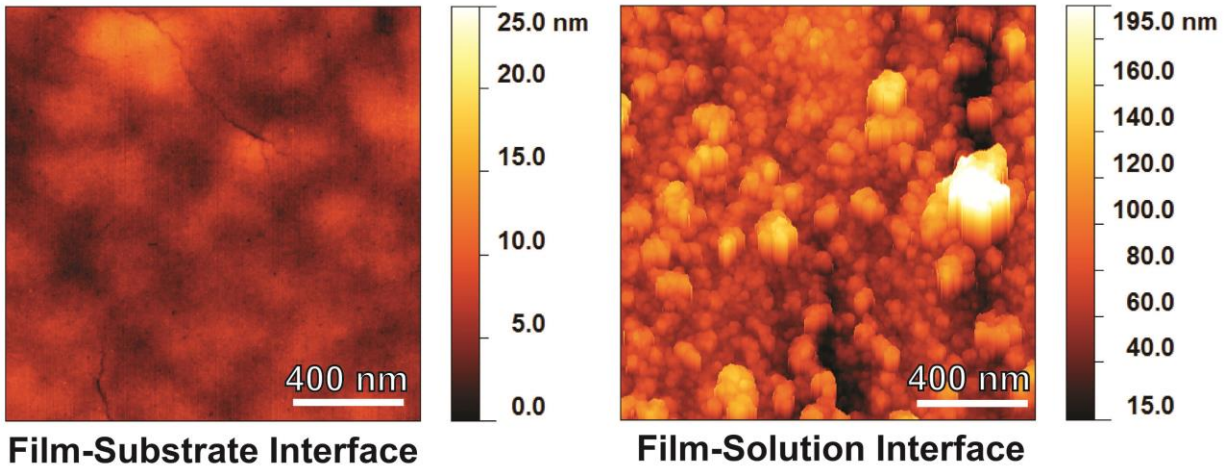

Figure 4.8: AFM images of the two surfaces of the delaminated PDA film.

rise to a rough granular structure at the film-solution interface.[17] The film-substrate interface is much smoother than the film-solution interface (R_{RMS} = 1.7 nm vs. 28.7 nm, respectively), which could account for greater adhesion of this interface with the PDMS due to lower asperities.[28] The film-substrate surface of PDA may also exhibit oriented catechol groups more conducive to adhesion compared to the film-solution surface (Figure 4.9). The adaptive orientation of catechols is a known factor in catecholamine adhesion.[2,29,30] Catechols adsorbed to the surface of SiO_2 during deposition may experience an orientational attractive force with the substrate not experienced by catechols at the film-solution interface.[3,4] The orientation-dependent adhesion of PDA films emphasizes the need to consider factors beyond mere catechol content when designing underwater adhesive materials

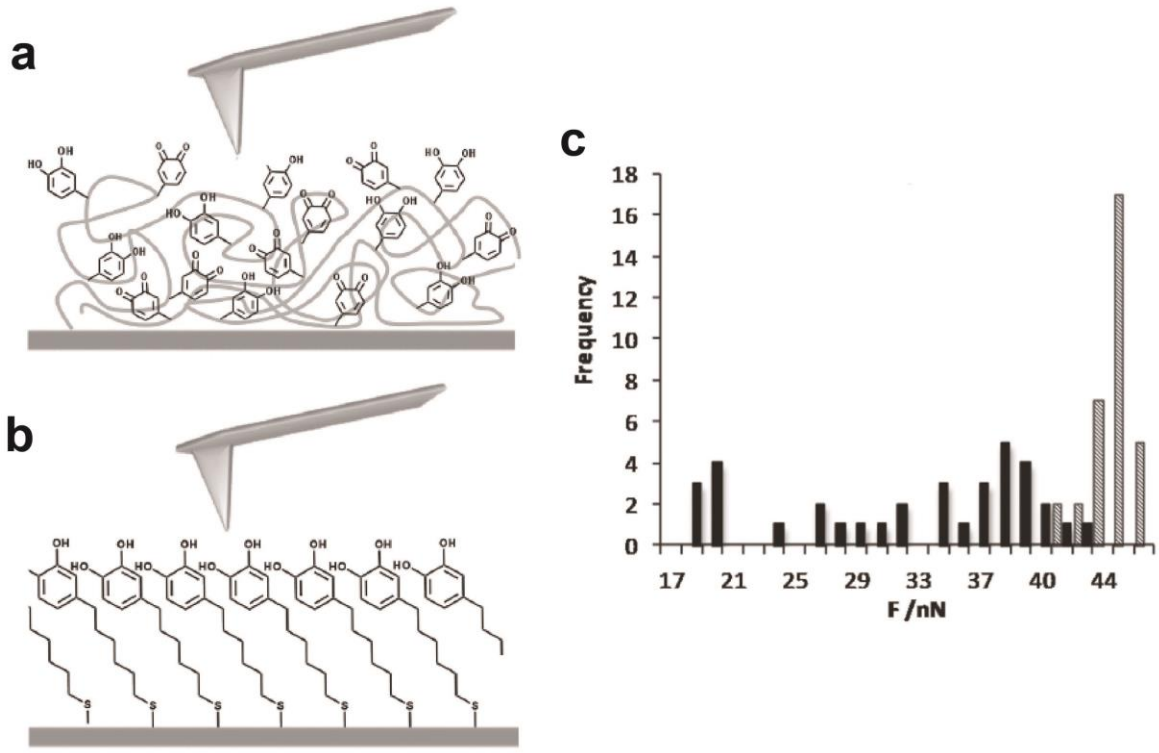

Figure 4.9: a) Schematic of AFM adhesion to an amorphous PDA film. b) Schematic of AFM adhesion to an oriented catechol monolayer c) Adhesive force of the catechol SAM is shown as grey bars and the PDA film as black bars. The average adhesive force of the catechol monolayer is greater than the maximum force measured with the PDA film. Reproduced from [30].

4.4.2 PDA elastic modulus is consistent with oligomeric aggregate model and can be enhanced by crosslinking with genipin

The relamination of PDA films on PDMS allowed characterization of their internal cohesive mechanics via thin film wrinkling. Adhering a thin film to a pre-stretched substrate of lesser stiffness and then releasing the substrate to its original length results in compressive

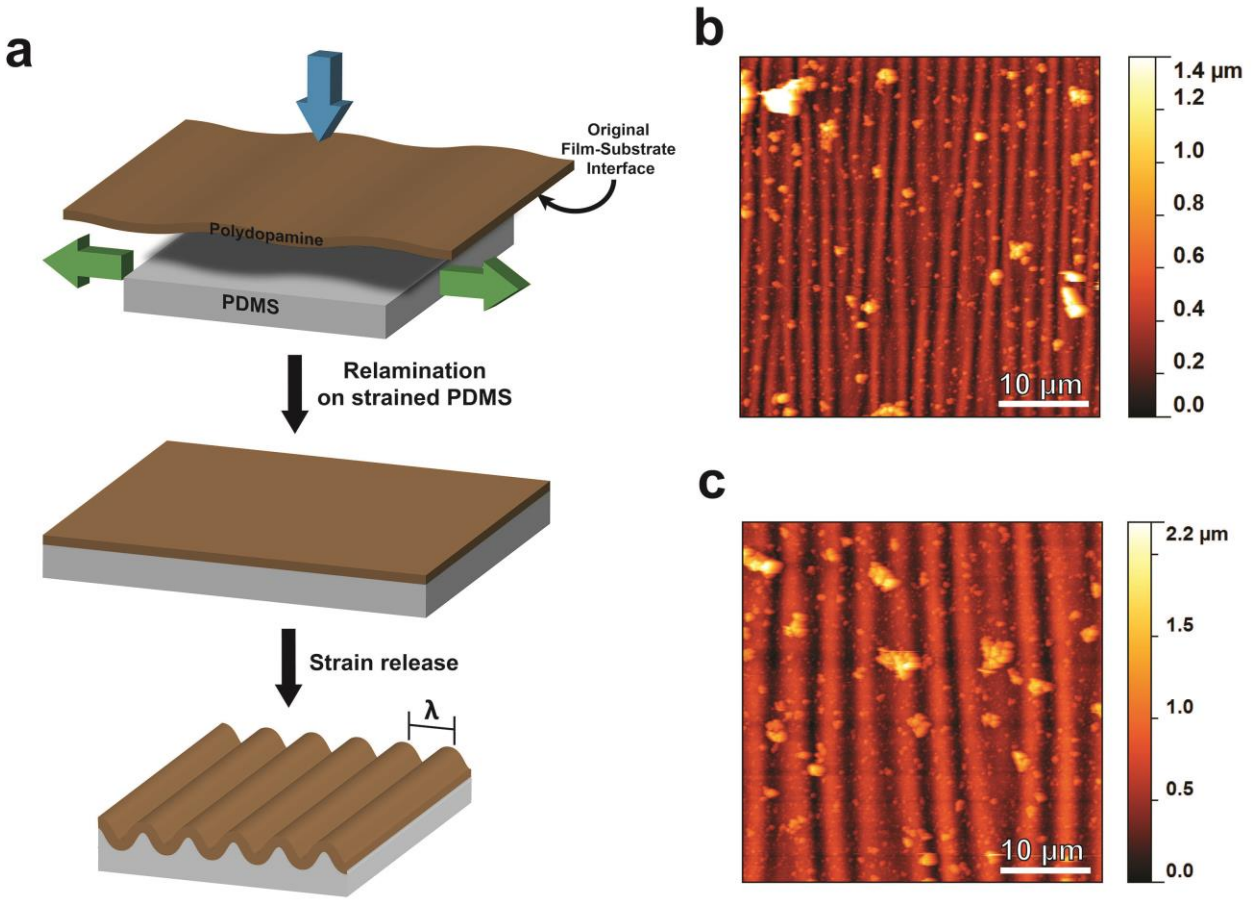

Figure 4.10: (a) Schematic of PDA film wrinkling achieved by relaminating a PDA film on a pre-strained PDMS substrate, then releasing the strain to compressively wrinkle the PDA film. (b) AFM scan of a wrinkled PDA film that had been delaminated in 200 mM NaCl + 50 mM Tris buffer at pH = 10. (c) AFM scan of a wrinkled genipin-crosslinked film.

periodic wrinkling of the thin film (Figure 4.10).[31] The wavelength of the wrinkling is related to the elastic modulus of the film through Eqn. 4.1:

$$E_f = 3E_s \frac{1-\nu_f^2}{1-\nu_s^2}\left(\frac{\lambda}{2\pi h}\right)^3 \quad (4.1)$$

where E_f and E_s are the elastic modulus of the film and substrate, respectively, ν_f and ν_s are the Poisson ratio of the film and substrate, respectively, h is the film thickness, and λ is the wavelength of the periodic wrinkling. The Poisson ratios were assumed to be $\nu_f = 0.3$ (also assumed in a previous report on PDA films[8]) and $\nu_s = 0.5$.[50] This characterization method allows for quantification of the bulk modulus of thin PDA films without detrimental interference from the underlying substrate encountered in nanoindentation measurements.[8]

The elastic modulus of PDA measured via thin film wrinkling (Figure 4.11) is generally consistent with theoretical modeling and previous nanoindentation measurements on melanin materials (Table 4.1). PDA films delaminated in 200 mM NaCl at pH = 9 exhibited an elastic modulus of 2.0 ± 0.9 GPa. Considering the granular structure of PDA films, this modulus value must derive both from the intermolecular attractive forces within the granules themselves, and

			Young's Modulus *E* (Gpa)	
	Material	**Method**	**Ambient (or 0% water for simulations)**	**In Water**
In Silico	**DHI Tetramers [42]**	**Simulation**	5.0 ± 1.7	2.3 ± 1.3
	DHI Monomers [8]	**Simulation**	2.6 ± 0.1	-
	DHI Monomers [8]	**Simulation ("crosslinked")**	4.4 0.1	-
Experimental	**Eumelanin [43]**	**Nanoindentation**	7.0 ± 2.8	1.4 ± 1.2
	Eumelanin [44]	**NanoIndentation**	6.8 ± 0.8	1.5 ± 0.3
	PDA [8]	**Nanoindentation**	4.3	-
	PDA [This Work]	**Film Wrinkling**	2.0 ± 0.9	-

Table 4.1: Young's moduli of different melanin-like materials.

also the cohesive forces acting at the granule interfaces. The fact that *in silico* modelling of PDA molecular ensembles gives greater moduli values (ca. 2.3–5.0 GPa) than measurements on bulk PDA films suggests that the intergranular cohesion is weaker than the intragranular cohesion in PDA.

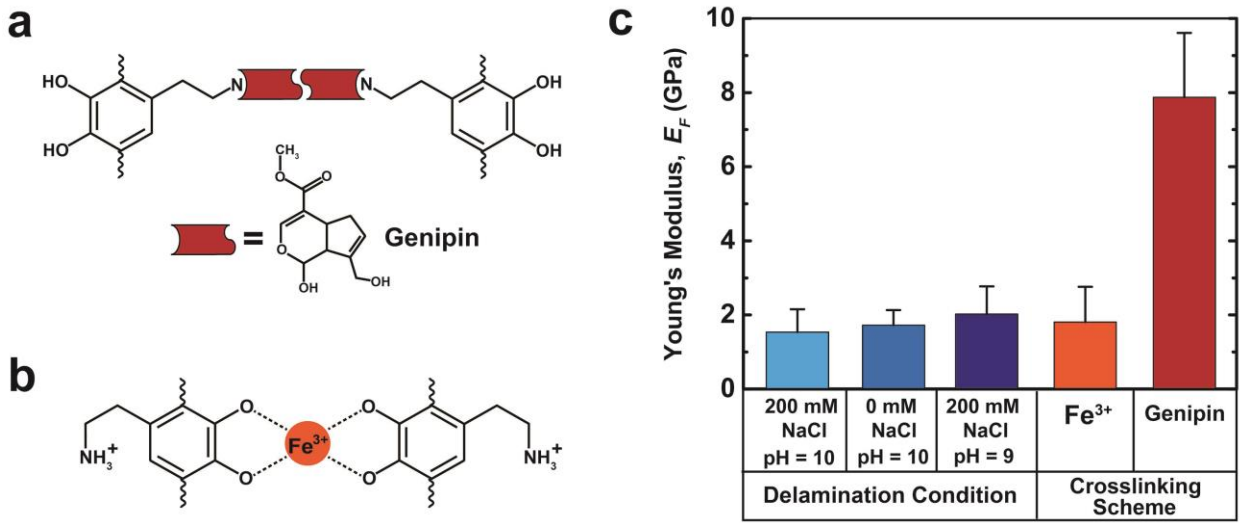

Figure 4.11: Illustration of the two crosslinking schemes investigated. (a) Amine crosslinking via genipin. (b) Catechol crosslinking via Fe^{3+} cations. (c) Young's modulus of PDA films as determined from the wrinkling wavelengths. Errors bars represent one standard deviation. The different delamination conditions did not have a statistically significant effect on the modulus ($P > 0.05$).

The mechanical robustness of PDA may be enhanced by internally crosslinking its aggregated oligomers and potentially serve to improve the long term stability[13,45-47] of PDA coatings in mechanically agitated environments. The term *crosslinking* is used here to describe linking between monomers or oligomers in polydopamine using species not native to polydopamine. Two different means of crosslinking the PDA films were explored: metal cation crosslinking via catechols and chemical crosslinking *via* primary amines (Figure 4.11). Fe^{3+} cations were chosen as a catechol crosslinking agent based on their known ability to enhance the mechanical robustness of other catecholic materials.[15,32] Iron chelation in the PDA films was confirmed *via* Raman spectroscopy (Figure A20). Genipin was chosen as an amine crosslinking

agent[33] based on its relatively low cytotoxicity[34–37] which is an important property for PDA's many potential biomedical applications.[38]

The results of the two crosslinking schemes are shown in Figure 4.11c. The iron chelated films did not exhibit any increase in elastic modulus over unmodified films, which may be due to the limited transport of Fe^{3+} through the films at the low pH of the 5 mM $FeCl_3$ solution (pH = 2.6). The positive surface charge in the films at this pH would inhibit the complete permeation of the Fe^{3+} cations throughout the film limiting the extent of crosslinking.[39] In contrast, PDA films incubated in genipin solution exhibited a >5x increase in modulus over the control: 7.9 ± 1.7 GPa vs. 1.5 ± 0.4 GPa. Covalent bonding of PDA monomers *in silico* was observed to increase PDA's elastic modulus,[8] so the increase in modulus of the PDA film soaked in genipin compared to the control is strong evidence that genipin is an effective crosslinking agent for PDA films. The use of amine groups for crosslinking is advantageous over catechol crosslinking since it preserves the adhesive functionality of catechols within the films. Amine crosslinking is similarly advantageous over proposed "oxidative crosslinking" of PDA,[8] because oxidation could lower the catechol population in favor of less adhesive quinones[2,27] or degrade the film composition.[40,41]

4.5 Conclusions

In summary, Chapter 4 has discussed the adhesive and cohesive mechanisms of PDA films and means for controlling them. PDA adhesion to metal oxides is multimodal and practical implementation of PDA must account for the surface-specific bonding mode between the catechol and the metal oxide. In particular, PDA's hydrogen-bonding adhesion mode to SiO_2 is susceptible to disruption in monovalent salt solutions, but may be stabilized by greater primary amine content in the films or addition of multivalent cations. The underwater adhesion of

delaminated PDA films depends on the surface orientation of the film. This observation emphasizes the fact that the mere presence of catechol groups is not sufficient for the underwater adhesion of PDA, but surface morphology and likely catechol density and orientation at the surface are also important. Surface-wrinkling measurements of the elastic modulus of PDA support the oligomeric aggregate model of PDA. Genipin is an effective crosslinking modality for PDA and present certain advantages over iron or oxidative crosslinking.

4.6 References

(1) Lee, H.; Scherer, N. F.; Messersmith, P. B. Single-Molecule Mechanics of Mussel Adhesion. *Proc. Natl. Acad. Sci.* **2006**, *103*, 12999–13003.

(2) Anderson, T. H.; Yu, J.; Estrada, A.; Hammer, M. U.; Waite, J. H.; Israelachvili, J. N. The Contribution of DOPA to Substrate-Peptide Adhesion and Internal Cohesion of Mussel-Inspired Synthetic Peptide Films. *Adv. Funct. Mater.* **2010**, *20*, 4196–4205.

(3) Qin, Z.; Buehler, M. Molecular Mechanics of Dihydroxyphenylalanine at a Silica Interface. *Appl. Phys. Lett.* **2012**, *101*, 1–5.

(4) Mian, S. A.; Yang, L. M.; Saha, L. C.; Ahmed, E.; Ajmal, M.; Ganz, E. A Fundamental Understanding of Catechol and Water Adsorption on a Hydrophilic Silica Surface: Exploring the Underwater Adhesion Mechanism of Mussels on an Atomic Scale. *Langmuir* **2014**, *30*, 6906–6914.

(5) Li, Y.; Qin, M.; Li, Y.; Cao, Y.; Wang, W. Single Molecule Evidence for the Adaptive Binding of DOPA to Different Wet Surfaces. *Langmuir* **2014**, *30*, 4358–4366.

(6) Maier, G. P.; Rapp, M. V.; Waite, J. H.; Israelachvili, J. N.; Butler, A. Adaptive Synergy between Catechol and Lysine Promotes Wet Adhesion by Surface Salt Displacement. *Science* **2015**, *349*, 628–632.

(7) Rapp, M. V.; Maier, G. P.; Dobbs, H. A.; Higdon, N. J.; Waite, J. H.; Butler, A.; Israelachvili, J. N. Defining the Catechol–Cation Synergy for Enhanced Wet Adhesion to Mineral Surfaces. *J. Am. Chem. Soc.* **2016**.

(8) Lin, S.; Chen, C.-T.; Bdikin, I.; Ball, V.; Grácio, J.; Buehler, M. J. Tuning Heterogeneous Poly(dopamine) Structures and Mechanics: In Silico Covalent Cross-Linking and Thin Film Nanoindentation. *Soft Matter* **2014**, *10*, 457–464.

(9) Liebscher, J.; Mrówczyński, R.; Scheidt, H. a; Filip, C.; Hădade, N. D.; Turcu, R.; Bende, A.; Beck, S. Structure of Polydopamine: A Never Ending Story? *Langmuir* **2013**, *29*, 10539–10548.

(10) Della Vecchia, N. F.; Avolio, R.; Alfè, M.; Errico, M. E.; Napolitano, A.; D'Ischia, M. Building-

Block Diversity in Polydopamine Underpins a Multifunctional Eumelanin-Type Platform Tunable through a Quinone Control Point. *Adv. Funct. Mater.* **2013**, *23*, 1331–1340.

(11) Hong, S.; Na, Y. S.; Choi, S.; Song, I. T.; Kim, W. Y.; Lee, H. Non-Covalent Self-Assembly and Covalent Polymerization Co-Contribute to Polydopamine Formation. *Adv. Funct. Mater.* **2012**, *22*, 4711–4717.

(12) Gracio, J. D. A.; Singh, Â. M. K.; Ruch, D.; Buehler, M. J.; Al, C. E. T.; Ball, V. Self-Assembly of Tetramers of 5,6-Dihydroxyindole Explains the Primary Physical Properties of Eumelanin: Experiment, Simulation, and Design. *ACS Nano* **2013**, 1524–1532.

(13) Wei, Q.; Haag, R. Universal Polymer Coatings and Their Representative Biomedical Applications. *Mater. Horizons* **2015**, *2*, 567–577.

(14) Klosterman, L.; Bettinger, C. J. Cation-Mediate Control of Polydopamine Film Oxidation and Iron Chelation. **2016**.

(15) Holten-Andersen, N.; Harrington, M. J.; Birkedal, H.; Lee, B. P.; Messersmith, P. B.; Lee, K. Y. C.; Waite, J. H. pH-Induced Metal-Ligand Cross-Links Inspired by Mussel Yield Self-Healing Polymer Networks with near-Covalent Elastic Moduli. *Proc. Natl. Acad. Sci. U. S. A.* **2011**, *108*, 2651–2655.

(16) Charkoudian, L. K.; Franz, K. J. Fe (III) -Coordination Properties of Neuromelanin Components : 5,6-Dihydroxyindole and 5,6-Dihydroxyindole-2-Carboxylic Acid. *Inorg. Chem.* **2006**, *45*, 3657–3664.

(17) Klosterman, L.; Riley, J. K.; Bettinger, C. J. Control of Heterogeneous Nucleation and Growth Kinetics of Dopamine-Melanin by Altering Substrate Chemistry. *Langmuir* **2015**, *31*, 3451–3458.

(18) Bernsmann, F.; Ponche, A.; Ringwald, C.; Hemmerlé, J.; Raya, J.; Bechinger, B.; Voegel, J.; Schaaf, P.; Ball, V. Characterization of Dopamine−Melanin Growth on Silicon Oxide. *J. Phys. Chem. C* **2009**, *113*, 8234–8242.

(19) Wei, H.; Ren, J.; Han, B.; Xu, L.; Han, L.; Jia, L. Stability of Polydopamine and poly(DOPA) Melanin-like Films on the Surface of Polymer Membranes under Strongly Acidic and Alkaline Conditions. *Colloids Surf. B. Biointerfaces* **2013**, *110C*, 22–28.

(20) Kim, S.; Gim, T.; Kang, S. M. Stability-Enhanced Polydopamine Coatings on Solid Substrates by iron(III) Coordination. *Prog. Org. Coatings* **2014**, *77*, 1336–1339.

(21) Peschel, G.; Belouschek, P.; Müller, M. M.; Müller, M. R.; König, R. The Interaction of Solid Surfaces in Aqueous Systems. *Colloid Polym. Sci.* **1982**, *260*, 444–451.

(22) Gao, B.; Su, L.; Tong, Y.; Guan, M.; Zhang, X. Ion Permeability of Polydopamine Films Revealed Using a Prussian Blue-Based Electrochemical Method. *J. Phys. Chem. B* **2014**, *118*, 12781–12787.

(23) Lebedev, A. V; Ivanova, M. V; Timoshin, A. a; Ruuge, E. K. Effect of Group II Metal Cations on Catecholate Oxidation. *Chemphyschem* **2007**, *8*, 1863–1869.

(24) Lebedev, a. V.; Ivanova, M. V.; Ruuge, E. K. Calcium-Dioxolene Complexes: Rate Constants of Pyrocatechol Oxidation in the Presence of Ca2+. *Biophysics (Oxf).* **2011**, *56*, 188–193.

(25) Lebedev AV , Ivanova MV , Timoshin AA, R. E. Effect of Calcium Cations on Acid-Base Properties and Free Radical Oxidation of Dopamine and Pyrocatechol. *Biomed. Khim.* **2008**, *54*,

687–695.

(26) Meagher, L. Direct Measurement of Forces between Silica Surfaces in Aqueous CaCl2 Solutions Using an Atomic Force Microscope. *J. Colloid Interface Sci.* **1992**, *152*, 293–295.

(27) Lee, B. P.; Chao, C.; Nunalee, F. N.; Motan, E.; Shull, K. R.; Messersmith, P. B.; Lee, B. P.; Chao, C.; Nunalee, F. N.; Motan, E.; et al. Rapid Gel Formation and Adhesion in Photocurable and Biodegradable Block Copolymers with High DOPA Content Rapid Gel Formation and Adhesion in Photocurable and Biodegradable Block Copolymers with High DOPA Content. *Macromolecules* **2006**, *39*, 1740–1748.

(28) Fuller, K. N. G.; D. Tabor, F. R. S. The Effect of Surface Roughness on the Adhesion of Elastic Solids. *Proc. R. Soc. Lond.* **1975**, *345*, 327–342.

(29) Lu, Q. Y.; Danner, E.; Waite, J. H.; Israelachvili, J. N.; Zeng, H. B.; Hwang, D. S. Adhesion of Mussel Foot Proteins to Different Substrate Surfaces. *J. R. Soc. Interface* **2013**, *10*, 11.

(30) Guardingo, M.; Bellido, E.; Miralles-Lluma, R.; Faraudo, J.; Sedo, J.; Tatay, S.; Verdaguer, A.; Busque, F.; Ruiz-Molina, D. Bioinspired Catechol-Terminated Self-Assembled Monolayers with Enhanced Adhesion Properties. *Small* **2014**, *10*, 1594–1602.

(31) Chung, J. Y.; Nolte, A. J.; Stafford, C. M. Surface Wrinkling: A Versatile Platform for Measuring Thin-Film Properties. *Adv. Mater.* **2011**, *23*, 349–368.

(32) Harrington, M. J.; Masic, A.; Holten-andersen, N.; Waite, J. H.; Fratzl, P. Iron-Clad Fibers : A Metal-Based Biological Strategy for Hard Flexible Coatings. *Science* **2010**, 216–220.

(33) Ninh, C.; Iftikhar, A.; Cramer, M.; Bettinger, C. J. Diffusion–reaction Models of Genipin Incorporation into Fibrin Networks. *J. Mater. Chem. B* **2015**, *3*, 4607–4615.

(34) Sung, H. W.; Huang, R. N.; Huang, L. L.; Tsai, C. C. In Vitro Evaluation of Cytotoxicity of a Naturally Occurring Cross-Linking Reagent for Biological Tissue Fixation. *J. Biomater. Sci. Polym. Ed.* **1999**, *10*, 63–78.

(35) Sung, H. W.; Liang, I. L.; Chen, C. N.; Huang, R. N.; Liang, H. F. Stability of a Biological Tissue Fixed with a Naturally Occurring Crosslinking Agent (Genipin). *J. Biomed. Mater. Res.* **2001**, *55*, 538–546.

(36) Liang, H.-C.; Chang, W.-H.; Lin, K.-J.; Sung, H.-W. Genipin-Crosslinked Gelatin Microspheres as a Drug Carrier for Intramuscular Administration: In Vitro and in Vivo Studies. *J. Biomed. Mater. Res. A* **2003**, *65*, 271–282.

(37) Chang, C. J. Effects of Nerve Growth Factor from Genipin-Crosslinked Gelatin in Polycaprolactone Conduit on Peripheral Nerve Regeneration - In Vitro and in Vivo. *J. Biomed. Mater. Res. - Part A* **2009**, *91*, 586–596.

(38) Lynge, M. E.; van der Westen, R.; Postma, A.; Städler, B. Polydopamine--a Nature-Inspired Polymer Coating for Biomedical Science. *Nanoscale* **2011**, *3*, 4916–4928.

(39) Yu, B.; Liu, J.; Liu, S.; Zhou, F. Pdop Layer Exhibiting Zwitterionicity: A Simple Electrochemical Interface for Governing Ion Permeability. *Chem. Commun. (Camb).* **2010**, *46*, 5900–5902.

(40) Del Frari, D.; Bour, J.; Ball, V.; Toniazzo, V.; Ruch, D. Degradation of Polydopamine Coatings by Sodium Hypochlorite: A Process Depending on the Substrate and the Film Synthesis Method.

Polym. Degrad. Stab. **2012**, *97*, 1844–1849.

(41) Ponzio, F.; Barthes, J.; Bour, J.; Michel, M.; Bertani, P.; Hemmerlé, J.; D'Ischia, M.; Ball, V. Oxidant Control of Polydopamine Surface Chemistry in Acids: A Mechanism-Based Entry to Superhydrophilic-Superoleophobic Coatings. *Chem. Mater.* **2016**, *28*, 4697–4705.

(42) Gracio, J. D. A.; Singh, Â. M. K.; Ruch, D.; Buehler, M. J.; Al, C. E. T.; Ball, V. Self-Assembly of Tetramers of 5,6-Dihydroxyindole Explains the Primary Physical Properties of Eumelanin: Experiment, Simulation, and Design. *ACS Nano* **2013**, 1524–1532.

(43) Bushan, B. *Handbook of Nanotechnology*; 2nd ed.; Springer: Berlin, 2007.

(44) Moses, D. N.; Mattoni, M. A.; Slack, N. L.; Waite, J. H.; Zok, F. W. Role of Melanin in Mechanical Properties of Glycera Jaws. *Acta Biomater.* **2006**, *2*, 521–530.

(45) Lewis, A. L.; Cumming, Z. L.; Goreish, H. H.; Kirkwood, L. C.; Tolhurst, L. A.; Stratford, P. W. Crosslinkable Coatings from Phosphorylcholine-Based Polymers. **2000**, *22*, 99–111.

(46) Oshima, A.; Ikeda, S.; Katoh, E.; Tabata, Y. Chemical Structure and Physical Properties of Radiation-Induced Crosslinking of Polytetrafluoroethylene. *Radiat. Phys. Chem.* **2001**, *62*, 39–45.

(47) Guo, Q. H.; Pintauro, P. N.; Tang, H.; O'Connor, S. Sulfonated and Crosslinked Polyphosphazene-Based Proton- Exchange Membranes. *J. Memb. Sci.* **1999**, *154*, 175–181.

(48) Lee, M.; Rho, J.; Lee, D. E.; Hong, S.; Choi, S. J.; Messersmith, P. B.; Lee, H. Water Detoxification by a Substrate-Bound Catecholamine Adsorbent. *Chempluschem* **2012**, *77*, 987–990.

(49) Park, H.-A.; Kim, Y. J.; Kwon, I. S.; Klosterman, L.; Bettinger, C. J. Lithium Purification from Aqueous Solutions Using Bioinspired Redox Active Melanin Membranes. *Polym. Int.* **2016**.

(50) Félix, A. S. C.; Iturbide-jiménez, F.; Licona-morán, B. Physical-Chemical Properties of PDMS Samples Used in Tunable Lenses. *Int. J. Eng. Sci. Innov. Technol.* **2014**, *3*, 563–571.

Chapter 5

Conclusions and Perspectives

5.1 Summary of work

This work describes the fundamental mechanisms by which polydopamine (PDA) coats and adheres to different surfaces and the compositional stability of the resulting films. Chapter 2 discussed the nucleation and growth kinetics of PDA films in light of existing paradigms for vacuum deposition of thin organic films. The qualitative effects of surface energy and deposition rates were observed to be similar between solution deposition of PDA and vacuum deposition of pentacene. However, the solution deposition of PDA introduces complicating factors not encountered in vacuum deposition. The deposition of PDA molecules with increasing pH depends on the competing factors of increased generation rate of PDA molecules versus increased solubility due to catechol ionization. The areal density and coverage of PDA islands is influenced by the surface charge and hydrophobicity of the substrate in aqueous solutions. These results emphasize that despite the universal coating ability of PDA, one must take into account the chemistry of the substrate to inform necessary deposition times for the desired surface coverage and thickness of the coating. Additionally, the surface and pH-dependent morphology of PDA coatings may affect internal cohesion and ion transport pathways through the coating due to higher granule interfacial area.

The results discussed in Chapter 3 emphasized the molecular heterogeneity and non-equilibrium character of as-synthesized PDA coatings. The catechol-derived oxidative evolution of PDA's composition is greatly influenced by redox-inactive metal cations such as Ca^{2+}, Na^{+}, and Mg^{2+}. The effects of Ca^{2+} were explored in depth and found to influence the surface charge

and cation-binding properties of PDA films. Therefore, PDA-incorporated devices exposed to high concentrations of metal cations (e.g. water purification) must consider the change in chemical properties of PDA over time (depending on operational pH). Conversely, alkaline cation solutions can act as a post-processing strategy to tune the composition of PDA films.

Chapter 4 discussed factors governing the adhesive stability and internal cohesion of PDA films. PDA film adhesion is a substrate, salt, and oxidation-dependent phenomenon. Long-term adhesive stability of PDA films can be promoted by higher dopamine concentrations during synthesis, incorporation of multivalent cations, and avoiding alkaline conditions and strongly oxidizing electrical bias. These results are particularly important for proposed passive or electrochemically-mediated water purification applications. Also, successful crosslinking of PDA with genipin via amine groups may enhance the long term molecular cohesion of PDA films while preserving their functional catechol moieties.

5.2 Future Perspectives

There are significant unresolved issues regarding catecholamine coatings that should guide future research:

1. How does film morphology and catechol orientation determine adhesion?

Considering the universal coating ability of PDA, it is peculiar that PDA particles and the surface of PDA films do not stick to other surfaces underwater. The orientation-dependent adhesion of PDA to PDMS discussed in Chapter 4 implies that surface morphology and catechol orientation at the surface are important factors governing bulk catecholamine adhesion. Quantification of adhesion energy as a function of surface roughness could isolate the morphological factor. Quantification of adhesion energy for the substrate-film interface of delaminated films as a

function of film synthesis conditions (e.g. substrate temperature, solution pH, granule density in films) could elucidate the importance of the interfacial chemistry.

2. How can the ratio of catechols to quinones in PDA films be quantified and related to adhesion?

Catechols mediate PDA's adhesion to polar surfaces while quinones inhibit it. Quinones can contribute to covalent bonding with organic surfaces and serve as conjugation sites for biomolecules and polymers. A comprehensive quantification of the ratio between these two redox states in relation to different processing conditions and adhesive properties would greatly enhance our understanding of catecholamine adhesion. Quantification via cyclic voltammetry is problematic as there is a large degree of irreversibility in cycling and it is not clear what the spatial distribution of electrochemically accessible monomers in the film are. Quantification of carbonyl vs. alcohol content via X-ray photoelectron spectroscopy (XPS)[1] – correlated with adhesion energy – could elucidate adhesion mechanisms in PDA at a fundamental level.

3. Can the catechol-derived adhesion in PDA be reversibly controlled?

The reversibility of catechol redox states presents the opportunity for reversibly controlling the adhesion of PDA films. Electrochemical cycling of the redox states is likely not viable considering the high degree of irreversibility observed in cyclic voltammograms of PDA. However, chemical oxidizing agents (e.g. O_2, dilute H_2O_2) and reducing agents (e.g. NADPH, ascorbate[2]) would not require electrically-conducting pathways in the film. Therefore, the adhesion of conformal or delaminated PDA films could be compared before and after redox cycling with chemical agents.

4. How does the granule size in PDA films affect the elastic modulus of the films or molecular transport through the films?

As the granule sizes in PDA films are decreased, the contribution of their interfacial area to the bulk properties of the film become more significant. Smaller granule size may therefore decrease the mechanical rigidity and toughness of the films due to lesser cohesive forces at the granule interfaces. The effect on elastic modulus could be quantified by the surface wrinkling technique described in Chapter 4. Additionally, greater interfacial area in the film may affect transport and absorption capacity of metal cations and organic molecules within the films. This phenomenon could be quantified using the methods described in reference [3].

Answers to these and other open questions will significantly enhance our understanding of bioinspired catecholamine coatings. Natural materials act as a source of innovation and challenge for researchers, and there is no doubt that future technological breakthroughs will continue to be drawn from them.

5.3 References

(1) Liebscher, J.; Mrówczyński, R.; Scheidt, H. a; Filip, C.; Hădade, N. D.; Turcu, R.; Bende, A.; Beck, S. Structure of Polydopamine: A Never Ending Story? *Langmuir* **2013**, *29*, 10539–10548.

(2) Kim, E.; Liu, Y.; Baker, C. J.; Owens, R.; Xiao, S.; Bentley, W. E.; Payne, G. F. Redox-Cycling and H2O2 Generation by Fabricated Catecholic Films in the Absence of Enzymes. *Biomacromolecules* **2011**, *12*, 880–888.

(3) Lee, M.; Rho, J.; Lee, D. E.; Hong, S.; Choi, S. J.; Messersmith, P. B.; Lee, H. Water Detoxification by a Substrate-Bound Catecholamine Adsorbent. *Chempluschem* **2012**, *77*, 987–990

Appendix

Chapter 2 Supporting Figures

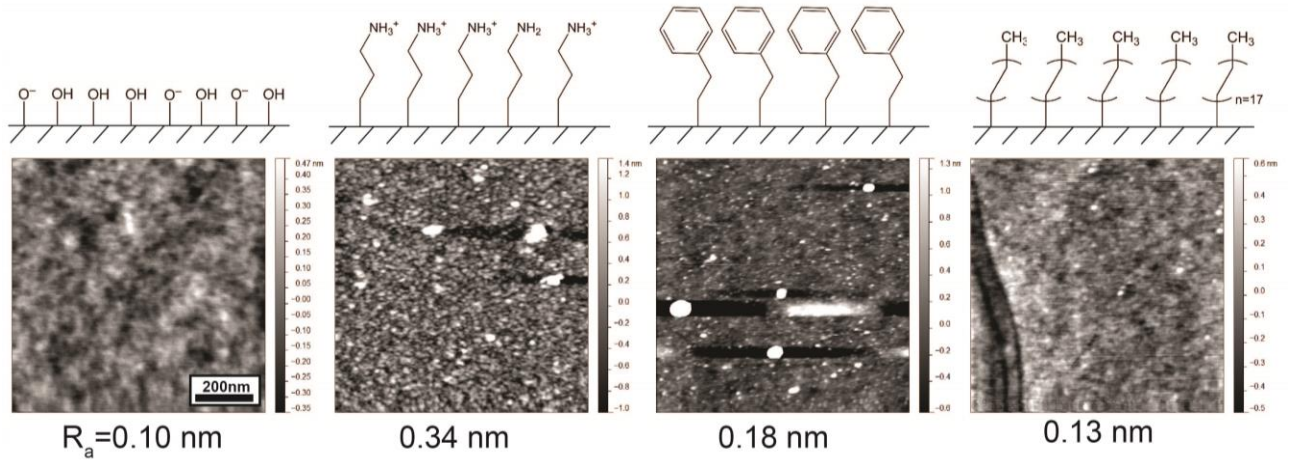

Figure A1: AFM scans of SiO_2 and SAM substrates before dopamine deposition. The average roughness of each scan are shown.

pH	8.17 ±0.02			8.50 ±0.05			8.95 ±0.04			9.46 ±0.02			9.97 ±0.02		
Sample Set	One	Two	Three	One	Two	Three	One	Two	Three	One	Two	Three	One	Two	Three
SiO_2	5			5	3		3	2		3	1		3	2	2
NH_3^+	4	4	3	3	3	3	3	4		2	3		3	4	
Ph	4	3	3	3	3	3	3	3		3	3		4	5	
CH_3	3	3	3	4		3	3	3		4	3		4	3	

Table A1: Sampling statistics for island densities. Each sample set consisted of five substrates (one for each pH) prepared in the same session. For the SiO_2, these also represent the sampling statistics for thickness values. The numbers in the table are the number of scans on each particular sample.

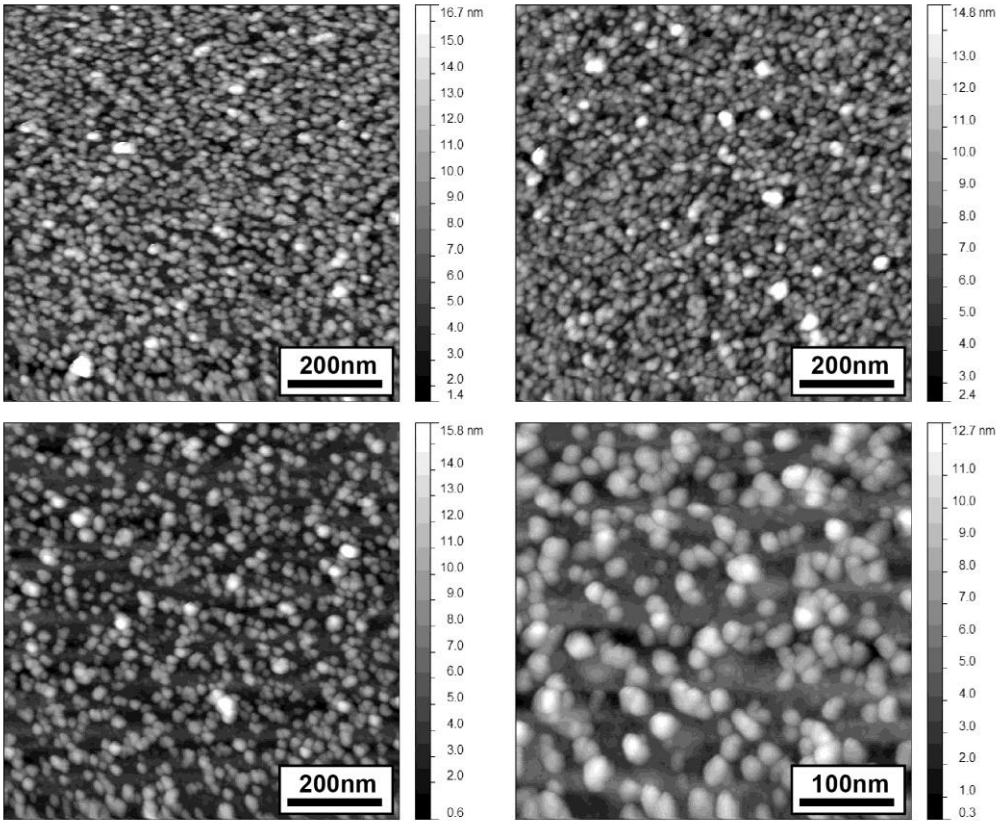

Figure A2: The morphology of PDA films on $-NH_3^+$ substrate at pH = 10. These data indicate the range of incomplete coverage observed.

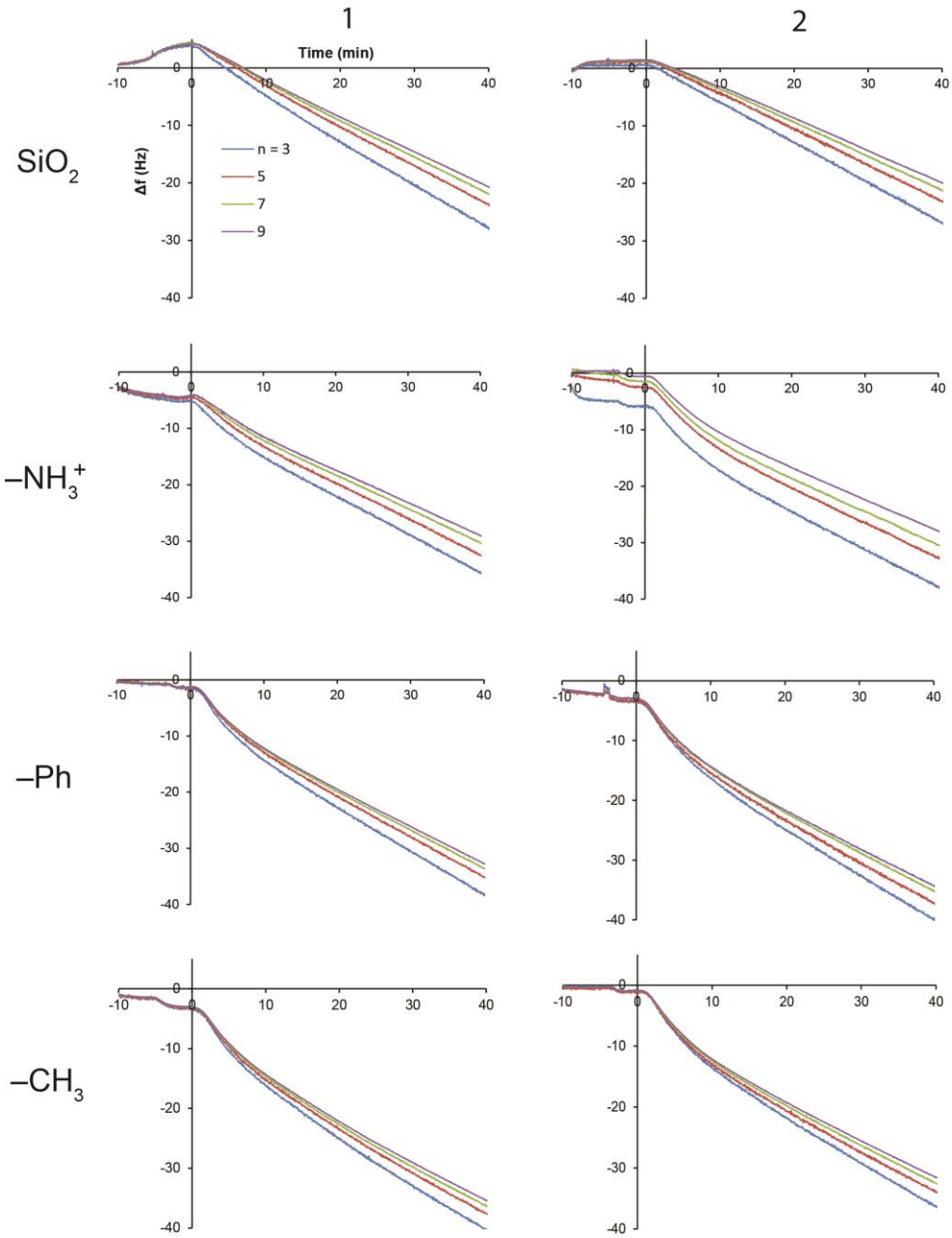

Figure A3: QCM-D frequency shifts at early times showing overtones 3-9.

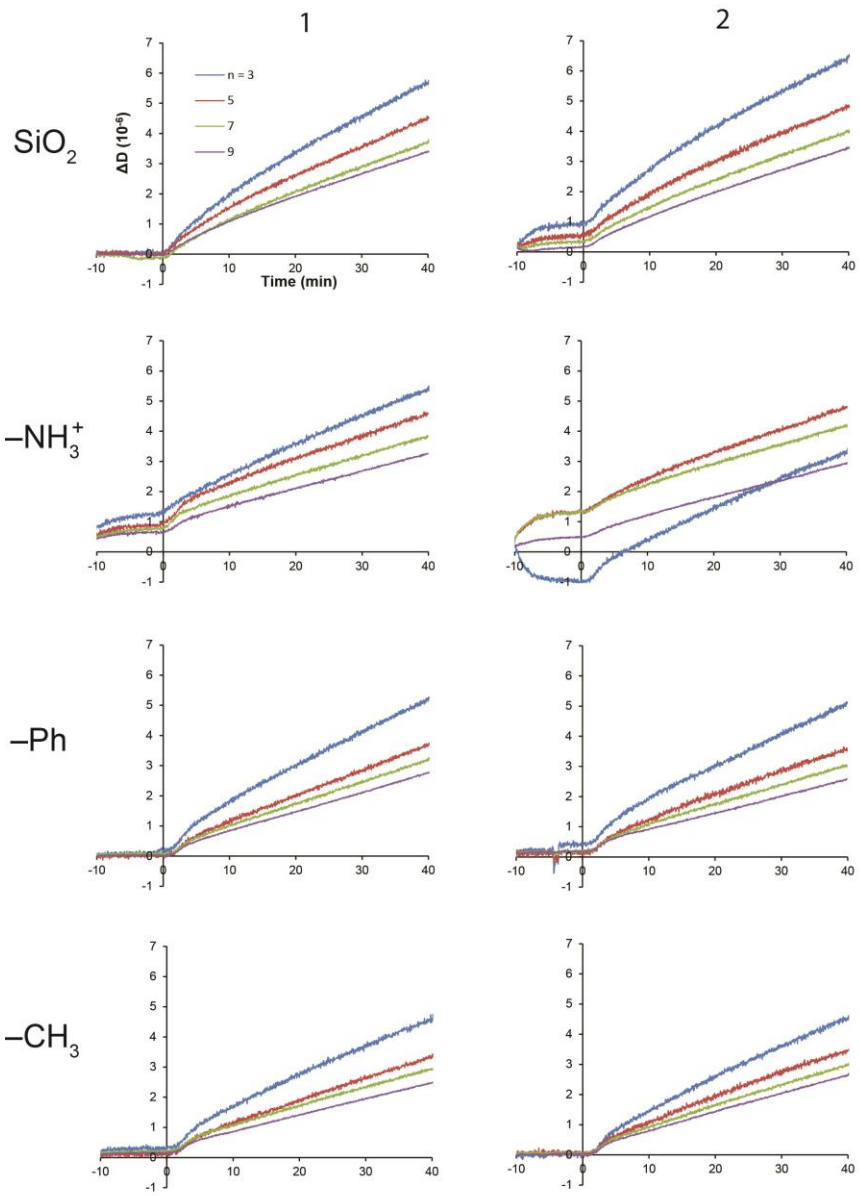

Figure A4: QCM-D dissipation shifts at early times showing overtones 3-9.

Sample	Contact Angle (°)	AFM thickness (nm)	Voigt Thickness (nm)	Viscosity (Pa·s ×10^{-3})	Shear Modulus (kPa)
S1	<10	9.6 ± 0.3	28.1	3.8	167
S2	<10	11.3 ± 1.3	31.8	3.1	171
A1	61.4 ± 1.5	13.3 ± 0.5	30.5	3.5	204
A2	81.7 ± 1.0	12.0 ± 0.8	30.1	3.3	197
P1	88.7 ± 0.7	13.5 ± 0.8	32.7	3.3	192
P2	84.3 ± 0.4	12.5 ± 0.9	30.6	3.4	203
O1	106.0 ± 0.6	13.6 ± 1.9	28.5	3.6	210
O2	102.5 ± 1.5	13.0 ± 1.4	31	3.3	189

Table A2: Parameters used in a Voigt model for the QCM-D data, and the contact angle (before deposition) and AFM thicknesses (after deposition) for each QCM sample. See references [1] and [2] for a description of the model, which was fit by my co-worker John Riley using the QCM-D software "QSoft401". AFM thicknesses were all determined by scratching the film as described in Chapter 2.

This model accounts for viscoelastic effects of the thicker film and adsorbed water mass at later times (>40 min). The greater final Voigt thicknesses (~30 nm) compared to AFM measurements (~12 nm) indicate a substantial hydrodynamically trapped water fraction in the bulk films, which may be due to the abundant –OH groups in PDA available for hydrogen bonding, or mesoscale porosity in the film.[3]

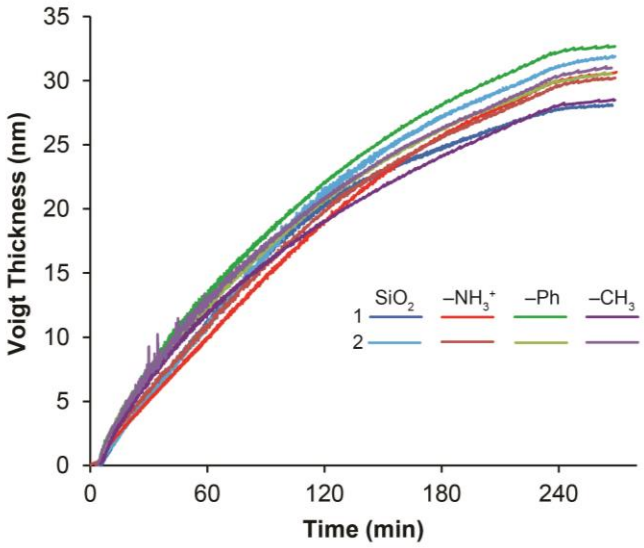

Figure A5: Voigt thickness of QCM-D PDA films vs. time (pH 8.5). The flow of dopamine precursor solutions was stopped after approximately 240 min.

Chapter 3 Supporting Figures

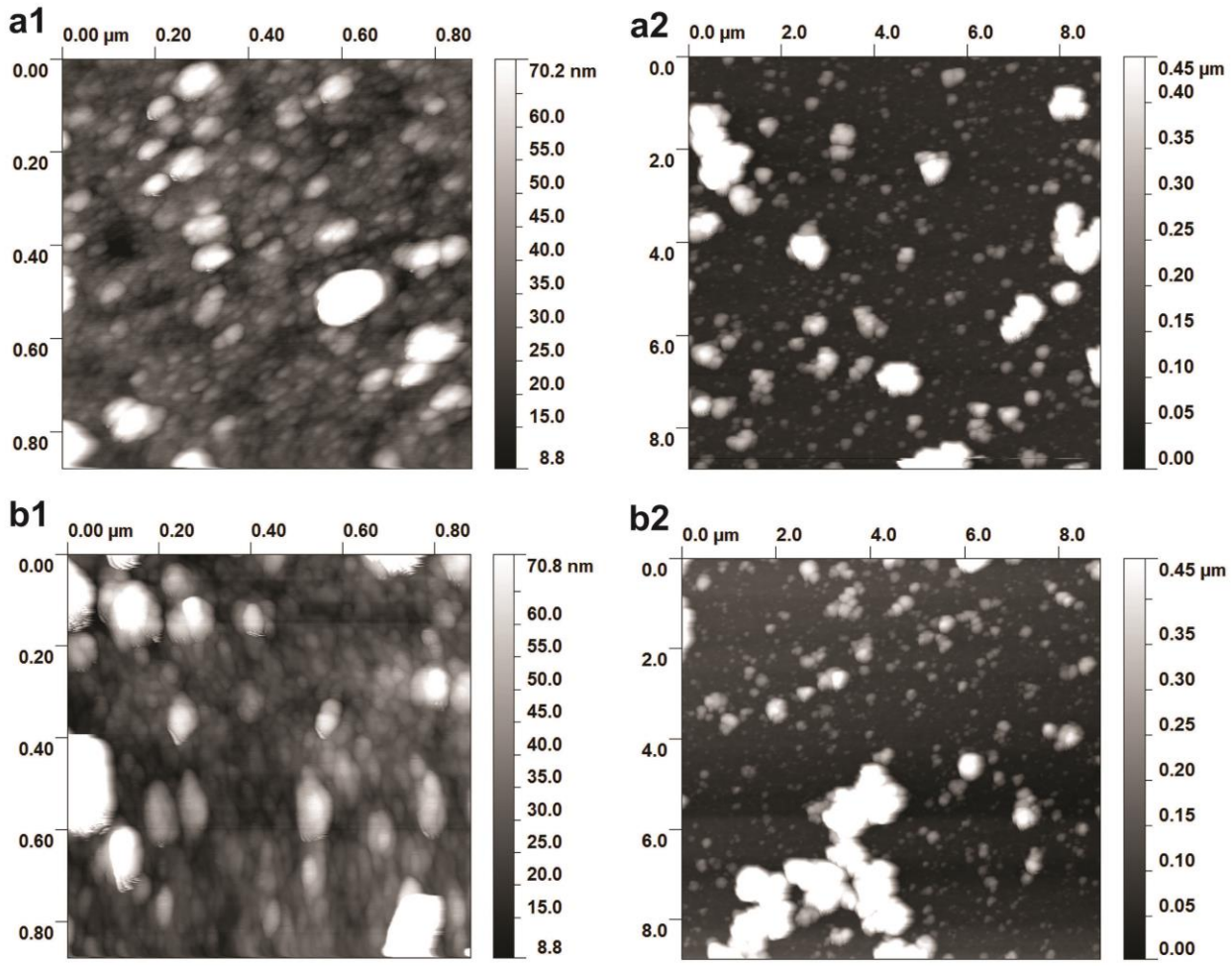

Figure A6: AFM scans of (a) pristine film (b) film incubated in 300 mM $CaCl_2$, 50 mM Tris buffer pH = 9.5 for 4 hr.

The oxidation products of dopamine deposit on various substrates as conformal films shown in Figure A6. The films nucleate as 3-dimensional islands[4] which grow and coarsen until they impinge on each other forming a network of cohesive granules with a characteristic length scale of 20-50 nm in diameter (Figure A6a1). The thickness of PDA films used in this study were determined by AFM to be 59 ± 3 nm (n = 6 measurements). Micron-scale precipitates of PDA from the deposition solution also deposit on the surface of the granular film. The UV-Vis spectrum of pristine PDA films is qualitatively similar to the deposition solution (Figure A7), indicating that similar products are formed in the films and the solution.

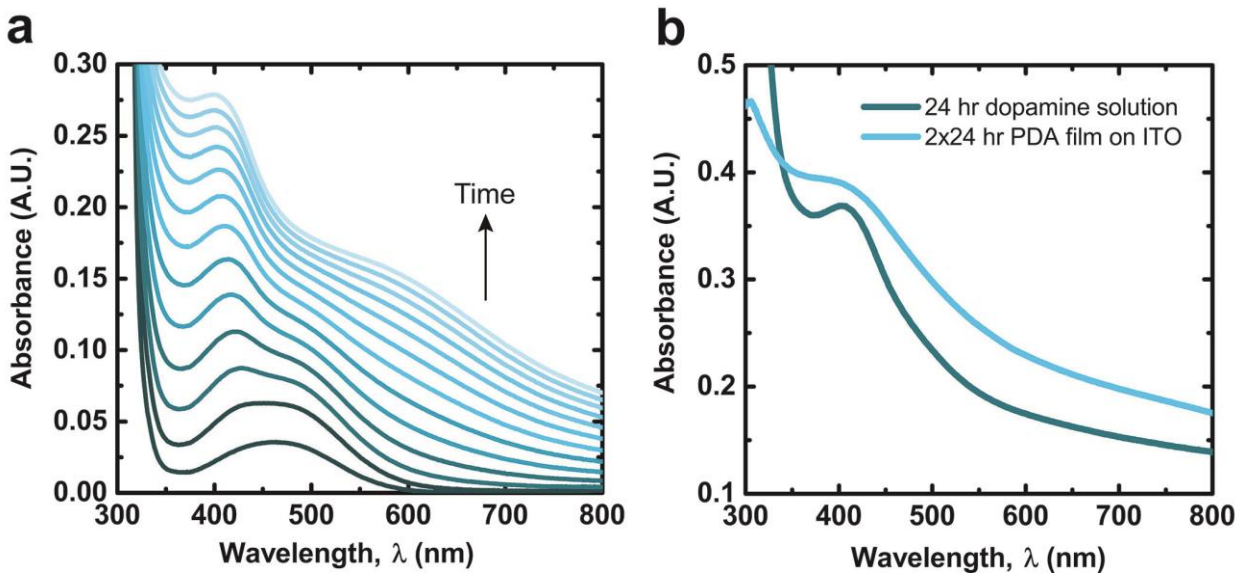

Figure A7: a) UV-Vis spectra of 2 mg/ml dopamine solution in pH 8.5 50 mM bicarbonate buffer. Scans were taken every 83 seconds. b) Spectra of dopamine solution after 24 hours (diluted 1:10 vol) and PDA film on ITO that sat in the dopamine solution for 24 hr then 24 hr again in a refreshed solution.

The spectrum of pristine PDA film shows a monotonic increase in absorption towards the UV region except for a peak at λ_{Abs} = 405 nm. This peak appears in the first several minutes of dopamine oxidation (Figure A7a). The peak's origin is not due to either dopaminochrome (λ_{Abs} = 475 nm) or dopamine-quinone (λ_{Abs} = 388 nm).[5] Considering that the peak appears to evolve out of the initial dopaminochrome peak it may be due to dimers of dopaminochrome and DHI which absorb around λ_{Abs} = 400 – 450 nm.[6]

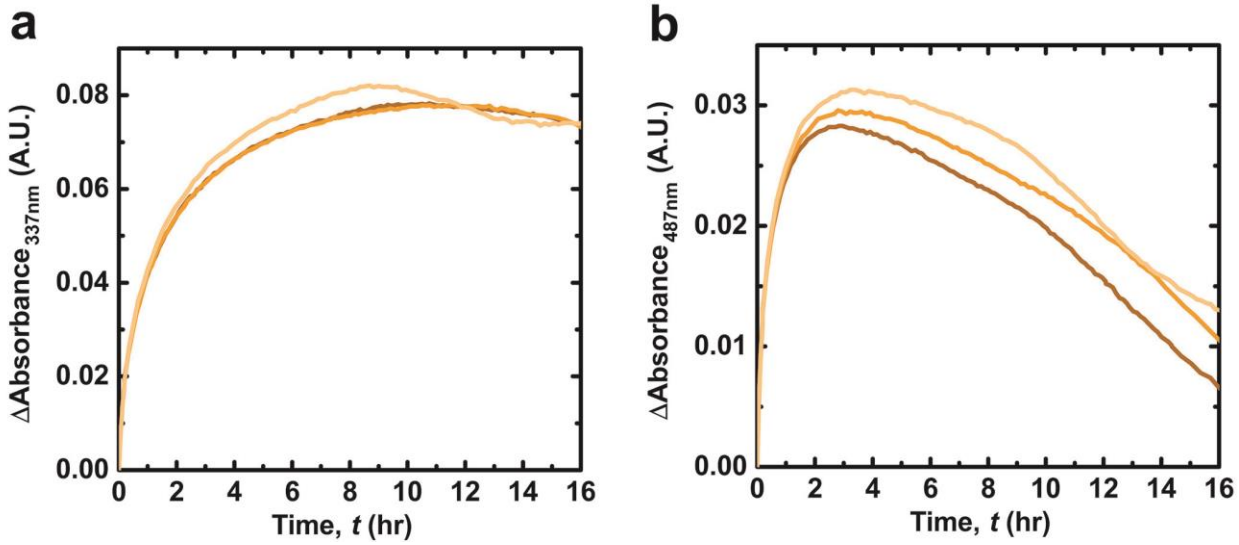

Figure A8: Absorbance vs. time for the peaks observed in subtracted film spectra on three different samples. Incubation solution was 300 mM $CaCl_2$, 50 mM Tris buffer pH = 9.5. a) λ_{Abs} = 337 nm b) λ_{Abs} = 487 nm

ΔA_{487nm} may decrease earlier than ΔA_{337nm} due to oxidative degradation of pre-existing convoluted visible chromophores that exist in the native film.[7]

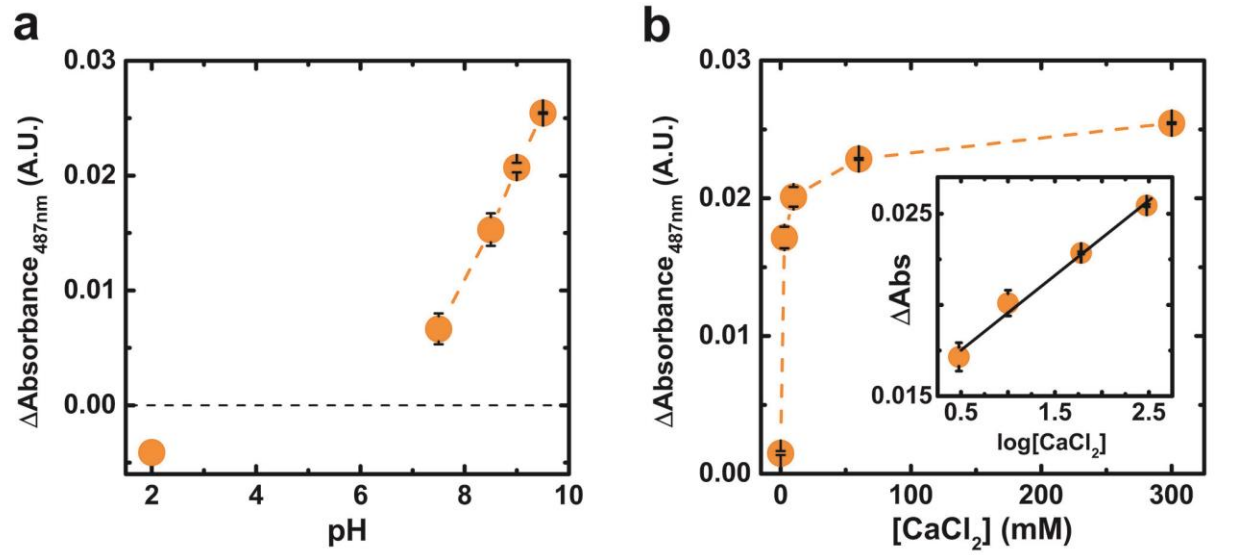

Figure A9: a) Subtracted spectra absorbance at λ_{Abs} = 487 nm after 1 hr as a function of pH in 300 mM $CaCl_2$, 50 mM Tris buffer. b) Subtracted spectra absorbance after 1 hr as a function of [$CaCl_2$] in 50 mM Tris buffer pH = 9.5. See Figure 2 for equivalent data at λ_{Abs} = 337 nm. Data are represented as the average ± std. dev. (n = 2).

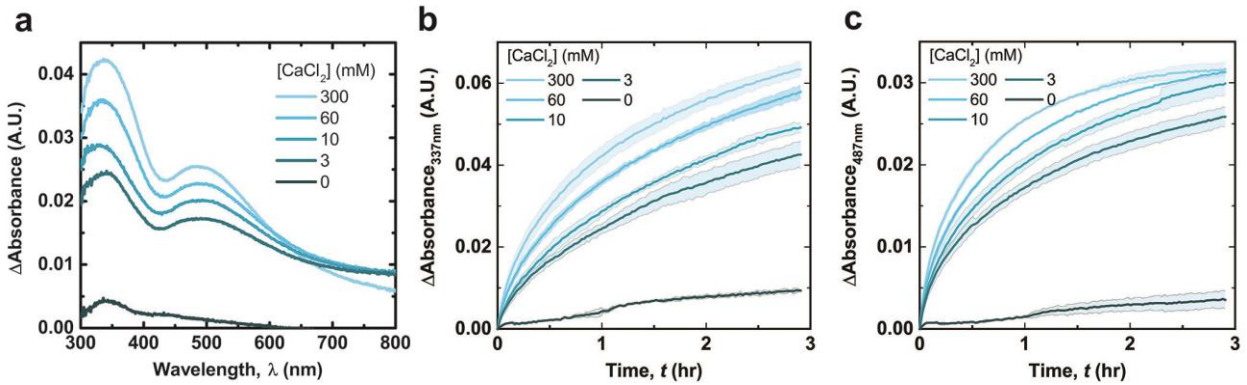

Figure A10: a) Subtracted spectra after 1 hr in 50 mM Tris buffer pH = 9.5. Average of two representative samples. b) Absorbance at λ_{Abs} = 377 nm over 3 hr. The light shaded regions correspond to the standard deviation of the two samples for each condition. c) Absorbance at at λ_{Abs} = 487 nm.

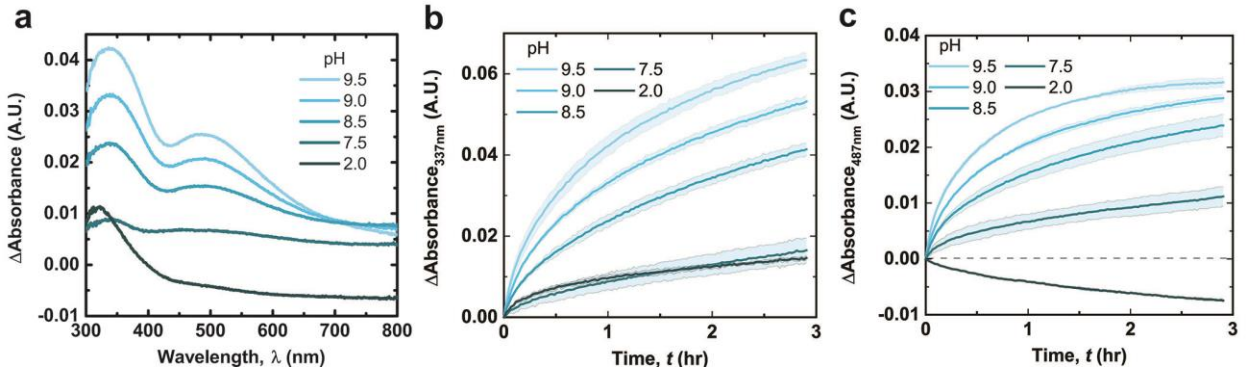

Figure A11: a) Subtracted spectra after 1 hr in 300mM $CaCl_2$ 50 mM Tris buffer. Average of two representative samples. b) Absorbance at λ_{Abs} = 377 nm over 3 hr. The light shaded regions correspond to the range defined by average ± std. dev. (n = 2). c) Absorbance at λ_{Abs} = 487 nm over 3 hr.

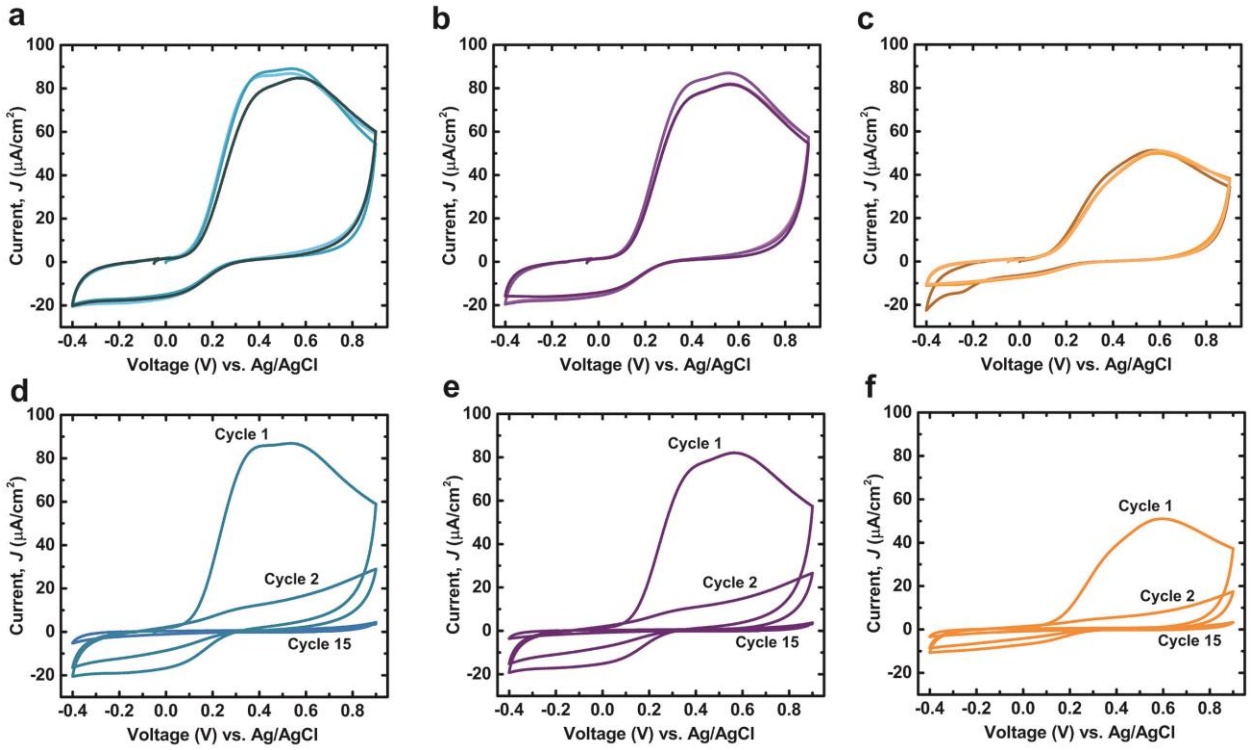

Figure A12: Cyclic voltammograms for three samples after they had been incubated for 4 hr in a) ddH_2O b) 50 mM Tris buffer pH = 9.5 c) 300 mM $CaCl_2$ 50 mM Tris buffer pH = 9.5. Also shown are cycles 2 and 15 for d) ddH_2O e) 50 mM Tris buffer pH = 9.5 f) 300 mM $CaCl_2$ 50 mM Tris buffer pH = 9.5.

The voltammograms of dopamine solutions at pH = 7.0 display the dopamine/quinone redox couple at $E°'$ = 182 mV and the dopaminochrome couple at $E°'$ = –228 mV.[5] The total oxidative current observed in PDA films up to 0.9 V (vs. Ag/AgCl) cannot be attributed to specific molecular species but may be due to the variable redox potentials of assorted oligomers in the films.

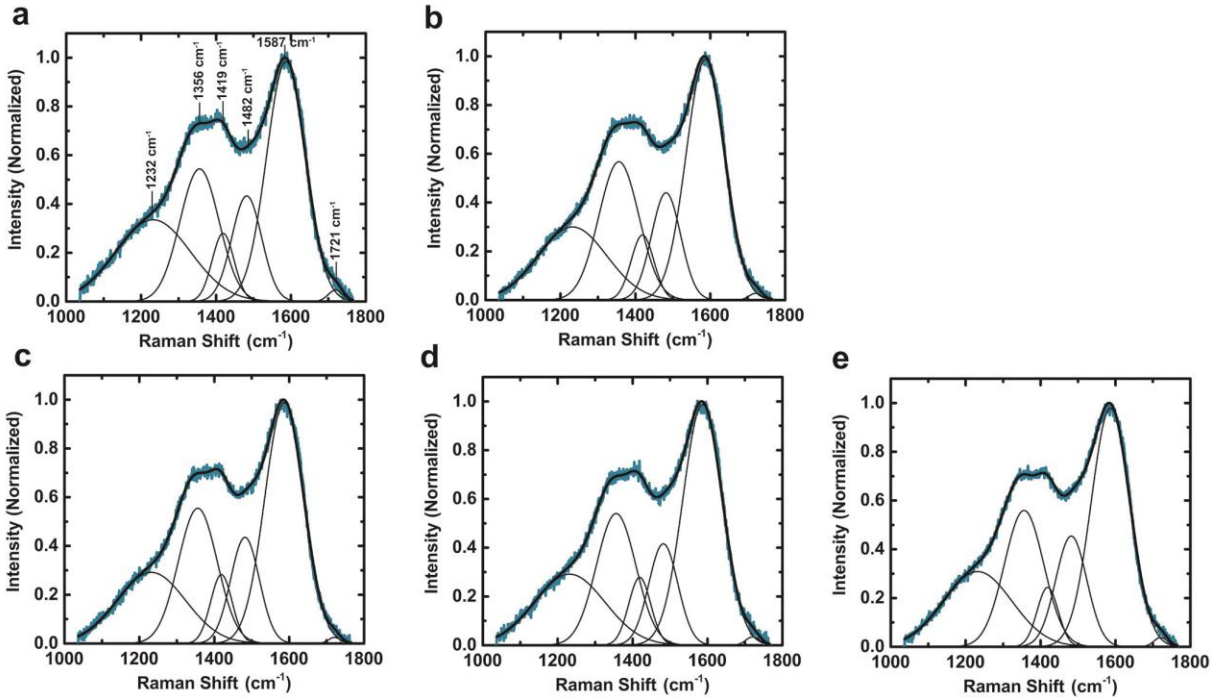

Figure A13: Deconvoluted Raman spectra of pristine PDA films before and after incubating in 5 mM iron solutions for 100 min. Peak positions were fixed at the same position for each deconvolution. a) Films with no iron exposure. b) $FeCl_3$ pH = 2.6 c) $FeCl_2$ pH = 2.6 d) $FeCl_2$ pH = 4.1 e) $FeCl_2$ pH = 5.1

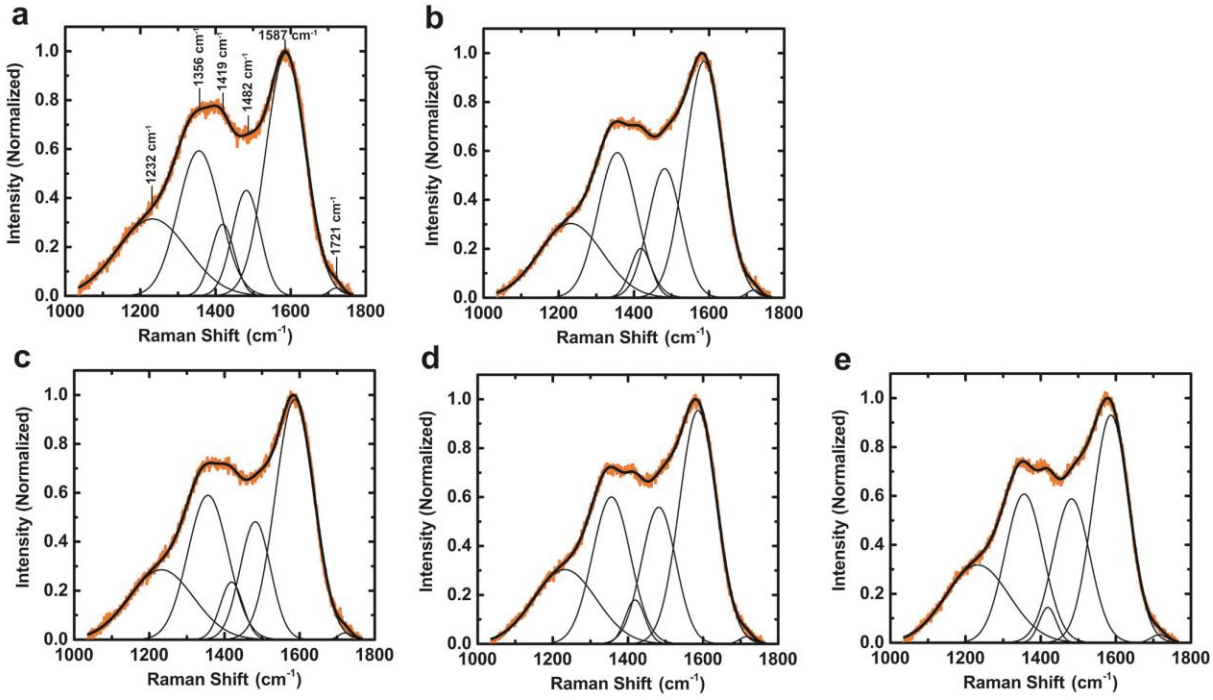

Figure A14: Deconvoluted Raman spectra of $CaCl_2$-oxidized PDA films before and after incubating in 5 mM iron solutions for 100 min. Peak positions were fixed at the same position for each deconvolution. a) Films with no iron exposure. b) $FeCl_3$ pH = 2.6 c) $FeCl_2$ pH = 2.6 d) $FeCl_2$ pH = 4.1 e) $FeCl_2$ pH = 5.1.

Chapter 4 Supporting Figures

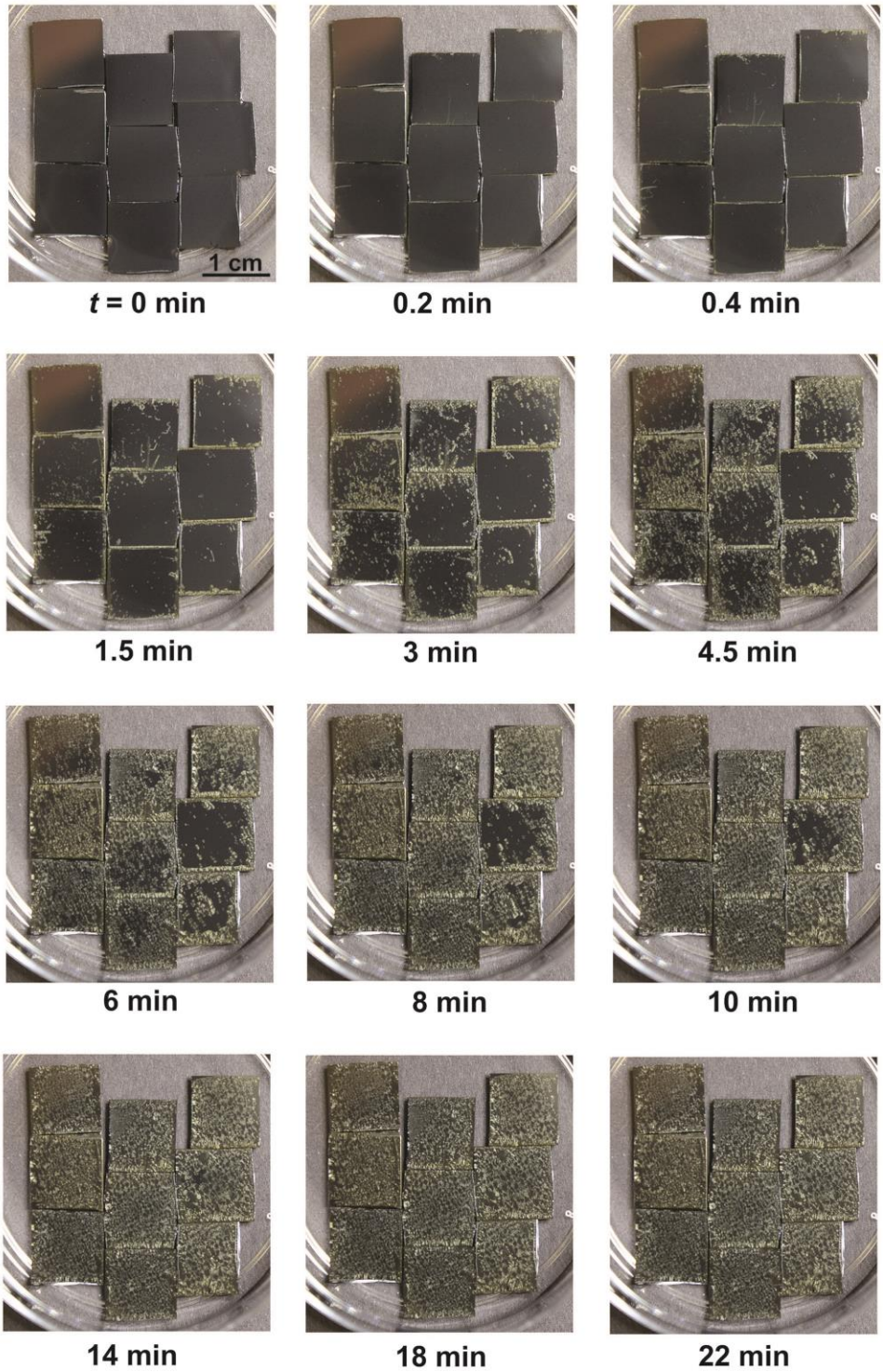

Figure A15: Delamination time lapse of PDA films (59 nm thickness on SiO_2; synthesized from 1 mg/ml dopamine) in 200 mM NaCl at pH = 9.5 (50 mM Tris Buffer).

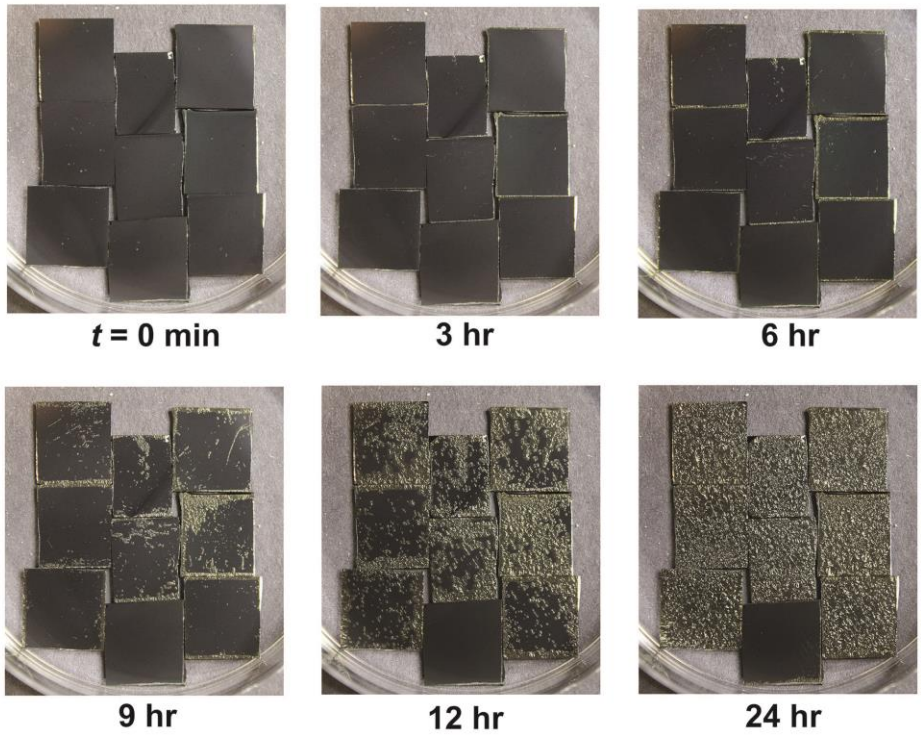

Figure A16: Delamination time lapse of PDA films (59 nm thickness on SiO_2; synthesized from 1 mg/ml dopamine) in 0 mM NaCl at pH = 10(50 mM Tris Buffer).

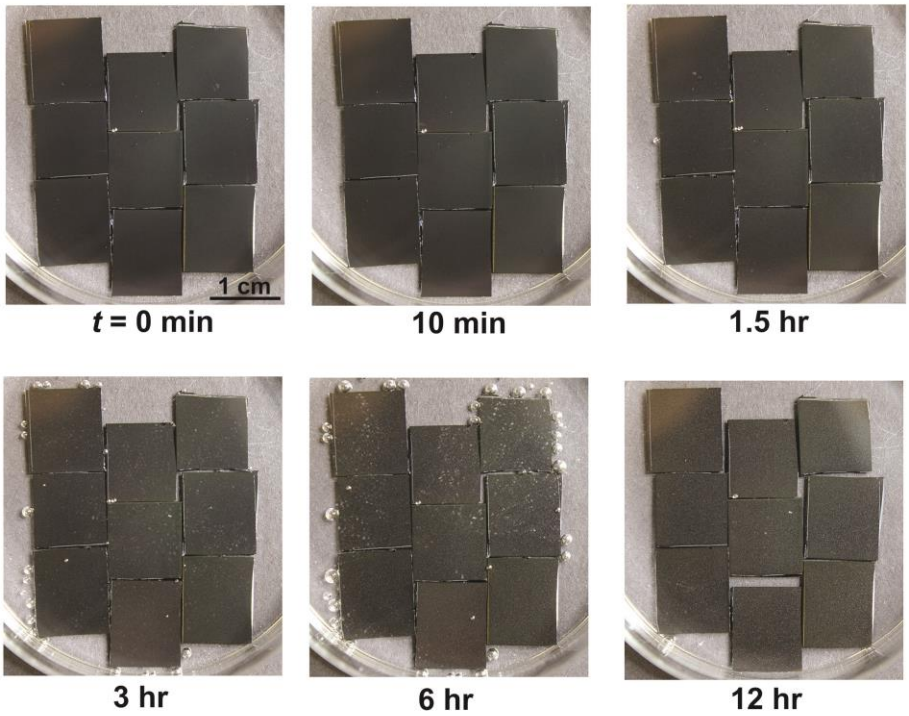

Figure A17: Time lapse of PDA films (59 nm thickness on SiO_2; synthesized from 1 mg/ml dopamine) in 200 mM NaCl + 200 mM $CaCl_2$ at pH = 10 (50 mM Tris Buffer). The visible white precipitate is $CaCO_3$.

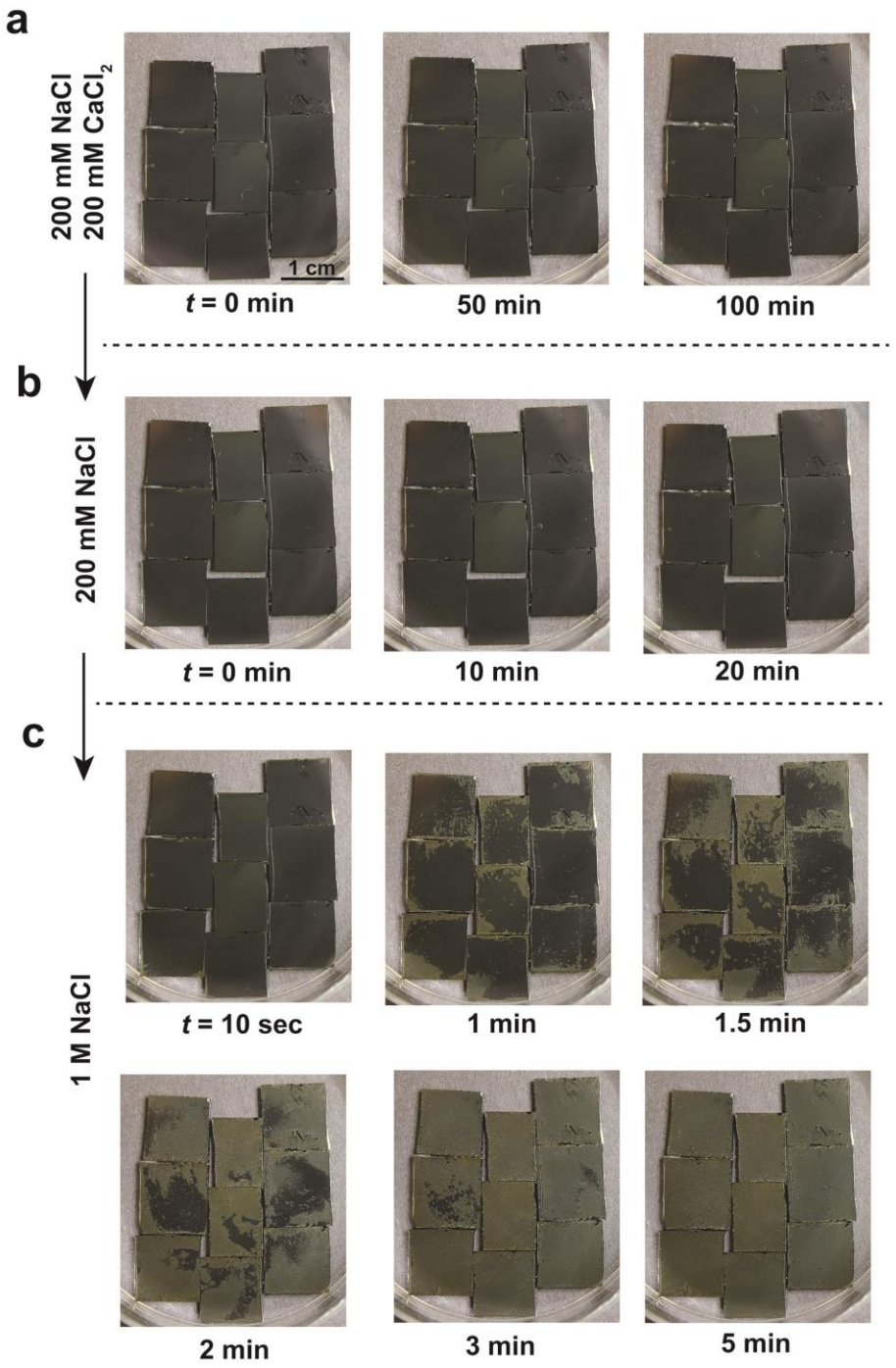

Figure A18: (a) Delamination time lapse of PDA films (59 nm thickness on SiO_2; synthesized from 1 mg/ml dopamine) in 200 mM NaCl + 200 mM $CaCl_2$ at pH = 10 (50 mM Tris Buffer) (b) the same films placed in 200 mM NaCl at pH = 10 (50 mM Tris Buffer) (c) the same films then placed in 1M NaCl at pH = 10 (50 mM Tris buffer).

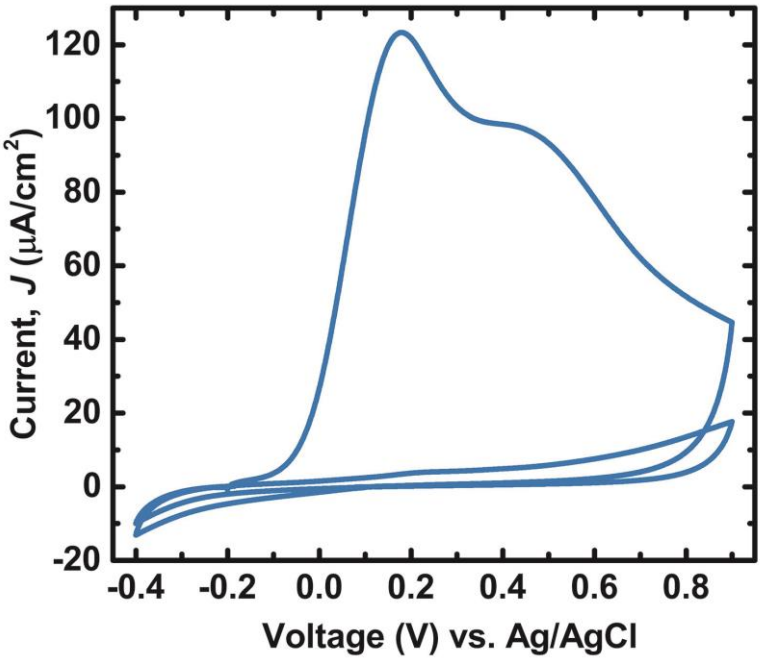

Figure A19: Cyclic voltammogram of PDA film on ITO in equivalent solution to the samples in Figure 4.7. Scan rate was 30 mV/s and was performed in ambient atmosphere. Two cycles are shown.

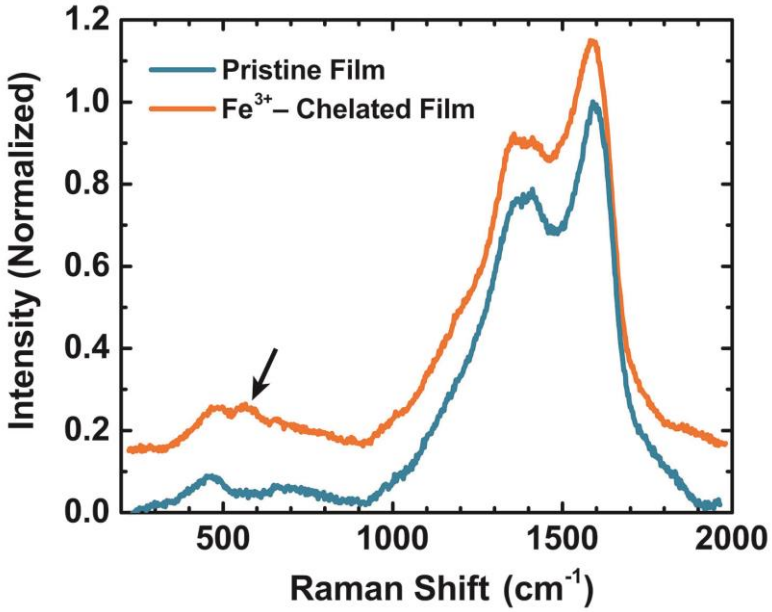

Figure A20: Raman spectra of a pristine PDA film and a PDA film after Fe^{3+} crosslinking. A new band appears at 560 cm^{-1} due to the five-membered chelate ring of catechol with iron.[8] The chelate vibrations of Fe-enediolate complexes are observed in the 500–600 cm^{-1} region in a variety of systems: 528 cm^{-1} for $Fe[oxalate_3]^{3-}$ and human tyrosine hydroxylase[9,10], 533 cm^{-1} for ferric tris-catecholate[11], 565 cm^{-1} for ferric-enterobactin[11], and 550 cm^{-1} for Fe-DOPA complexes.[12]

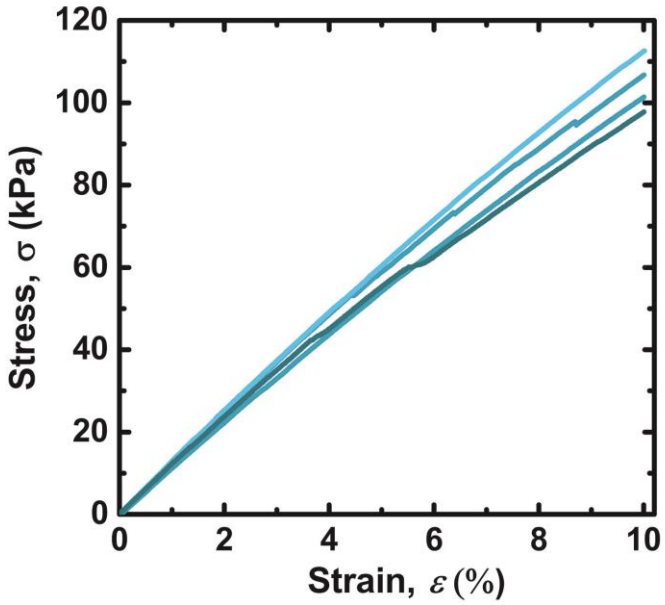

Figure A21: Stress-strain curves of PDMS elastomer samples used to determine their modulus (n = 4).

$n = 4$	Elastic Modulus E_S (MPa)	Standard Deviation (Mpa)
PDMS	1.08	0.07

$n = 6$	Thickness h (nm)	Standard Deviation (nm)
PDA Film	59	4

	$n = 5$	Wavelength λ (μm)	Standard Deviation (μm)
Delamination Condition	**200 mM NaCl pH = 10**	2.70	0.33
	0 mM NaCl pH = 10	2.80	0.20
	200 mM NaCl pH = 9	2.96	0.33
Crosslinking Scheme	**Fe^{3+}**	2.85	0.45
	Genipin	4.65	0.31
	No Genipin (Control)	2.69	0.24

		Elastic Modulus E_F (GPa)	Propagated Error (GPa)
Delamination Condition	**200 mM NaCl pH = 10**	1.5	0.7
	0 mM NaCl pH = 10	1.7	0.6
	200 mM NaCl pH = 9	2.0	0.9
Crosslinking Scheme	**Fe^{3+}**	1.8	1.0
	Genipin	7.9	2.5
	No Genipin (Control)	1.5	0.6

Table A3: Data obtained for determining the modulus of PDA: (a) Modulus of PDMS substrate (b) Thickness of PDA films (synthesized from 1 mg/ml dopamine for 24 + 24 hr deposition) (c) Wrinkling wavelengths of the different samples (d) Calculated moduli of the different films with propagated error incorporating the uncertainty in the PDMS modulus and PDA film thickness.

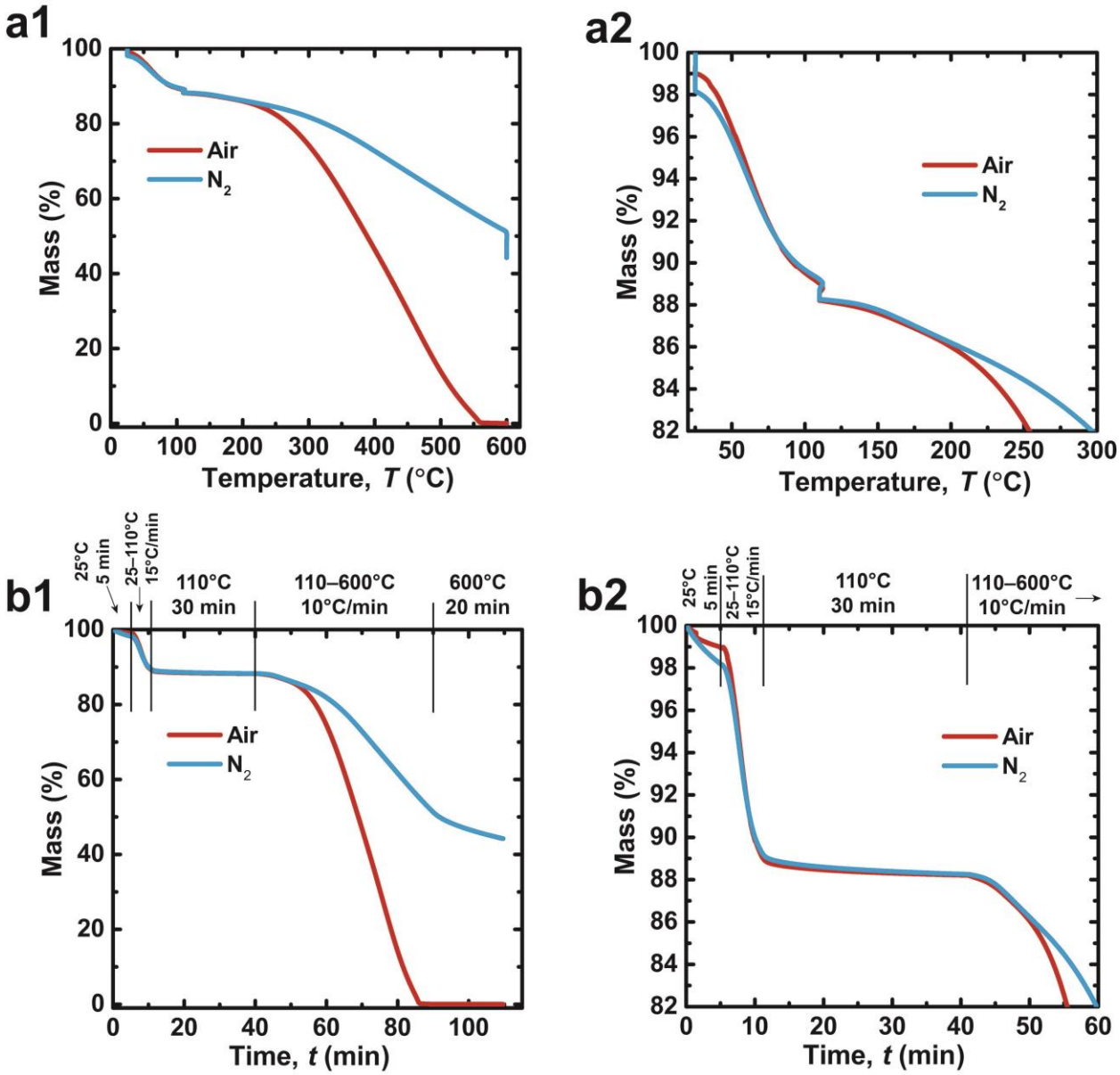

Figure A22: Thermogravimetric analysis of a PDA powder prepared from 4 mg/ml dopamine solution at pH = 8.5 for 24 hr reaction time. a1,2) Mass loss vs. temperature b1,2) Mass loss vs. time with heating procedure shown above. The mass loss at 25°C is attributed to the dry gas flow through the sample chamber resulting in moisture evaporation from the sample. The water loss was 12 wt% for both tests. Testing was performed using a Q50 TGA (TA Instruments; Delaware, USA) and 60 ml/min sample gas flow. Sample powder had been washed with ddH_2O to remove residual buffer salt, freeze dried for 48hr, and sat in ambient for 72hr before testing.

References

(1) Voinova, M. V; Rodahl, M.; Jonson, M.; Kasemo, B. Viscoelastic Acoustic Response of Layered Polymer Films at Fluid-Solid Interfaces : Continuum Mechanics Approach. *Phys. Scr.* **1999**, *59*, 391–396.

(2) Reviakine, I.; Johannsmann, D.; Richter, R. P. Hearing What You Cannot See and Visualizing What You Hear : *Anal. Chem.* **2011**, *83*, 8838–8848.

(3) Bridelli, M. G.; Crippa, P. R. Infrared and Water Sorption Studies of the Hydration Structure and Mechanism in Natural and Synthetic Melanin. *J. Phys. Chem. B* **2010**, *114*, 9381–9390.

(4) Klosterman, L.; Riley, J. K.; Bettinger, C. J. Control of Heterogeneous Nucleation and Growth Kinetics of Dopamine-Melanin by Altering Substrate Chemistry. *Langmuir* **2015**, *31*, 3451–3458.

(5) Zhang, F.; Dryhurst, G. Oxidation Chemistry of Dopamine: Possible Insights into the Age-Dependent Loss of Dopaminergic Nigrostriatal Neurons. *Bioorg. Chem.* **1993**, *21*, 392–410.

(6) Pezzella, A.; Crescenzi, O.; Panzella, L.; Napolitano, A.; Land, E. J.; Barone, V.; D'Ischia, M. Free Radical Coupling of O-Semiquinones Uncovered. *J. Am. Chem. Soc.* **2013**, *135*, 12142–12149.

(7) Tran, M. L.; Powell, B. J.; Meredith, P. Chemical and Structural Disorder in Eumelanins: A Possible Explanation for Broadband Absorbance. *Biophys. J.* **2006**, *90*, 743–752.

(8) Samokhvalov, A.; Liu, Y.; Simon, J. D. Characterization of the Fe(III)-Binding Site in Sepia Eumelanin by Resonance Raman Confocal Microspectroscopy. *Photochem. Photobiol.* **2004**, *80*, 84–88.

(9) Fujita, J.; Martell, A. E.; Nakamoto, K. Infrared Spectra of Metal Chelate Compounds. VI. A Normal Coordinate Treatment of Oxalato Metal Complexes. *J. Chem. Phys.* **1962**, *36*, 324.

(10) Michaud-Soret, I.; Andersson, K. K.; Que, L.; Haavik, J. Resonance Raman Studies of Catecholate and Phenolate Complexes of Recombinant Human Tyrosine Hydroxylase. *Biochemistry* **1995**, *34*, 5504–5510.

(11) Salama, S.; Stong, J. D.; Neilands, J. B.; Spiro, T. G. Electronic and Resonance Raman Spectra of iron(III) Complexes of Enterobactin, Catechol, and N-Methyl-2,3-Dihydroxybenzamide. *Biochemistry* **1978**, *17*, 3781–3785.

(12) Harrington, M. J.; Masic, A.; Holten-andersen, N.; Waite, J. H.; Fratzl, P. Iron-Clad Fibers : A Metal-Based Biological Strategy for Hard Flexible Coatings. *Science* **2010**, 216–220.